FACULDADE DE ENGENHARIA DA UNIVERSIDADE DO PORTO
Masters in Mechanical Engineering

Master Dissertation

Dynamics of carbon nanotube mass sensors

Diogo Henrique de Almeida Pinheiro
up201806159@up.pt

Supervisor
Hamed Akhavan

October 9, 2023

U.PORTO
FEUP FACULDADE DE ENGENHARIA
UNIVERSIDADE DO PORTO

Abstract

The dynamic behavior of a carbon nanotube (CNT) is influenced by small masses that may be attached to it. This behavior variation can be used to quantify the mass value of these small particles. Shell models, significantly simpler than molecular dynamics models, can be used to simulate the behavior of these structures and predict the effect of the existence of concentrated masses in their dynamics. A review of the different modeling approaches of this structure is made, as well as different production processes and experimental work with nano-oscillators based on CNTs which have already been used to detect and measure masses. In this dissertation, Sanders-Koiter's theory thin shell theory is applied to a cylindrical shell in order to represent a single-walled nanotube. The p-version finite element method is used to discretize the domain. The nanotube is modeled by only one element.

The developed model is modally compared with molecular dynamics results showing satisfactory results. The dynamic response to a non-linear electrostatic action is obtained by integrating in time the equations of motion. For this, Newmark's method is used. The obtained response in time is then compared with results from a beam model. This way, the model is validated. The feasibility of disregarding membrane inertia and longitudinal inertia in favor of reducing complexity and consequently computational load is also discussed.

Finally, a concentrated mass is added to the model. Natural frequencies and forms of vibration are calculated and validated. The effect of the presence of a coupled mass in the vibration modes of the CNT is studied and its use for transducing mass is explored. An equation that relates frequency shift with the value of the mass is proposed. The influence of the CNT geometry on its sensitivity as a mass transducer is analyzed. Errors due to possible mass decentralizations are quantified by studying the dependence of the system's natural frequencies on the location of the concentrated mass. The amplitude of the forced response of the system is related to the value of the localized mass and the feasibility of this mechanism being used as a mass transducer is discussed.

Keywords: Carbon Nanotubes; Shell Model; Mass Sensor; Nano Electromechanical System; Electrostatic; Oscillator

Resumo

O comportamento dinâmico de um nanotubo de carbono (CNT) é influenciado por pequenas massas que a ele possam estar acopladas. Esta variação de comportamento pode ser utilizada como uma forma de quantificar o valor da massa destas pequenas partículas. Modelos de casca, significativamente mais simples que modelos de dinâmica molecular, podem ser utilizados para modelar o comportamento destas estruturas e prever o efeito da existência massas concentradas no nanotubo. Uma revisão das diferentes abordagens de modelação desta estrutura é feita, bem como diferentes processos de produção e trabalhos experimentais com nano-osciladores baseados em CNTs os quais já foram usados para detetar e medir massas.

Nesta dissertação, a teoria de Sanders-Koiter para cascas finas é aplicada a uma casca cilíndrica a fim de representar um nanotubo de camada singular. A versão p do método dos elementos finitos é utilizada para discretizar o domínio. O nanotubo, neste caso, é modelado apenas por um elemento.

O modelo desenvolvido é modalmente comparado com modelos de dinâmica molecular apresentando resultados satisfatórios. A resposta dinâmica a uma atuação eletrostática não-linear é obtida integrando no tempo as equações de movimento. Para tal, o método de Newmark é utilizado. A resposta obtida é então comparada com resultados provenientes de um modelo de viga disponíveis na literatura. Desta forma, o modelo é validado. A viabilidade de desprezar a inercia de membrana e a inércia longitudinal em prol da redução de complexidade e consequentemente carga computacional é também discutida.

Por fim, uma massa concentrada é acrescentada ao modelo. Frequências e formas naturais de vibração são calculadas e validadas. O efeito da presença de uma massa acoplada nos primeiros modos de vibração do CNT é estudado e a sua utilização transdutor de massa é explorada. Uma equação que relaciona a frequência fundamental do oscilador e o valor da massa é proposta. A influência da geometria do CNT na sua sensibilidade como transdutor de massa é analisada. Os erros devido a possíveis descentramentos da massa são quantificados, estudando a dependência das frequências naturais do sistema com a localização da massa concentrada. A amplitude da resposta forçada do sistema é relacionada com o valor da massa localizada e é estudada a viabilidade deste mecanismo ser utilizado para quantificar o valor da massa.

Palavras-Chave: Nanotubo de carbono; Modelo de Casca; Sensor de Massa; Sistema Nano Eletromecânico; Eletrostático; Oscilador

Acknowledgments

I would like to express my heartfelt gratitude to the professors who have been instrumental in shaping my academic journey over the last five years. I wish to express my deep gratitude to Dr. Hamed Akhavan, my supervisor, and Professor Pedro Leal Ribeiro, whose invaluable guidance and mentorship have been instrumental in the development of this thesis.

I am deeply indebted to my parents, whose unwavering support, encouragement, and sacrifices have been my pillars of strength throughout this academic pursuit. Your belief in me has been a constant source of motivation, and I am forever grateful for your love and guidance. To my sister and grandparents, thank you for always being there for me, offering encouragement, and providing a loving and nurturing environment in which I could thrive.

I extend my appreciation to my university colleagues, whose camaraderie and collaborative spirit have enriched my academic experience. Last but certainly not least, I want to thank my girlfriend for her unwavering support, patience, and understanding. This thesis represents the culmination of years of hard work, dedication, and the collective support of those around me. Without the contributions of these individuals, this achievement would not have been possible.

Thank you all for being an integral part of my academic journey.

Table of Contents

List of Figures

List of Tables

List of Abbreviations

AC	Alternating current
CC	Clamped-clamped boundary conditions
CNT	Carbon nanotube
CVD	Chemical vapor deposition
DC	Direct current
DFT	Density functional theory
FEM	Finite element method
MD	Molecular dynamics
MEMS	Micro-electro-mechanical systems
MWCNT	Multi-walled carbon nanotube
NEMS	Nano-electro-mechanical systems
PECVD	Plasma-enhanced chemical vapor deposition
SEM	Scanning electron microscope
SWCNT	Single-walled carbon nanotube
TEM	Transmission electron microscope

List of Symbols

Greek Symbols

α_c	Rayleigh damping mass coefficient
β	Parameter of Newmark´s method
β_c	Rayleigh damping stiffness coefficient
γ	Parameter of Newmark´s method
$\gamma_{\theta z}$	Transverse shear strain
$\gamma_{x\theta,0}$	Shear membrane strain component on the middle surface
$\gamma_{x\theta}$	Shear membrane strain
γ_{xz}	Transverse shear strain
γ_{yz}	Transverse shear strain
δK	Variation of the kinetic energy
Δt	Time step
δU	Variation of the potential energy
δ	Dirac delta
δW	Variation of virtual work of the external pressure field
$\varepsilon_{\theta,0}$	Normal strain component in θ direction on the middle surface
$\varepsilon_{\theta\theta}$	Normal strain in θ direction
$\varepsilon_{x,0}$	Normal strain component in x direction on the middle surface
ε_{xx}	Normal strain in x direction
ε_{zz}	Normal strain in z direction
ε_0	Permeability of vaccum
ζ	Damping ratio
ζ_m	Damping ratio of mode m
ζ_n	Damping ratio of mode n
θ	Circumferential coordinate
θ^p	Circumferential position of the concentrated mass - θ coordinate
ν	Poisson's ratio
ξ	Natural coordinate in the x direction
ξ^p	Longitudinal position of the concentrated mass - ξ coordinate
ρ	Mass density
$\sigma_{\theta\theta}$	Normal stress in the θ direction
$\sigma_{\theta z}$	Transverse shear stress

σ_{xx} Normal stress in the x direction
σ_{xz} Transverse shear stress
σ_{yz} Transverse shear stress
$\tau_{x\theta}$ Shear membrane stress
χ Aspect ratio
Ω Surface area of the shell
ω Frequency
Ω_{AC} Frequency ratio - ratio between ω_{AC} and fundamental natural frequency of the CNT
ω_{AC} Frequency of the alternating component of V
ω_m Natural frequency of mode m
ω_n Natural frequency of mode n
ω_1 Fundamental natural frequency

Roman Symbols

a_0 Auxiliary variable of Newmark´s method
a_1 Auxiliary variable of Newmark´s method
a_2 Auxiliary variable of Newmark´s method
a_3 Auxiliary variable of Newmark´s method
a_4 Auxiliary variable of Newmark´s method
a_5 Auxiliary variable of Newmark´s method
a_6 Auxiliary variable of Newmark´s method
a_7 Auxiliary variable of Newmark´s method
$\widetilde{a}$ Inter-atomic spacing of the carbon atoms
b Distance of the CNT to the gate
C Capacitance per unit length
d Diameter
E Young's modulus
E_{elec} Electrostatic energy
F_{elec} Electrostatic force per unit length
f_r Transverse shape function for longitudinal coordinate
g_r Internal membrane shape functions for longitudinal coordinate
h Thickness
$i\theta$ Auxiliary variable
$i\xi$ Auxiliary variable
$j\theta$ Auxiliary variable
$j\xi$ Auxiliary variable
K Kinetic energy
k_θ Curvature in the θ direction
$k_{x\theta}$ Shear curvature
k_x Curvature in the x direction
l Length of the nanotube
$\mathscr{L}_u$ Equation of motion for the axial component

$\mathscr{L}_u^{CM}$	Equation of motion considering a concentrated mass for the axial component
$\mathscr{L}_v$	Equation of motion for the tangential component
$\mathscr{L}_v^{CM}$	Equation of motion considering a concentrated mass for the tangential component
$\mathscr{L}_w$	Equation of motion for the radial component
$\mathscr{L}_w^{CM}$	Equation of motion considering a concentrated mass for the radial component
m	Longitudinal nodes number (for ξ)
$M_{\theta\theta}$	Internal moment in θ direction
M_{conc}	Attached concentrated mass
$M_{x\theta}$	Internal shear moment
M_{xx}	Internal moment in x direction
m_x	Concentrated mass per unit length
n	Circumferential nodes number (for θ)
N	Number of shape function of each displacement component in each direction
$N_{\theta\theta}$	Internal normal force in the θ direction
$N_{x\theta}$	Internal shear normal force
N_{xx}	Internal normal force in the x direction
p_u	External pressure field in the axial direction
p_v	External pressure field in the circumferential direction
p_w	External pressure field in the perpendicular direction
pgu	Number of shape functions employed to displacement u_0 in the x coordinate
pgv	Number of shape functions employed to displacement v_0 in the x coordinate
ptu	Number of shape functions employed to displacement u_0 in the θ coordinate
ptv	Number of shape functions employed to displacement v_0 in the θ coordinate
ptw	Number of shape functions employed to displacement w_0 in the θ coordinate
pw	Number of shape functions employed to displacement w_0 in the x coordinate
$\mathscr{P}_{ext}$	External pressure field
q_{ij}^u	Generalized displacements for u_0
q_{ij}^v	Generalized displacements for v_0
q_{ij}^w	Generalized displacements for w_0
$\ddot{q}_{ij}^u$	Generalized accelerations for u_0
$\ddot{q}_{ij}^v$	Generalized accelerations for v_0
$\ddot{q}_{ij}^w$	Generalized accelerations for w_0
R	Radius of a single-walled carbon nanotube
r	Multiplier of zig-zag carbon bonds of hexagonal lattice

s	Multiplier of zig-zag carbon bonds of hexagonal lattice
t	Time variable
t_1	Initial time
t_2	Final time
tu_n	Axial shape functions for θ
tv_n	Circumferential shape functions for θ
tw_n	Transverse shape functions for θ
U	Potential energy
u	Axial displacement
$\dot{u}$	Axial velocity
u_0	Middle surface axial displacement
$\dot{u}^0$	Middle surface axial velocity
$\ddot{u}^0$	Middle surface axial acceleration
v	Circumferential displacement
$\dot{v}$	Circumferential velocity
V	Voltage
V_{AC}	Alternating current voltage
V_{DC}	Direct current voltage
v_0	Middle surface circumferential displacement
$\dot{v}^0$	Middle surface circumferential velocity
$\ddot{v}^0$	Middle surface circumferential acceleration
w	Transverse displacement
$\dot{w}$	Transverse velocity
W	Work of external pressure field
w_0	Middle surface transverse displacement
$\dot{w}^0$	Middle surface transverse velocity
$\ddot{w}^0$	Middle surface transverse acceleration
x	Longitudinal coordinate of the system
x^p	Longitudinal position of the concentrated mass - x coordinate
z	Coordinate perpendicular to the shell

Vectors and Matrices

$\{\delta_1\}$	Vector of shape functions for longitudinal displacements
$\{\delta_2\}$	Vector of shape functions for transverse displacements
$\{\delta_3\}$	Vector of shape functions for radial displacements displacements
$\{\Delta q\}$	Vector of variation of displacement
$\{a_1\}$	Lattice vector
$\{a_2\}$	Lattice vector
$\{C_h\}$	Chiral vector
$\{de^0\}$	Middle surface displacements vector
$\{P\}^{t+\Delta t}{}_{eff}$	Effective load vector of Newmark's method
$\{P_i\}$	Subvector of generalized force for the direction of i
$\{q\}$	Generalized displacements vector
$\{\dot{q}\}^t$	Generalized velocity vector
$\{\ddot{q}\}^t$	Generalized acceleration vector
$\{\ddot{q}_i(t)\}$	Subvector of generalized accelerations for the direction of i
$[C]$	Damping matrix
$[K]$	Stiffness matrix
$[K]_{eff}$	Effective stiffness matrix of Newmark's method
$\left[K_{ij}\right]$	Stiffness submatrix
$[M]$	Mass matrix
$\left[M_{ij}\right]$	Mass submatrix
$\left[M_{ij}^{CM}\right]$	Mass submatrix with concentrated mass
$[N]$	Shape functions matrix

Chapter 1

Introduction

1.1. General Overview and Motivation

CNTs have earned an appropriate spot in the fields of engineering, materials science, medicine, biology, electronics, and energy production thanks to the most recent developments in nanoscience and nanotechnology. Since Iijima [1], who invented the study of the synthesis of molecular carbon structures in the form of fullerenes and later reported the creation of needle-like tubes of finite carbon structure, the helical tubules of graphene sheets, and the carbon nanotubes, in 1991, ongoing research and the resulting number of publications on the topic have taken a major role for the scientific community.

Carbon nanotubes are often used as ultrahigh frequency nanoelectromechanical resonators (as their reduced size and high rigidity amplify the resonant frequency and reduce its energy consumption, improving its sensitivity), including sensors, oscillators, charge detectors, field emission devices [2], NEMS devices used to mass and biological detection [3].

The study of the vibration characteristics of CNTs is closely related to these applications and depend on the capability of predicting the vibrational response under certain conditions. Thus, the existence of a model capable of acquiring the response both on transient and steady-state regimes reveals its extreme importance. Various methods have been used to investigate the vibrations of carbon nanotubes (CNTs). These include molecular dynamics simulations, which have been employed in several studies [4–7]. Such simulations are considered reliable and have been found to produce results that are close to experimental studies. Additionally, continuum models using beam or shell theories have been published in different studies as well [8–11].

In this dissertation, the linear model of single-walled carbon nanotubes is developed by employing the Sanders-Koiter theory and using the p-version finite element method to aid with the discretization and implementation, while molecular dynamics and different continuum model results are used to validate the proposed model. The response under a non-linear forced regime, due to an electrostatic interaction, will be computed by applying Newmark's method.

1.2. Objectives

This master thesis presents a comprehensive investigation into the dynamic behavior of carbon nanotubes (CNTs) under the influence of electrostatic actuation, with the ultimate goal of developing CNT-based mass sensors for detecting very small masses. The study incorporates a continuum shell model representation for CNTs to efficiently simulate their behavior (when compared with molecular dynamics). Electrostatic actuation, a widely employed technique in micro and nanoelectromechanical systems (MEMS/NEMS), is introduced into the computational model to explore its impact on CNT vibrations.

The objectives of this research are threefold: first, to incorporate the effect of electrostatic actuation into a computational model for CNTs, represented as cylindrical shells. Second, to validate the model's accuracy by comparing its predictions with results from molecular dynamics simulations or experimental data available in the literature. The validation process ensures the model's reliability and ability to accurately reproduce real-world scenarios. Finally to include a concentrated mass, and study its influence on the system's vibrational properties and response under a forced regime.

Using the validated model, the study investigates the vibrations of CNTs under forced excitation induced by electrostatic forces. The analysis extends to CNTs with and without attached masses, seeking to understand these masses' influence on the nanotubes' dynamic behavior. This investigation is particularly crucial in the context of nano-mass sensors, as it sheds light on how attached masses affect the vibrations and overall performance of the CNTs as sensing elements.

The findings of this research contribute to the advancement of nanoelectromechanical systems (NEMS) and offer promising prospects for sensitive mass sensing applications. By leveraging the insights gained from this study, researchers can develop more effective CNT-based nano-mass sensors capable of detecting molecules or other minuscule masses. The integration of electrostatic actuation and the continuum shell model represents a significant step toward the practical realization of such advanced sensing devices.

In conclusion, this master thesis bridges the gap between continuum shell modeling and electrostatic actuation in the context of CNT dynamics. The results presented herein provide valuable knowledge for the development of cutting-edge nano-mass sensors with potential applications in various fields, including molecular detection and nanoscale mass measurements.

1.3. Thesis Structure

This thesis is composed of six chapters, including the Introduction (Chapter 1) and the Conclusion (Chapter 6). Chapter 2 consists of a literature review. In Chapter 3 the model presented in this thesis is introduced and deduced. Chapter 4 focuses on the validation and results analysis of this model. In Chapter 5 a concentrated mass is introduced into the problem and the results are analyzed. In a more detailed way, the Chapters 2 to 5 are briefly described below.

Chapter 2 begins with a small introduction to CNTs explaining their morphology and resuming the way that carbon atoms' arrangement in space affects their properties. Then the different applications of CNTs are explored, dedicating a section to carbon nanotube

resonators, and their ability to act as sensors. The main difficulties presented in the literature of modeling CNT-based resonators are identified. Then, different approaches to the CNT model are reviewed, with special attention dedicated to continuum models (beam and shell) and molecular dynamic models. Finally, different experiments with carbon nanotube resonators are revised.

In Chapter 3 the problem analyzed is presented and a thin shell model is deduced as well as an expression to compute capacitive forces induced on the CNT. In the first place, we present the Kirchhoff-Love assumptions and discuss the limitations of the thin shell theory. Sanders-Koiter thin shell theory is then employed and invoking Hamilton's Principle and the strong form of the governing equations of the problem is written. After, p-version FEM is used and the problem is presented in its weak form; FEM matrices are assembled and equations are written in a matrix way. Aiming to decrease computational effort, models neglecting membrane inertia are deduced in this chapter. Considering an electrostatic interaction with a ground plane, an expression for the externally applied pressure on the CNT is proposed. Chapter 3 closes by exhibiting the algorithm used to integrate the equations of motion in time and the way the non-linearity of the force was addressed.

Chapter 4 is dedicated to validating the model developed in the previous chapter and analyzing its results. Starting with a convergence analysis for all full and condensed models, we conclude on the number of shape functions needed. A comparison aiming to evaluate the influence of membrane inertia on the natural frequencies of clamped CNT was done. After that, the natural frequency values obtained using the proposed model are put side-by-side with those documented in the literature, and the models are validated. Different CNT morphologies are explored. Then, characteristic natural mode shapes of vibration are identified and documented. Finally, the response in time of a clamped-clamped CNT resonator is computed for different excitation frequencies and the model is validated with literature values.

Chapter 5 is dedicated to studying the possibility of using a CNT oscillator as a mass sensor. A concentrated mass is added to the previously developed model and the effect on natural frequency values is reported as well as compared to the literature. The impact of the concentrated mass on the natural mode shapes of vibration is also analyzed. The position of the concentrated mass is also studied. To conclude the steady-state response in time of a clamped-clamped CNT resonator is computed, now with an attached mass. The effect of this mass on the dynamic response is presented and discussed.

Chapter 6 resumes all the conclusions of this work and discusses directions for future work.

Chapter 2

Carbon Nano Tubes

Carbon nanotubes have attracted a lot of investigation since their initial discovery [1]. Since then, other researchers have noted extraordinary mechanical and physical features for this novel type of carbon. Carbon nanotubes have enormous prospects for the development of fundamentally new material systems, from special electrical properties and thermal conductivity, higher than diamond, to mechanical capabilities where the stiffness, strength, and resilience exceed any existing material [12].

Thinking of a graphene sheet in which the atoms are laid out in a hexagonal way and imagining it rolling forming a cylinder is the best way to understand what is a CNT. This chain of thoughts can be used to derive the CNT's equivalent diameter, based on the carbon atoms arrangement. The layout of the CNT structure defines its morphology, which will affect its properties.

The development of nanoelectromechanical systems (NEMS) and their application as nanoresonators created a promising future for CNTs in which they can be used as sensors, due to their exceptional dynamic behavior, small size, and low current consumption.

This chapter will start with an overview of CNT's morphology presenting the different arrangements that carbon atoms can have in such structures. After that, the main methods used for the production of carbon nanotubes are stated as well as their advantages and disadvantages. Later a review of CNT's applications is done with special attention to carbon nanotube resonators. In this section, the main challenges of CNT-based resonators are presented. Afterwards, the different approaches to CNT modeling are highlighted going in-depth with molecular dynamics - the general concept of Molecular Dynamics (MD) is explained. A review of different models is done. Finally, comes an overview of practical experiments with CNT resonators.

2.1. Morphology and Characteristics of Carbon Nanotubes

Graphite sheets that have been folded into tubes make up carbon nanotubes (Figure 2.1). In contrast to diamond, which develops as a 3D crystal structure with each carbon atom having four nearest neighbors arranged in a tetrahedron, graphite forms as a 2D sheet of carbon atoms stacked in a hexagonal pattern. Each carbon atom in this instance has three close neighbors. Nanotube properties depend on atomic orientation (a result of the rolling direction), the tube diameter, and length. The two types of CNTs are single-walled

carbon nanotubes (SWCNTs) and multi-walled carbon nanotubes (MWCNTs), with the latter being an aggregate of concentric SWCNTs, each of which can express a different chirality and are connected to one another by van der Waals bonds. Single-walled CNTs are preferred for basic studies because intra-tube interactions increase the complexity of the study.

At the atomic level, the nanotube's structure is primarily specified by its chirality, which is determined by the chiral vector, $\{C_h\}$, and chiral angle, θ. The following equation may be used to describe the chiral vector [13]:

$$\{C_h\} = r\{a_1\} + s\{a_2\} \tag{2.1}$$

Where (r, s) are the multipliers of the zig-zag carbon bonds of hexagonal lattice, and ($\{a_1\}$, $\{a_2\}$) are the vectors of the same lattice.

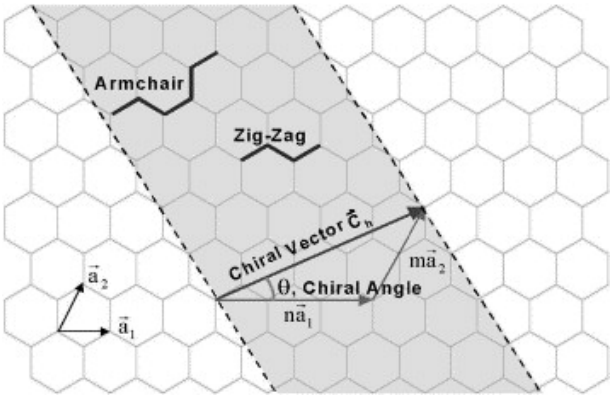

Fig. 2.1. Carbon nanotube cylindrical projection in the plane; hexagonal graphene sheet - representation of a chiral vector; reprinted from [12] with permission from Elsevier

The vector's slope in relation to a starting place, the zigzag, is represented by the chiral angle. Thus, the basic lattice orientation may be divided into three main categories: the default zig-zag (0°), the armchair (30°) (Figure 2.2), and the intermediate (chiral), which has a different angle from the other two. The chiral vector may be defined for a zig-zag nanotube as (r,0) and for an armchair nanotube as (s,s), as shown in Figures 2.1 and 2.2, respectively. These limiting examples, known as zig-zag and armchair, are based on the geometry of the carbon bonds. The next equation uses this vector to define the tube's diameter as well:

$$d = \frac{\widetilde{a}}{\pi}\sqrt{r^2 + rs + s^2} \tag{2.2}$$

where $\widetilde{a}$ corresponds to the inter-atomic spacing of the carbon atoms. For graphene sheets $\widetilde{a} = 0.246$ nm. The same value will be used for CNT's.

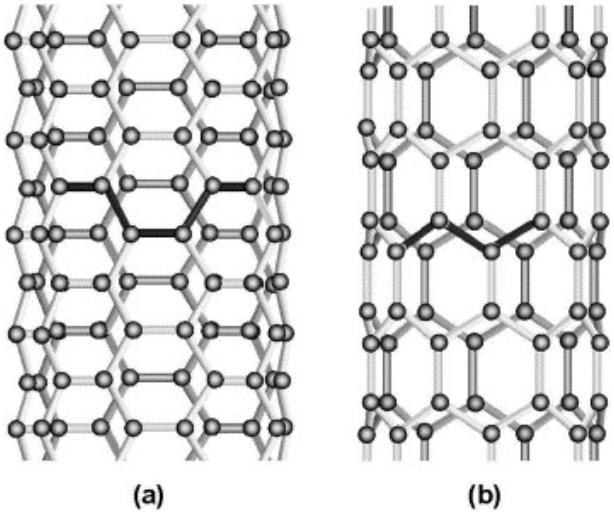

Fig. 2.2. Schematic representation of an armchair (a) and a zig-zag (b) carbon nanotube atomic structure; reprinted from [12] with permission from Elsevier

2.2. Production

This section presents an overview of the various methods employed for CNT synthesis with a focus on the specific techniques used in the context of CNT-based mass sensors.

The first ever synthesized CNT consisted of a MWCNT and this was obtained using an electric-arc discharge technique [1]. Later, using a similar process (arc-discharge process) the first SWCNT was synthesized [14]. Ever since the discovery of CNT, and with the development of research, different processes to synthesize CNT have emerged. Different methods were developed, existing now a variety of alternatives besides Arc-discharge [15], as Laser ablation [16], Gas-phase catalytic growth from carbon monoxide [17] and CVD [18–20].

The arc-discharge method (Figure 2.3) uses high-purity graphene rods as anode and cathode. The CNT emerges in a helium atmosphere while voltage is applied to form a stable arc. The anode is consumed and material is deposited on the cathode. SWCNT can be obtained by adding to the electrode a small number of metallic catalyst particles [15].

Laser ablation (Figure 2.4) was first used to produce fullerenes and later improved to produce SWCNT. A laser vaporizes a graphite object at temperatures near 1200ºC in a controlled atmosphere. To produce SWCNT graphite must be supplemented with cobalt and nickel. CNTs are collected on a water-cooled target [16].

When producing on a large scale, the need for extra complex purification methods must be taken into account for the selection of the production method. Arc-discharge and laser ablation cannot be continuous processes since it is necessary to periodically break the production to replace the carbon source material and requires extensive purification processes. Gas-phase techniques use gases as the source of carbon, allowing for continuous production. With these processes, it is also possible to collect the product while producing which also results in a more pure CNT compared to the already stated methods [12].

Using carbon monoxide as the carbon source, Nikolaev et al. [17] reported the gas-phase manufacturing of single-walled carbon nanotubes. They stated that the highest

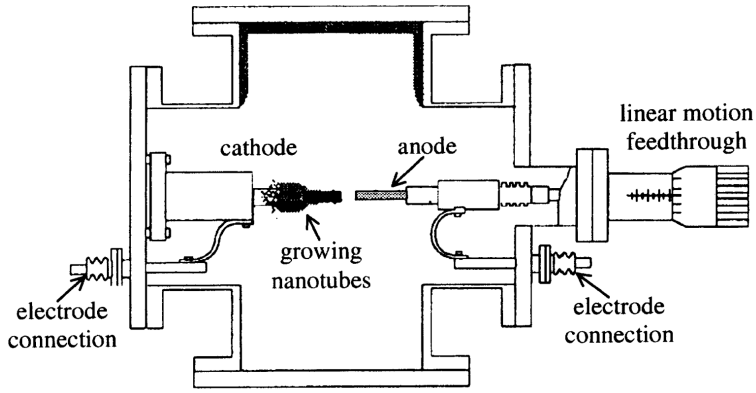

Fig. 2.3. An illustration of the arc-discharge process; reprinted from [12] with permission from Elsevier

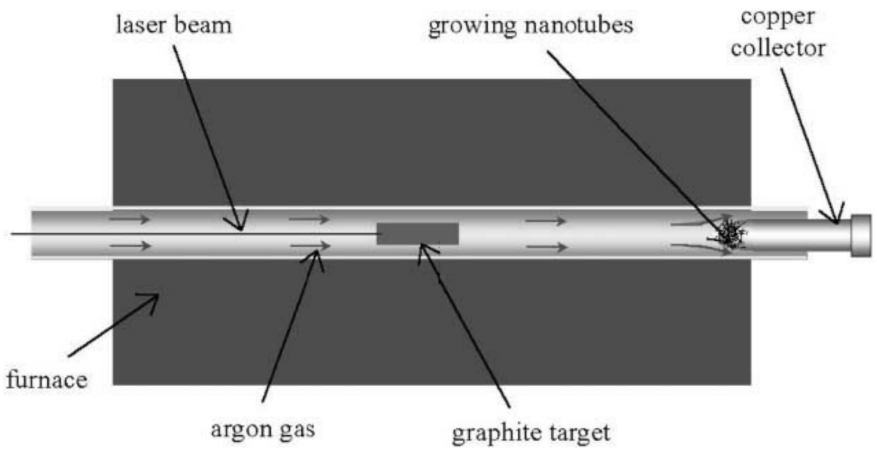

Fig. 2.4. Process flow diagram for laser ablation; reprinted from [12] with permission from Elsevier

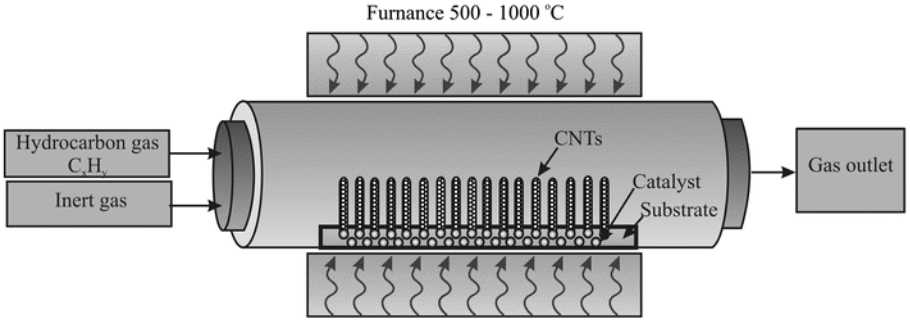

Fig. 2.5. Simplified scheme of a CVD reactor for CNTs synthesis [21]

yielding strength of a SWCNT was obtained at the highest accessible pressure and temperature (10 atm and 1200 ºC). This method has been improved to yield significant amounts of remarkably pure single-walled carbon nanotubes. The designated HiPco nanotubes (high-pressure conversion of carbon monoxide) have drawn a lot of attention since Carbon Nanotechnologies Inc. (Houston, TX) commercialized the method for the mass manufacturing of highly pure single-walled carbon nanotubes [12].

Hydrocarbon gases are used as the carbon source in other gas-phase processes, chemical vapor deposition - CVD [18–20] to produce both single and multi-walled carbon nanotubes (Figure 2.5). Hydrocarbon-grown nanotubes may have significant amorphous carbon deposits on their surface and need further purifying procedures since hydrocarbons pyrolyze easily on surfaces heated beyond 600 and 700ºC [17]. Although the quality of the nanotubes as-processed is impacted by the dissociation of hydrocarbons at low temperatures, the lower processing temperature (compared to HiPco) makes it possible for carbon nanotubes to grow on a wide range of substrates, including glass [22]. A substrate coated with a nickel catalyst may be used in CVD procedures, with ammonia serving as the catalytic gas and acetylene serving as the carbon source [18, 19].

Furthermore, a DC power may be applied, generating plasma that will enhance the reaction (up to 40 times faster) [20]. The use of plasma will help with the synthesis of well-aligned, straight carbon nanotubes on a variety of substrates, giving name to the plasma-enhanced chemical vapor deposition technique (PECVD). PECVD can produce precisely aligned arrays of carbon nanotubes with excellent control over their characteristics, but at a higher cost, whereas CVD can do it at a lower cost with less consistent control over the product's properties [12].

2.3. Applications

The excellent mechanical, electrical, and thermal properties make carbon nanotubes suitable for several engineering and science applications. In electronics, CNTs' excellent electrical conductivity promotes research for their use in transistors, interconnects, and electronic devices [23–25]. Composite materials (polymers, ceramics, and metals) are being reinforced with CNTs to improve both their rigidity and strength [26, 27]. The application of CNT into composites is also being studied to increase the conductivity of the materials [28] and CNTs are being included in heat exchangers [29]. CNTs are even

being explored in the drug delivery and imaging fields, due to their ability to carry certain molecules until a defined targeted cell [30–32]. There are various fields of application of CNTs and each one takes advantage of different characteristical properties of them.

In this work, we will focus on the application of the carbon nanotube as sensors. These structures when used on a resonator application can be used to transduce force and measure minute masses with a high accuracy. Since the objective of this thesis is to study the dynamics of a carbon nanotube resonator being used as a mass sensor further research on this topic will be done in the next section.

2.4. Carbon Nanotubes Resonators

Nanoelectromechanical systems (NEMS) have been made possible by recent technical developments [33–35]. NEMS are nanoscale devices with integrated mechanical (often a vibrating beam or plate) and electrical (resistors, capacitors, inductors, etc.) components that may operate in many conditions and serve a variety of functions. Nanomechanical resonators, often known as nanoresonators in general, are a specific type of NEMS device that has drawn significant attention from researchers worldwide because of their distinctive characteristics and wide-ranging applications. Nano resonators may detect the presence of very small particles (on the order of 10^{-21} g, for example), as the addition of the particle mass results in a shift in the resonance frequency of such devices.

Additionally, nanoresonators have high-quality factors [36, 37] and operate at extremely high frequencies (from MHz to GHz) [38], enabling high-resolution frequency output. Due to their unique set of characteristics, microresonators are the ideal choice for resonant sensors [39] that enable the ultra-sensitive detection of mass [40–42], force [43, 44], location [44], temperature fluctuations [45–48], biological entities [49, 50], linked resonance [51], and biochemical processes [52, 53].

Nano resonators enable label-free [54, 55] sensing and detection of biological molecules [56, 57] and cells [58], as well as biomolecular interactions [59]. As a result, they may be employed as lab-on-chip biosensors [60]. A micro resonator's dynamical behavior directly affects how well it performs [61]. Therefore, improving the detection sensitivity and creating a new generation of nano-scale resonators require a thorough understanding of the dynamics of nanomechanical resonators. Reducing a resonator's mass is one of the most efficient methods to raise its sensitivity. Due to their low mass, high rigidity, small cross-section, and distinctive electrical characteristics, carbon nanotubes are being suggested as potential candidates for use in nanoresonators [62–65].

Resonators made of carbon nanotubes (CNTs) are nanoscale devices that consist of a CNT (which can be either doubly clamped or cantilevered) placed at a set distance from a rigid electrode (referred to as the gate). An electrostatic interaction between the CNT and the gate below typically drives a CNT resonator. A voltage that is biased toward the gate is provided to the CNT. This causes the CNT to accumulate more charges, leading to an electrostatic attraction between the CNT and the gate.

The applied voltage may have both DC and AC components, which causes the CNT resonator to respond in a static and dynamic manner, respectively. To be more precise, the CNT is first given a DC voltage that causes it to deflect to a new, equilibrium state [66]. The CNT is then subjected to an AC voltage, which causes it to oscillate around the

deflected position. It should be emphasized that the flexibility and inexpensive cost of electrostatic actuation make it more popular than other methods of actuation [67].

The process of analysis of the dynamic behavior of a Carbon Nanotube Resonator includes some big challenges [67]:

- **Electrostatic Load** - As already stated, CNT resonators are often actuated through an electrostatic interaction between the CNT and the gate. This interaction results in a distributed pressure on the CNT, whose magnitude and distribution depend on the CNT's proximity to the gate (depending on the CNT's displacement). This strong non-linearity introduces a big complexity to the problem. The distribution of the pressure also depends on the CNT boundary conditions, i.e. if it is doubly clamped or cantilevered; hence, it is important to develop accurate models for electrostatic load distribution.

- **Carbon Nanotube Modeling** - It can be challenging to create a realistic model of the carbon nanotube. The complexity of the model will be defined by the phenomena that will be analyzed. The cost of computing will rise along with model complexity. Later, the different approaches to CNT modeling will be presented and discussed.

- **Sources of non-linearity** - CNT resonators may experience vibrations of high amplitude. In this case, it is necessary to have a model that accounts for the geometrical non-linearity caused by stretching and rotation, electrostatic load non-linearity, damping non-linearity, and also non-linearity induced by interlayer molecular forces - van der Waals forces [68].

- **Manufacturing Defects** - It is likely that the produced device contains a variety of flaws due to manufacturing uncertainty at the nanoscale. A realistic model can consider the impact of these flaws.

2.5. CNT Modeling

The need for correct, accurate, and more simple models that describe the mechanical and electrical properties of carbon nanotubes is the main driver of research in this area. These models will allow for a reliable prediction of results that are comparable to the results of experiments and will allow for the proper investment in CNT-containing devices.

At the nanoscale, experimental studies are not only difficult to carry out but also expensive, necessitating the use of high-resolution transmission electron microscopes. Additionally, the natural frequencies of various vibration modes within the frequency spectrum are difficult to separate and identify (partially because they are of close values). This way, studies based on computational models continue to be the most reasonable way to analyze nanostructures.

As a result, three different ways to model nanostructures are identified [69]: atomistic modeling, hybrid atomistic-continuum modeling, and continuum modeling.

The first, atomistic modeling, uses techniques like density functional theory (DFT) [70, 71] and molecular dynamics [4, 72]. By combining the mechanical strain energy of the limited volume element of the continuum model with the molecular potential energy of

a nanostructured device, hybrid atomistic-continuum modeling, a blend method between the first and third ones, allows for the introduction of interatomic potentials into the continuum analysis [73]. Finally, the classical (local) beam, plate, and shell theories, which are included in continuum modeling, allow for an analysis of nanostructures that is similar to that of large-scale systems. The major benefits of continuum modeling are related to its generally simpler formulation and the fact that it is lighter and easier to implement from a computational point of view [11], providing an accurate tool to study different circumstances [74]. As a consequence, a continuous model supports the modeling and investigation of particular phenomena in nanotubes, such as buckling, wave propagation, free vibration, nonlinear vibration, and energy exchange [8, 73]. In the following subsections, a general overview of both, molecular dynamics and continuum models applied to CNTs will be done. Following that, several works on this theme will be reviewed and presented.

2.5.1 Molecular Dynamics

The majority of atomistic analyses of CNT vibrations use molecular dynamics. Even though none are carried out as a thesis aim, this section provides a quick introduction to the idea and practice of molecular dynamics simulations - MD - which is utilized in this dissertation as a bibliographical reference to verify the findings of continuum models.

As a result of the early applications in liquid dynamics, molecular dynamics became one of the earliest simulation techniques. Since the 1970s, when the structure and dynamics of macromolecules were first studied, various other fields of interest, including chemistry and biology, have used this method as computer efficiency and algorithmic research advanced [75].

Molecular dynamics simulations can follow two different approaches. The first, known as a classical molecular dynamic simulation, views molecules as classical objects since their atoms are equivalent to masses and their bonds to stiffness, and both are governed by general classical mechanics principles. The second kind, known as quantum molecular dynamic simulations, explicitly accounts for the fact that chemical bonds are quantum in nature by applying the electron density function to the valence electrons that govern bonding and classical dynamics to the ions [2, 75].

A classical MD simulation essentially employs a particle approach to solve Newton's second law-based particle dynamics governing equations [79]. The simulation begins by specifying each particle's boundary conditions to calculate the system's potential function, $U(r_1,...,r_n)$, which depends on each atom's location. This potential describes the potential energy of n interacting atoms according to their positions in space $r_i = (x_i, y_i, z_i)$. Each ith atom experiences the following acting force:

$$\{F_i\} = -\nabla_{\boldsymbol{r}_i} U(\boldsymbol{r}_1, \ldots, \boldsymbol{r}_n) = -\left(\frac{\partial U}{\partial x}, \frac{\partial U}{\partial y}, \frac{\partial U}{\partial z}\right) \tag{2.3}$$

An essential input is each atom's beginning location (r_i) as well as their starting velocities (v_i). The potential energy from bound or non-bonded interactions may be split. Stretching, bending, dihedral angle torsion, and out-of-plane torsion are all examples of interactions that occur between bounded atoms. Non-bonded atoms primarily express

potential energy through van der Waals forces. The stated interactions are illustrated in Figure 2.6.

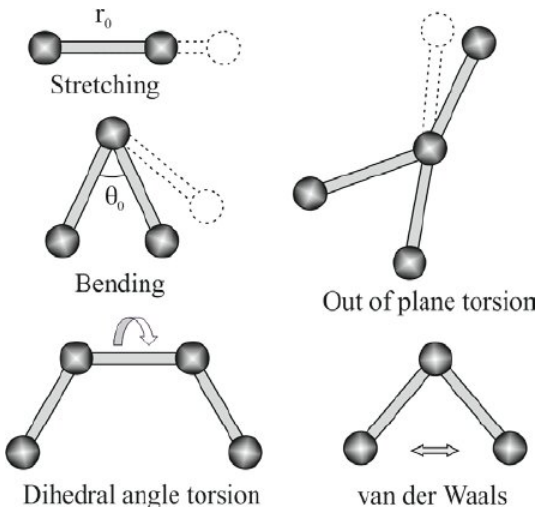

Fig. 2.6. Inter-atomic interactions in molecular mechanics; reprinted from [13] with permission from Elsevier

It's important to realize that the idea of an atom is inaccurate in the context of quantum physics. As distinct nuclei may exchange electrons, decentralized electronic clouds emerge and have an impact on chemical bonding. Transitional characteristics of the electronic cloud are neglected and an average field is considered. This way, and considering Newton's second law, the MD problem consists of solving the following system of equations:

$$\{F_i\} = m_i \frac{\partial^2 \{r_i(t)\}}{\partial t^2} \tag{2.4}$$

The Verlet algorithm is frequently used to determine the solution involving atomic discretization and iterative numerical integration. The equation below provides the fundamental Verlet algorithm [2]:

$$\{r_i(t+\Delta t)\} \approx 2\{r_i(t)\} - \{r_i(t-\Delta t)\} + \frac{\{F_i(t)\}}{m_i}\Delta t^2 \tag{2.5}$$

It is crucial to realize that the molecular dynamics simulation approach is quite expensive to compute because of the complexity and range of the discretization required.

Studies based on molecular models

The behavior of a nano resonator has been investigated in several studies using molecular dynamics simulations [76]. For instance, Kim and Park [77] demonstrated how the application of a tensile strain significantly improves the nanoresonator quality factor (Q-factor) by examining the energy dissipation of a doubly clamped copper nanoresonator that is subject to flexural oscillations.

With the aid of molecular dynamics simulations, Vallabhaneni et al. [78] investigated the quality factors of resonance connected to the axial and transverse vibrations of single-walled CNT resonators. They looked into the impact of device dimensions and chirality,

as well as temperature, on the resonance frequency and quality factor, and discovered discrepancies between the outcomes of MD simulations and traditional theories of energy dissipation.

The fundamental frequency shift of a cantilevered carbon nanotube resonator holding a finite nanoparticle was reported by Yoon and Hwang [79]. After examining the resonance frequencies of a carbon nanotube resonator, Kang and Kwon [80] discovered that the resonance frequency of the CNT may be controlled by adjusting its length using an axial position controller. Lee and Kang [81] studied the vibrational behavior of cantilevered carbon nanotube resonators containing an attached nanocluster, they noticed that the mass, position, and linear density of the attached nanocluster had a significant impact on the effective density factor, which could affect the shift of resonance frequency.

Nourmohammadi et al. [82] used classical molecular dynamics to simulate the fundamental longitudinal mode oscillations of silicon and nickel nanowires and nanofilms at room temperature in the canonical ensemble. They looked at various techniques for estimating linear and nonlinear damping in nanomechanical resonators. In their research of the longitudinal-mode oscillations of an amorphous silicon nano resonator as a function of frequency and temperature, Mukherjee et al. [83] utilized isothermal molecular dynamics simulations and found that damping is a weak function of frequency at ambient temperature.

2.5.2 Continuum Model

The behavior of nanoresonators based on continuum models has been the subject of several investigations in the literature. In this part, we will first go through the papers most pertinent to this thesis, specifically those dealing with electrically activated carbon nanotube resonators. The research on nanoresonators — which need not be electrically activated or made of CNTs — and their applications in mass detection will next be reviewed. Nano resonators may often be modeled using a continuous beam theory since they are typically quite long and considered one dimension.

The Euler-Bernoulli and Timoshenko theories can capture the dynamic response of such systems due to their significant length-to-diameter or length-to-thickness ratios [67]. The first neglects rotational inertia and shear effects and the second is used for thick, short-length, higher modes with rotary inertia. These theories have obvious limits since a CNT is closer to a nanoshell than to a beam, yet they are frequently used to explain shells because they are simpler than shell theories, despite the latter producing superior results.

In this dissertation, a continuum model based on Kirchhoff-Love assumptions will be built, leading primarily to the conclusion that, because the shell's thickness is so small compared to other dimensions, transverse shear stresses and transverse normal stresses may be disregarded. The findings of the linear field investigation are remarkably consistent across several shell theories, such as Donnell's, Flügge's, or Sanders-Koiter's [11]. Sanders-Koiter's theory is chosen to lay the foundation and present opportunities for nonlinear field growth in the future.

Studies based on continuum models

Numerous researchers have used continuum models to examine the linear and nonlinear behaviors of electrically driven CNT resonators [84–86]. Ouakad and Younis [87] utilized an Euler-Bernoulli beam model of the CNT to analyze the nonlinear dynamics of carbon nanotube resonators that are doubly clamped and cantilevered and are electrically actuated under both DC and AC actuation. They employed the single-mode Galerkin approximation and the shooting method to numerically solve the reduced-order model.

Rasekh et al. [88] carried out more research and looked at the nonlinear behavior of electrostatically activated clamped-clamped CNT resonators. They discovered that the van der Waals forces don't have a significant role in gaps of 2 nm and more. In another study, Li and Chou [89] examined the possibility of a nanomechanical resonator that used carbon nanotubes, both cantilevered and bridging, to detect mass. They found that there was a direct correlation between the resonance frequency and the attached mass, with a logarithmic relationship.

In a study on the axial buckling of SWCNTs, Silvestre et al. [90] conducted a comparison between the Sanders-Koiter thin shell theory and the Donnell shallow shell theory. The results indicated that the Sanders-Koiter theory was more effective and accurate in reproducing the buckling stresses and mode forms of axially compressed nanotubes. Amabili [91] has authored a book that provides thorough foundations for the majority of relevant ideas and methods for nonlinearity in shells and plates. Starting with initial work on linear vibrations from a local shell theory (Sanders-Koiter), Strozzi et al. [8] have done several investigations on nonlinearity. While researching and confirming the inadequacy of reduced Donnell's theory in explaining CNTs' vibrational properties, they also constructed a reduced model [9]. Based on the earlier study, the same authors conducted a study on circumferential flexural vibrational modes, taking into account the impact of various CNT properties like aspect ratio and chirality, along with various boundary conditions, and concentrating on the stability of vibration modes [8].

2.6. Experimental Investigation

As already stated, the interest in studying the behavior of CNTs has been huge ever since their discovery. Besides the theoretical models, different research groups worldwide have studied CNT resonators' behavior experimentally.

These studies started with the work of Sazonova et al. [92] who first reported the electrical actuation of CNTs in a clamped-clamped arrangement. They were capable of reproducing the different modes predicted by theoretical models. This work demonstrated the capability of CNTs to work as force transducers. They also documented the possibility of tuning the resonance frequency. The deformed shape of the CNT under load is presented in Figure 2.7 obtained using a scanning electron microscope (SEM).

Peng et al. [93] used a similar setup and demonstrated that it can be used as an exceptionally sensitive mass detector with a resolution of 10^{-18} [g]. Garcia-Sanchez et al. [94] developed a method to measure the displacement of CNTs achieving a resolution of sub-nanometer. This method was then used to detect bending-mode vibrations; this team was capable of capturing high-frequency modes of a CNT.

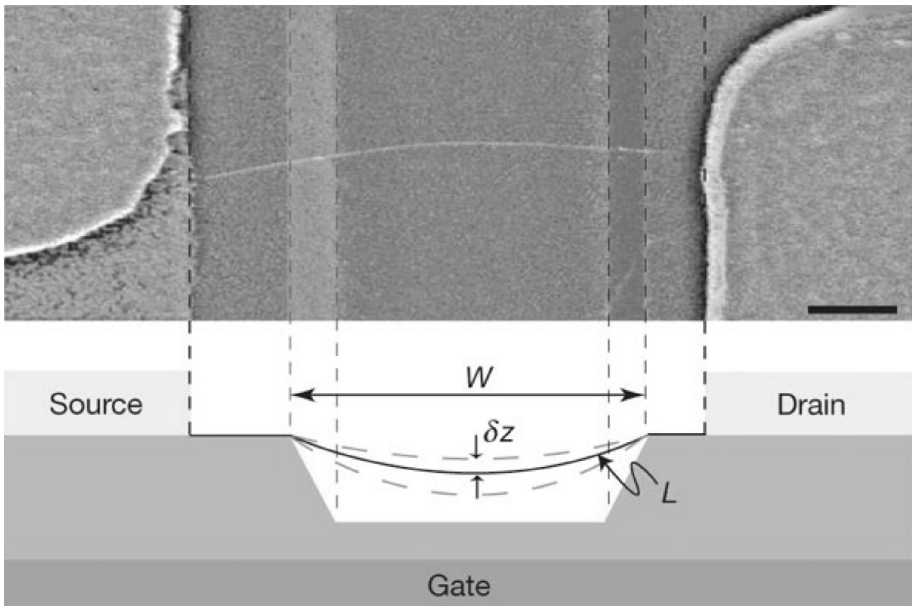

Fig. 2.7. Image of a clamped CNT under bending obtained with SEM and the scheme of the device geometry [66]

Advances in using CNT oscillators as mass sensors happened with the work of Chiu et al. [95]: based on the resonance frequency shift effect was capable of sensing nano scale masses attached to the CNT. Improvements to the used technique are reported and may conceivably permit a resolution on the order of the proton mass 1 [yg] (1 yoctogram $= 10^{-24}$ gram).

Lassagne et al. [96] in their experiments with doubly clamped single-walled CNTs, studied the intensity of electro-mechanical coupling in a capacitive actuation, being strong enough to lead the system into a nonlinear regime. Cho et al. [97] studied the nonlinear behavior of a doubly clamped CNT resonator by recording its steady-state response to different excitation frequencies. The effect of a concentrated mass on this value was also analyzed, representing one more step closer to the use of a CNT oscillator as a mass sensor.

Eichler et al. [98] developed an important study, analyzing the damping of systems based on carbon structures, mainly CNTs. It was shown that the damping of such systems highly depends on the displacement and so must be considered non-linear. Castellanos-Gomez et al. [99] studied the tunability of a doubly clamped CNT resonator and were capable of experimentally permuting between mode-softening and mode-hardening non-linear behaviors, adjusting the gate static voltage. Further on this adjustability of CNT resonators, Ning et al. [100] introduced a new design of resonators that not only enabled tuning by gate voltage but also permitted adjustability, pulling in an axial direction the CNT applying a preload on this.

This review demonstrated that with the current knowledge and technological resources it is possible to produce CNT-based resonators and use them as high-sensitivity sensors (for detecting small masses or transducing force).

Chapter 3

Model Development - CNT Ressonator

3.1. Introduction and Outline

In this chapter the formulation of a continuum model for a single-walled carbon nanotube (as seen in Figure 3.1) will be presented. The electrostatic interaction resulting from a voltage difference between the CNT and an electrode plate will also be modeled. Applying Newmark's method, it will be possible to compute the CNT's nonlinear response induced by electrostatic forces.

The CNT-based resonator is made up of a single-walled CNT with the following dimensions: length L, diameter D, and thickness h. The CNT is positioned at a distance b from the gate below.

As was already stated, the carbon nanotubes are simply folded sheets of graphene, for that reason some works consider their thickness equal to the diameter of the carbon atoms in that sheet. Therefore, using a thin shell theory to describe a CNT is correct. The definition of a thin shell is a three-dimensional body having two closely spaced curved surfaces, where the distance between the surfaces is minimal in relation to the length and diameter of the body. The middle surface of the shell is the collection of points that lie in the center of the two surfaces. The thickness of the shell at a certain place is defined as the distance between surfaces measured in the radial direction, normal to the central surface. When modeling a CNT a common value to use as the thickness of the shell is the diameter of a carbon atom. This value is normally considered constant throughout the body resulting in governing equations being simpler to solve.

A flat plate can be seen as a specific case of a shell, and vice versa, a shell may be seen as a generalization of a plate. Shallow shells are designated as such due to their large radius or small curvature, according to many theories that extrapolate shell models from plates. Several publications assume linear elasticity with isotropic and homogeneous materials for both plates [101] and shells [102] and concluded that the difference between an-isotropic and isotropic models is not significant.

Note that the nanotube model will be treated as an isotropic, homogeneous material in the shell theories covered in this dissertation, and the tube is viewed as a thin shell. In order to satisfy the requirement for property descriptions, many comparable mechanical and geometrical characteristics have been put forth, enabling the translation between atomistic modeling and continuum modeling properties. Research on the nonlinear responses of

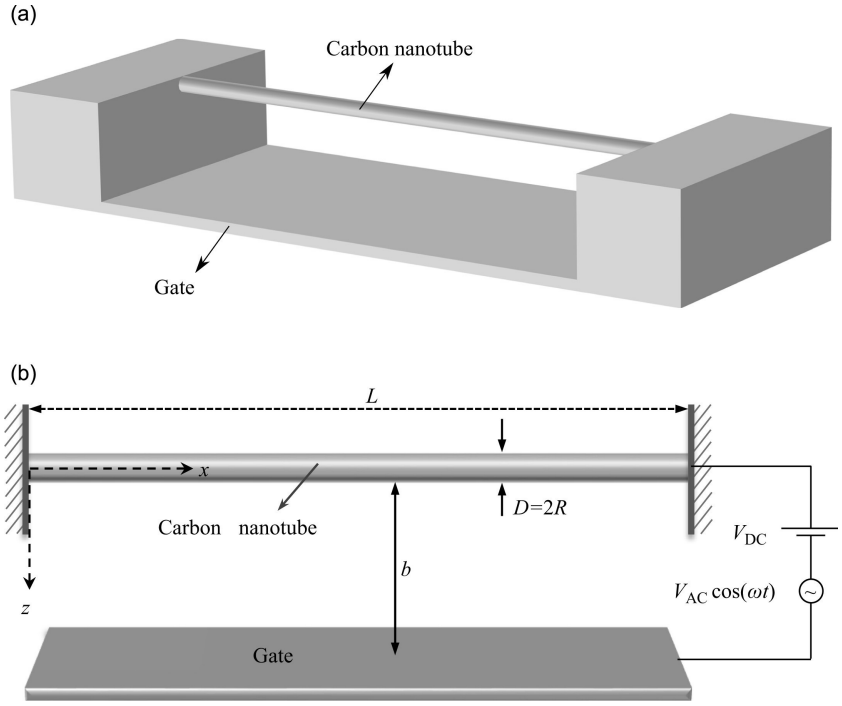

Fig. 3.1. Proposed problem Scheme - (a) 3D schematic of a CNT-based resonator (b) simplified schematic of a CNT-based resonator showing the system geometrical parameters; reprinted from [72] with permission from Elsevier

CNTs with high amplitudes was done by [103] Yakobson et al. The Poisson's ratio, Young's modulus, and wall thickness that were reported in this paper are going to be used in this dissertation. Shear deformation and rotating inertia effects are also disregarded [104].

A particular thin shell theory is examined and chosen for the current dissertation, among different thin shell theories. Sanders-Koiter's theory will be used in this dissertation, especially regarding its documented behavior in the nonlinear dynamic domain, as for linear motions the difference between theories such as Flügge's, Donnell's, or Sanders-Koiter, for example, is not significant [11, 105]. Sanders-Koiter's theory is chosen with the intention of laying the foundation and presenting opportunities for nonlinear field growth in the future.

3.2. Kirchhoff-Love Assumptions

Kirchhoff's hypothesis, which states that normals to the undeformed middle surface stay straight and normal to the deformed middle surface and experience no extension, is defined for plate bending. This idea is similar to the thin beam theory developed by Euler and Bernoulli, which is only true for narrow beams with very thin thicknesses relative to their length. These assumptions are transposed to the strain field neglecting the shear components γ_{xz} and γ_{yz} and the normal to the membrane strain component ε_{zz}.

$$\begin{cases} \gamma_{xz} = 0 \\ \gamma_{yz} = 0 \\ \varepsilon_{zz} = 0 \end{cases} \tag{3.1}$$

Applying Hooke's Law it is possible to conclude that transverse shear stresses come as:

$$\sigma_{xz} = \sigma_{yz} = 0 \tag{3.2}$$

The stated assumptions in Equation (3.1) were then adapted by Love [106] to thin shells and defined as the Kirchhoff-Love hypothesis. This hypothesis can be written in cylindrical coordinates:

$$\begin{cases} \gamma_{xz} = 0 \\ \gamma_{\theta z} = 0 \\ \varepsilon_{zz} = 0 \end{cases} \tag{3.3}$$

Following the Hooke's Law, the transverse shear stresses come as:

$$\sigma_{xz} = \sigma_{\theta z} = 0 \tag{3.4}$$

3.3. Sanders-Koiter Thin Shell Theory

Following Sanders's procedure [91, 107] in order to apply the theory to a cylindrical shell, and considering the cylindrical coordinates (x, θ, z), comes the displacement field as:

$$\begin{aligned} u(x,\theta,z,t) &= u^0(x,\theta,t) - z\frac{\partial w^0(x,\theta,t)}{\partial x} \\ v(x,\theta,z,t) &= v^0(x,\theta,t) - \frac{z}{R}\frac{\partial w^0(x,\theta,t)}{\partial \theta} \\ w(x,\theta,z,t) &= w^0(x,\theta,t) \end{aligned} \tag{3.5}$$

where $u^0(x,\theta,t)$, $v^0(x,\theta,t)$ and $w^0(x,\theta,t)$) refer to the displacement components in the middle surface of the cylinder, Ω, presented in the Figure 3.2

$$\begin{aligned} \varepsilon_{x,0} &= \frac{\partial u^0}{\partial x} \\ \varepsilon_{\theta,0} &= \frac{1}{R}\frac{\partial v^0}{\partial \theta} + \frac{w^0}{R} \\ \gamma_{x\theta,0} &= \frac{1}{R}\frac{\partial u^0}{\partial \theta} + \frac{\partial v^0}{\partial x} \\ k_x &= -\frac{\partial^2 w^0}{\partial x^2} \\ k_\theta &= \frac{1}{R^2}\frac{\partial v^0}{\partial \theta} - \frac{1}{R^2}\frac{\partial^2 w^0}{\partial \theta^2} \\ k_{x\theta} &= -2\frac{1}{R}\frac{\partial^2 w^0}{\partial x \partial \theta} + \frac{1}{2R}(3\frac{\partial v^0}{\partial x} - \frac{1}{R}\frac{\partial u^0}{\partial \theta}) \end{aligned} \tag{3.6}$$

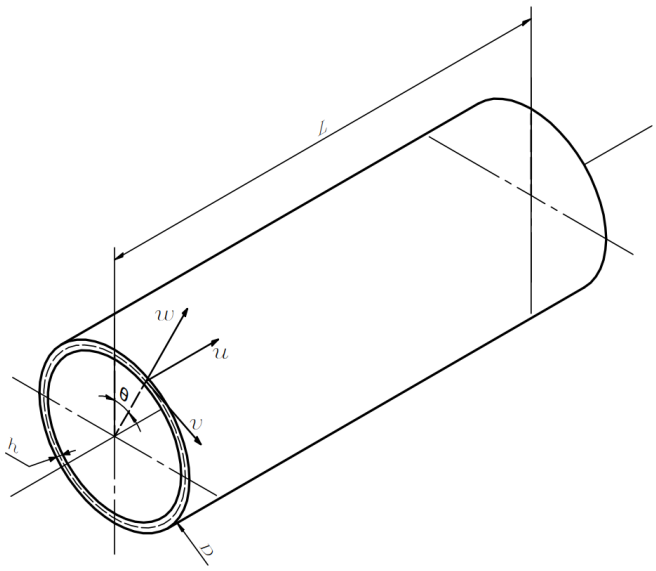

Fig. 3.2. Geometry of a cylindrical shell - cylindrical coordinates

being the strains ε_{xx}, $\varepsilon_{\theta\theta}$, $\gamma_{x\theta}$ of the point at z distance from the middle surface given by:

$$\begin{aligned} \varepsilon_{xx} &= \varepsilon_{x,0} + zk_x \\ \varepsilon_{\theta\theta} &= \varepsilon_{\theta,0} + zk_\theta \\ \gamma_{x\theta} &= \gamma_{x\theta,0} + zk_{x\theta} \end{aligned} \tag{3.7}$$

3.3.1 Hamilton's Principle

Invoking Hamilton's Principle [108], the total variation of the mechanical energy over a period of time is null:

$$\int_{t_1}^{t_2} (\delta K - \delta U + \delta W)\, \mathrm{d}t = 0 \tag{3.8}$$

where δK is the variation of kinetic energy, δU is the variation of potential energy, and δW is the variation of virtual work of forces that either do not have a potential function (non-conservative forces) or whose potential function is not included in U. For the sake of simplicity, these forces are labeled $non-conservative$.

The variation of potential energy δU is given by:

$$\begin{aligned} \delta U &= \int_\Omega \int_{-\frac{h}{2}}^{\frac{h}{2}} (\sigma_{xx}\delta\varepsilon_{xx} + \sigma_{\theta\theta}\delta\varepsilon_{\theta\theta} + \tau_{x\theta}\delta\gamma_{x\theta})\, \mathrm{d}z\, \mathrm{d}\Omega \\ &= \int_\Omega \int_{-\frac{h}{2}}^{\frac{h}{2}} \left[\sigma_{xx}(\delta\varepsilon_{x,0} + z\delta k_x) + \sigma_{\theta\theta}(\delta\varepsilon_{\theta\theta} + z\delta k_\theta) + \tau_{x\theta}\left(\delta\gamma_{x\theta,0} + z\delta k_{x\theta}\right)\right] \mathrm{d}z\, \mathrm{d}\Omega \end{aligned} \tag{3.9}$$

Since the internal membrane forces and moments dependencies on the general stress field can be expressed as

$$\{N_{xx}, N_{\theta\theta}, N_{x\theta}, M_{xx}, M_{\theta\theta}, M_{x\theta}\} = \int_{-\frac{h}{2}}^{\frac{h}{2}} \left(1 - \frac{z}{R}\right) \{\sigma_{xx}, \sigma_{\theta\theta}, \tau_{x\theta}, z\sigma_{xx}, z\sigma_{\theta\theta}, z\tau_{x\theta}\} \, \mathrm{d}z \tag{3.10}$$

The variation of potential energy δU can be expressed as:

$$\begin{aligned} \delta U = \underbrace{\int_0^{2\pi} \int_0^{l}}_{\int_\Omega} & (N_{xx}\delta\varepsilon_{x,0} + N_{\theta\theta}\delta\varepsilon_{\theta\theta} + N_{x\theta}\delta\gamma_{x\theta,0} + M_{xx}\delta k_x + M_{\theta\theta}\delta k_\theta \\ & + M_{x\theta}\delta k_{x\theta}) \underbrace{R \, \mathrm{d}x \, \mathrm{d}\theta}_{d\Omega} \end{aligned} \tag{3.11}$$

The variation of kinetic energy δK is given by:

$$\begin{aligned} \delta K &= \int_0^{2\pi} \int_0^{l} \int_{-\frac{h}{2}}^{\frac{h}{2}} \rho(\dot{u}\delta\dot{u} + \dot{v}\delta\dot{v} + \dot{w}\delta\dot{w}) dz R \, \mathrm{d}x \, \mathrm{d}\theta \\ &= \int_0^{2\pi} \int_0^{l} \int_{-\frac{h}{2}}^{\frac{h}{2}} \rho \left[\left(\dot{u}^0 - z\frac{\partial \dot{w}^0}{\partial x} \right) \left(\delta\dot{u}^0 - z\frac{\partial \delta\dot{w}^0}{\partial x} \right) \right. \\ &\quad \left. + \left(\dot{v}^0 - \frac{z}{R}\frac{\partial \dot{w}^0}{\partial \theta} \right) \left(\delta\dot{v}^0 - \frac{z}{R}\frac{\partial \delta\dot{w}^0}{\partial \theta} \right) + \dot{w}^0\delta\dot{w}^0 \right] R \, \mathrm{d}x \, \mathrm{d}\theta \\ &= \int_0^{2\pi} \int_0^{l} \rho \left[h\dot{u}^0\delta\dot{u}^0 + \frac{h^3}{12}\frac{\partial \dot{w}^0}{\partial x}\frac{\partial}{\partial x}\left(\delta\dot{w}^0\right) + h\dot{v}^0\delta\dot{v}^0 \right. \\ &\quad \left. + \frac{h^3}{12}\frac{1}{R^2}\frac{\partial \dot{w}^0}{\partial \theta}\frac{\partial}{\partial \theta}\left(\delta\dot{w}^0\right) + h\dot{w}^0\delta\dot{w}^0 \right] R \, \mathrm{d}x \, \mathrm{d}\theta \\ &= \int_0^{2\pi} \int_0^{l} \left[\rho h \left(\dot{u}^0\delta\dot{u}^0 + \dot{v}^0\delta\dot{v}^0 + \dot{w}^0\delta\dot{w}^0 \right) \right. \\ &\quad \left. + \frac{\rho h^3}{12} \left[\frac{\partial \dot{w}^0}{\partial x}\frac{\partial}{\partial x}\left(\delta\dot{w}^0\right) + \frac{1}{R^2}\frac{\partial \dot{w}^0}{\partial \theta}\frac{\partial}{\partial \theta}\left(\delta\dot{w}^0\right) \right] \right] R \, \mathrm{d}x \, \mathrm{d}\theta \end{aligned} \tag{3.12}$$

Considering that an external pressure field $\mathscr{P}_{ext} = (p_u, p_v, p_w)$ is applied on the shell, the work of the non-conservative forces, δW, can be expressed as:

$$\delta W = \int_0^{2\pi} \int_0^{l} \left(p_u\delta u^0 + p_v\delta v^0 + p_w\delta w^0 \right) R \, \mathrm{d}x \, \mathrm{d}\theta \tag{3.13}$$

Finally, applying Hamilton's principle and simplifying we obtain:

$$
\begin{aligned}
&\int_{t_1}^{t_2} (\delta K - \delta U + \delta W)\, \mathrm{d}t = 0 \\
\Rightarrow &\int_{t_1}^{t_2} \left[\int_\Omega \rho h \left[\dot{u}^0 \delta \dot{u}^0 + \dot{v}^0 \delta \dot{v}^0 + \dot{w}^0 \delta \dot{w}^0 \right] + \frac{\rho h^3}{12} \left[\frac{\partial \dot{w}^0}{\partial x} \frac{\partial}{\partial x} \left(\delta \dot{w}^0 \right) + \frac{1}{R^2} \frac{\partial \dot{w}^0}{\partial \theta} \frac{\partial}{\partial \theta} \left(\delta \dot{w}^0 \right) \right] \mathrm{d}\Omega \right. \\
&- \int_\Omega \left[N_{xx} \delta \left(\frac{\partial u^0}{\partial x} \right) + N_{\theta\theta} \delta \left(\frac{1}{R} \frac{\partial v^0}{\partial \theta} + \frac{w^0}{R} \right) + N_{x\theta} \delta \left(\frac{1}{R} \frac{\partial u^0}{\partial \theta} + \frac{\partial v^0}{\partial x} \right) + M_{xx} \delta \left(-\frac{\partial^2 w^0}{\partial x^2} \right) \right. \\
&\left. + M_{\theta\theta} \delta \left(\frac{1}{R^2} \frac{\partial v^0}{\partial \theta} - \frac{1}{R^2} \frac{\partial^2 w^0}{\partial \theta^2} \right) + M_{x\theta} \delta \left(-2 \frac{1}{R} \frac{\partial^2 w^0}{\partial x \partial \theta} + \frac{1}{2R} \left(3 \frac{\partial v^0}{\partial x} - \frac{1}{R} \frac{\partial u^0}{\partial \theta} \right) \right) \right] \mathrm{d}\Omega \\
&\left. + \int_\Omega \left[p_u \delta u^0 + p_v \delta v^0 + p_w \delta w^0 \right] \mathrm{d}\Omega \right] \mathrm{d}t = 0
\end{aligned}
\tag{3.14}
$$

Integrating by parts gives:

$$
\begin{aligned}
&\int_{t_1}^{t_2} \left[- \int_\Omega \left[\rho h \left(\ddot{u}^0 \delta u^0 + \ddot{v}^0 \delta v^0 + \ddot{w}^0 \delta w^0 \right) + \frac{\rho h^3}{12} \left(\frac{\partial^2 \ddot{w}^0}{\partial x^2} \delta w^0 + \frac{1}{R^2} \frac{\partial^2 \ddot{w}^0}{\partial \theta^2} \delta w^0 \right) \right] \mathrm{d}\Omega \right. \\
&+ \int_\Omega \left(\frac{\partial N_{xx}}{\partial x} \delta u_0 + \frac{1}{R} \frac{\partial N_{\theta\theta}}{\partial \theta} \delta v_0 - \frac{N_{\theta\theta}}{R} \delta w_0 + \frac{1}{R} \frac{\partial N_{x\theta}}{\partial \theta} \delta u_0 + \frac{\partial N_{x\theta}}{\partial x} \delta v_0 + \frac{\partial^2 M_{xx}}{\partial x^2} \delta w_0 \right. \\
&+ \frac{1}{R^2} \frac{\partial M_{\theta\theta}}{\partial \theta} \delta v_0 + \frac{1}{R^2} \frac{\partial^2 M_{\theta\theta}}{\partial \theta^2} \delta w_0 + \frac{2}{R} \frac{\partial^2 M_{x\theta}}{\partial x \partial \theta} \delta w_0 + \frac{3}{2R} \frac{\partial M_{x\theta}}{\partial x} \delta v_0 - \frac{1}{2R^2} \frac{\partial M_{x\theta}}{\partial \theta} \delta u_0 \Big) \mathrm{d}\Omega \\
&\left. \left. + \int_\Omega \left(p_u \delta u^0 + p_v \delta v^0 + p_w \delta w^0 \right) \mathrm{d}\Omega \right] \mathrm{d}t = 0 \right.
\end{aligned}
\tag{3.15}
$$

Selecting the terms affected by each degree of freedom for each equation:

$$
\begin{aligned}
-\rho h \ddot{u}^0 + \frac{\partial N_{xx}}{\partial x} + \frac{1}{R} \frac{\partial N_{x\theta}}{\partial \theta} - \frac{1}{2R^2} \frac{\partial M_{x\theta}}{\partial \theta} + p_u &= 0 \\
-\rho h \ddot{v}^0 + \frac{1}{R} \frac{\partial N_{\theta\theta}}{\partial \theta} + \frac{\partial N_{x\theta}}{\partial x} + \frac{1}{R^2} \frac{\partial M_{\theta\theta}}{\partial \theta} + \frac{3}{2R} \frac{\partial M_{x\theta}}{\partial x} + p_v &= 0 \\
-\rho h \ddot{w}^0 + \underbrace{\frac{\rho h^3}{12} \left[\frac{\partial^2 \ddot{w}^0}{\partial x^2} + \frac{1}{R^2} \frac{\partial^2 \ddot{w}^0}{\partial \theta^2} \right]}_{\text{rotary inertia}} - \frac{N_{\theta\theta}}{R} + \frac{\partial^2 M_{xx}}{\partial x^2} + \frac{1}{R^2} \frac{\partial M_{\theta\theta}}{\partial \theta} + \frac{2}{R} \frac{\partial^2 M_{x\theta}}{\partial x \partial \theta} + p_w &= 0
\end{aligned}
\tag{3.16}
$$

Neglecting the rotary inertia from the equation because it only affects higher frequencies and has little impact on the CNTs' vibration, as well as switching the signals in the equations to eventually arrive at a positive definite mass matrix and positive semidefinite stiffness matrix, maintaining mechanical coherence, come the final equations of motion with dependence on the forces and moments:

$$
\begin{aligned}
\rho h\ddot{u}^0 - \frac{\partial N_{xx}}{\partial x} - \frac{1}{R}\frac{\partial N_{x\theta}}{\partial \theta} + \frac{1}{2R^2}\frac{\partial M_{x\theta}}{\partial \theta} &= p_u \\
\rho h\ddot{v}^0 - \frac{1}{R}\frac{\partial N_{\theta\theta}}{\partial \theta} - \frac{\partial N_{x\theta}}{\partial x} - \frac{1}{R^2}\frac{\partial M_{\theta\theta}}{\partial \theta} - \frac{3}{2R}\frac{\partial M_{x\theta}}{\partial x} &= p_v \\
\rho h\ddot{w}^0 + \frac{N_{\theta\theta}}{R} - \frac{\partial^2 M_{xx}}{\partial x^2} - \frac{1}{R^2}\frac{\partial M_{\theta\theta}}{\partial \theta} - \frac{2}{R}\frac{\partial^2 M_{x\theta}}{\partial x \partial \theta} &= p_w
\end{aligned}
\tag{3.17}
$$

To solve the equations of motion in terms of displacement it is important to relate this with the internal forces and moments. Since an isotropic material, is being considered, this comes as:

$$
\begin{aligned}
N_{xx} &= \frac{Eh}{1-\nu^2}\left[\frac{\partial u^0}{\partial x} + \nu\left(\frac{1}{R}\frac{\partial v^0}{\partial \theta} + \frac{w^0}{R}\right)\right] \\
N_{\theta\theta} &= \frac{Eh}{1-\nu^2}\left(\frac{1}{R}\frac{\partial v^0}{\partial \theta} + \frac{w^0}{R} + \nu\frac{\partial u^0}{\partial x}\right) \\
N_{x\theta} &= \frac{Eh}{2(1+\nu)}\left(\frac{1}{R}\frac{\partial u^0}{\partial \theta} + \frac{\partial v^0}{\partial x}\right) \\
M_{xx} &= \frac{Eh^3}{12\,(1-\nu^2)}\left(-\frac{\partial^2 w^0}{\partial x^2} + \nu\frac{1}{R^2}\frac{\partial v^0}{\partial \theta} - \nu\frac{1}{R^2}\frac{\partial^2 w^0}{\partial \theta^2}\right) \\
M_{\theta\theta} &= \frac{Eh^3}{12\,(1-\nu^2)}\left(\frac{1}{R^2}\frac{\partial v^0}{\partial \theta} - \frac{1}{R^2}\frac{\partial^2 w^0}{\partial \theta^2} - \nu\frac{\partial^2 w^0}{\partial x^2}\right) \\
M_{x\theta} &= \frac{Eh^3}{24(1+\nu)}\left(-\frac{2}{R}\frac{\partial^2 w^0}{\partial x \partial \theta} + \frac{3}{2R}\frac{\partial v^0}{\partial x} - \frac{1}{2R^2}\frac{\partial u^0}{\partial \theta}\right)
\end{aligned}
\tag{3.18}
$$

Using these equations to relate the internal forces and moments with the displacements on the shell, and applying them to the already obtained equations of motion, it is possible to get the equations of motion with respect to displacements. Those are the three main equations that describe the thin shell. In order to apply them and extract a weak formulation, further work is presented in the next sections.

$$
\begin{aligned}
&\rho h\ddot{u}^0 - \frac{Eh}{1-\nu^2}\left[\frac{\partial^2 u^0}{\partial x^2} + \frac{1-\nu}{2}\frac{1}{R^2}\frac{\partial^2 u^0}{\partial \theta^2} + \nu\frac{1}{R}\frac{\partial w^0}{\partial x} + \frac{1+\nu}{2}\frac{1}{R}\frac{\partial^2 v^0}{\partial x \partial \theta}\right] \\
&- \frac{Eh^3}{24(1+\nu)R^3}\left[\frac{\partial^3 w^0}{\partial x \partial \theta^2} - \frac{3}{4}\frac{\partial^2 v^0}{\partial x \partial \theta} + \frac{1}{4R}\frac{\partial^2 u^0}{\partial \theta^2}\right] = p_u
\end{aligned}
\tag{3.19}
$$

$$
\begin{aligned}
&\rho h\ddot{v}^0 - \frac{Eh}{1-\nu^2}\left[\frac{1}{R^2}\frac{\partial^2 v^0}{\partial \theta^2} + \frac{1}{R^2}\frac{\partial w^0}{\partial \theta} + \frac{1+\nu}{2}\frac{1}{R}\frac{\partial^2 u^0}{\partial x \partial \theta} + \frac{1-\nu}{2}\frac{\partial^2 v^0}{\partial x^2}\right] \\
&- \frac{Eh^3}{12\,(1-\nu^2)}\left[\frac{1}{R^4}\frac{\partial^2 v^0}{\partial \theta^2} - \frac{1}{R^4}\frac{\partial^3 w^0}{\partial \theta^3} - \frac{3-\nu}{2}\frac{1}{R^2}\frac{\partial^3 w^0}{\partial x^2 \partial \theta}\right. \\
&\left. + \frac{9(1-\nu)}{8R^2}\frac{\partial^2 v^0}{\partial x^2} - \frac{3(1-\nu)}{8R^3}\frac{\partial^2 u^0}{\partial x \partial \theta}\right] = p_v
\end{aligned}
\tag{3.20}
$$

$$\rho h\ddot{w}^0 + \frac{Eh}{1-\nu^2}\left[\frac{1}{R^2}\frac{\partial v^0}{\partial\theta} + \frac{w^0}{R^2} + \nu\frac{1}{R}\frac{\partial u^0}{\partial x}\right] + \frac{Eh^3}{12(1-\nu^2)}\left[\frac{\partial^4 w^0}{\partial x^4}\right.$$
$$\left. - \frac{3-\nu}{2R^2}\frac{\partial^3 v^0}{\partial x^2\partial\theta} + \frac{2}{R^2}\frac{\partial^4 w^0}{\partial x^2\partial\theta^2} - \frac{1}{R^4}\frac{\partial^3 v^0}{\partial\theta^3} + \frac{1}{R^4}\frac{\partial^4 w^0}{\partial\theta^4} + \frac{1-\nu}{2}\frac{1}{R^3}\frac{\partial^3 u^0}{\partial x\partial\theta^2}\right] = p_w \tag{3.21}$$

3.4. Full Model

3.4.1 P-version Finite Element Method

To evaluate a structure and improve the convergence of its solution, the finite element method is utilized in two primary versions. The earliest and most often used is the h-version finite element technique, which bases the accuracy of its calculations on changing the number of elements in an object and increasing them (refining the mesh). As the size of the components gets smaller the number of elements rises and convergence is achieved.

The p-version finite element method is another viable option. It typically uses fewer elements but relies on more shape functions (increasing the order of the polynomials, if the shape functions are in fact polynomials, which is frequently the case) and generalized coordinates to increase the accuracy of the results. Here, the number and size of the elements typically remain fixed, while the displacement field is changeable and refined by employing more shape functions. The approach is referred to be hierarchical by some writers since the previously used functions are retained in improved approximations. According to [109], the p-version FEM offers a lot of benefits over the conventional h-version FEM since it requires fewer components and degrees of freedom while retaining the flexibility of the h-version FEM to provide superior results. As in the case of the current investigation, the p-version also permits the modeling of straightforward structures with a single element, which reduces computing effort and shows a greater convergence ratio.

3.4.2 Boundary Conditions and Shape Functions

A set of shape functions must be chosen for the p-version FEM. For the current model, Rodrigues' form of Legendre's orthogonal polynomials [110–112] are chosen for the x coordinate. To easily implement this set of functions the doming in x coordinate was a-dimensionalized with respect to the nanotube length with the origin at the middle of the CNT. The relation between ξ, the new longitudinal coordinate and x is given by:

$$\xi = \frac{2x-l}{l} \tag{3.22}$$

This way, the internal membrane displacements will be defined as a linear combination of the functions given by:

$$g_r(\xi) = \sum_{n=0}^{\mathrm{Int}(r/2)} \frac{(-1)^n(2r-2n-5)!!}{2^n n!(r-2n-1)!}\xi^{r-2n-1}, r>2 \tag{3.23}$$

On the other hand, for the transverse displacements, the shape functions will be selected from:

$$f_r(\xi) = \sum_{n=0}^{\mathrm{Int}(r/2)} \frac{(-1)^n (2r-2n-7)!!}{2^n n!(r-2n-1)!} \xi^{r-2n-1}, r > 4 \tag{3.24}$$

noting that $r!! = r(r-2)...(2 \text{ or } 1)$, $0!! = (-1)!! = 1$, that $Int(r/2)$ denotes the integer part of $r/2$ and that terms respecting the condition $(r-2n-1)! < 0$ are ignored.

The chosen shape functions must respect the geometric boundary conditions of the system.

Being the CNT clamped on both sides (CC), the following boundary conditions can be written:

$$\begin{aligned} u^0 = v^0 = w^0 = 0, \quad for \quad x = 0 \quad \wedge \quad x = l \\ \frac{\partial w^0}{\partial x} = 0, \quad for \quad x = 0 \quad \wedge \quad x = l \end{aligned} \tag{3.25}$$

All the presented boundary conditions are geometrical and so, must be respected by the used shape functions. The primary distinction between internal membrane shape functions and out-of-plane/transverse shape functions is that the former, designated $g_r(\xi)$, has a null value for $\xi = -1$ and $\xi = 1$, whereas the latter, designated $f_r(\xi)$, has both a null value and a slope for these two values.

On the basis of [9], a distinct set of functions is chosen for the θ coordinate. It is a collection of trigonometric harmonic functions that are frequently used to describe the dynamics along cylindrical coordinates.

$$\begin{aligned} tu_n(\theta) &= \cos(n\theta), \quad n \in \mathbb{N} \\ tv_n(\theta) &= \sin(n\theta), \quad n \in \mathbb{N}^{\setminus\{0\}} \\ tw_n(\theta) &= \cos(n\theta), \quad n \in \mathbb{N} \end{aligned} \tag{3.26}$$

The vector of generalized displacements and a form function combination matrix may be used to calculate the middle surface displacements as follows:

$$\begin{aligned} \left\{de^0\right\} &= \left\{ \begin{array}{c} u^0 \\ v^0 \\ w^0 \end{array} \right\} = [N]\{q\} \\ &= \left[\begin{array}{ccc} \{\delta_1\}^T & 0 & 0 \\ 0 & \{\delta_2\}^T & 0 \\ 0 & 0 & \{\delta_3\}^T \end{array} \right] \{q\} \end{aligned} \tag{3.27}$$

where,

$$\begin{aligned} \{\delta_1\}^T &= \left\{ f^u_{1x} f^u_{1\theta}, f^u_{1x} f^u_{2\theta}, \ldots, f^u_{\text{pgux}}, f^u_{ptu\theta} \right\} \\ \{\delta_2\}^T &= \left\{ f^v_{1x} f^v_{1\theta}, f^v_{1x} f^v_{2\theta}, \ldots, f^v_{\text{pgv}\,x}, f^v_{ptv\theta} \right\} \\ \{\delta_3\}^T &= \left\{ f^w_{1x} f^w_{1\theta}, f^w_{1x} f^w_{2\theta}, \ldots, f^w_{pwx}, f^w_{ptw\theta} \right\} \end{aligned} \tag{3.28}$$

and $\{q\}^T$ is defined as:

$$\{q\}^T = \left\{q^u_{11};q^u_{12};\ldots;q^u_{pgu-ptu};\quad q^v_{11};q^v_{12};\ldots;q^v_{pgv-ptv};\quad q^w_{11};q^w_{12};\ldots;q^w_{pw-ptw}\right\} \quad (3.29)$$

where *ptu*, *ptv*, and *ptw* define, respectively, the number of shape functions assigned to the displacements of u^0, v^0 and w^0 in the coordinate of x, and *pgu*, *pgv*, and *pw* define, respectively, the number of shape functions allocated to the displacement components of u^0, v^0 and w^0 in the coordinate of θ.

3.4.3 Galerkin Method and Matrix Assembly

The already presented governmental equations of the problem (Equations (3.19), (3.20) and (3.21)) were written in the strong form. Applying the Galerkin method [113] and using the same group of functions as shape functions and weight functions and after that, integrating by parts we will obtain the weak form of the equations and it will be possible to compute the finite element method matrices

$$\begin{aligned}
&\int_0^{2\pi}\int_0^l f^u_r(x)f^u_s(\theta)\mathscr{L}_u(x,\theta,t)\mathrm{d}xR\,\mathrm{d}\theta = 0\\
&\int_0^{2\pi}\int_0^l f^v_r(x)f^v_s(\theta)\mathscr{L}_v(x,\theta,t)\mathrm{d}xR\,\mathrm{d}\theta = 0\\
&\int_0^{2\pi}\int_0^l f^w_r(x)f^w_s(\theta)\mathscr{L}_w(x,\theta,t)\mathrm{d}xR\,\mathrm{d}\theta = 0
\end{aligned} \quad (3.30)$$

where,

$$\begin{aligned}
\mathscr{L}_u(x,\theta,t) =& \rho h\underbrace{\frac{\partial^2 u^0}{\partial t^2}}_{ter(1)} - \frac{Eh}{1-\nu^2}\left[\underbrace{\frac{\partial^2 u^0}{\partial x^2}}_{ter(2)} + \underbrace{\frac{1-\nu}{2}\frac{1}{R^2}\frac{\partial^2 u^0}{\partial\theta^2}}_{ter(3)} + \underbrace{\nu\frac{1}{R}\frac{\partial w^0}{\partial x}}_{ter(4)} + \underbrace{\frac{1+\nu}{2}\frac{1}{R}\frac{\partial^2 v^0}{\partial x\partial\theta}}_{ter(5)}\right]\\
&+\frac{Eh^3}{24(1+\nu)R^3}\left[\underbrace{\frac{\partial^3 w^0}{\partial x\partial\theta^2}}_{ter(6)} - \underbrace{\frac{3}{4}\frac{\partial^2 v^0}{\partial x\partial\theta}}_{ter(7)} + \underbrace{\frac{1}{4R}\frac{\partial^2 u^0}{\partial\theta^2}}_{ter(8)}\right] - \underbrace{p_u}_{ter(9)} = 0
\end{aligned} \quad (3.31)$$

$$\begin{aligned}\mathscr{L}_v(x,\theta,t) =& \rho h \underbrace{\frac{\partial^2 v^0}{\partial t^2}}_{ter(10)} - \frac{Eh}{1-\nu^2}\left[\underbrace{\frac{1}{R^2}\frac{\partial^2 v^0}{\partial \theta^2}}_{ter(11)} + \underbrace{\frac{1}{R^2}\frac{\partial w^0}{\partial \theta}}_{ter(12)} + \underbrace{\frac{1+\nu}{2}\frac{1}{R}\frac{\partial^2 u^0}{\partial x \partial \theta}}_{ter(13)} + \underbrace{\frac{1-\nu}{2}\frac{\partial^2 v^0}{\partial x^2}}_{\text{ter}(14)}\right] \\ & - \frac{Eh^3}{12(1-\nu^2)}\left[\underbrace{\frac{1}{R^4}\frac{\partial^2 v^0}{\partial \theta^2}}_{ter(15)} - \underbrace{\frac{1}{R^4}\frac{\partial^3 w^0}{\partial \theta^3}}_{ter(16)} - \underbrace{\frac{3-\nu}{2}\frac{1}{R^2}\frac{\partial^3 w^0}{\partial x^2 \partial \theta}}_{ter(17)}\right. \\ & \left. + \underbrace{\frac{9(1-\nu)}{8R^2}\frac{\partial^2 v^0}{\partial x^2}}_{ter(18)} - \underbrace{\frac{3(1-\nu)}{8R^3}\frac{\partial^2 u^0}{\partial x \partial \theta}}_{ter(19)}\right] - \underbrace{p_v}_{ter(20)} = 0\end{aligned} \tag{3.32}$$

$$\begin{aligned}\mathscr{L}_w(x,\theta,t) =& \rho h \underbrace{\frac{\partial^2 w^0}{\partial t^2}}_{ter(21)} + \frac{Eh}{1-\nu^2}\left[\underbrace{\frac{1}{R^2}\frac{\partial v^0}{\partial \theta}}_{ter(22)} + \underbrace{\frac{w^0}{R^2}}_{ter(23)} + \underbrace{\nu\frac{1}{R}\frac{\partial u^0}{\partial x}}_{ter(24)}\right] \\ & + \frac{Eh^3}{12(1-\nu^2)}\left[\underbrace{\frac{\partial^4 w^0}{\partial x^4}}_{ter(25)} - \underbrace{\frac{3-\nu}{2R^2}\frac{\partial^3 v^0}{\partial x^2 \partial \theta}}_{ter(26)} + \underbrace{\frac{2}{R^2}\frac{\partial^4 w^0}{\partial x^2 \partial \theta^2}}_{ter(27)}\right. \\ & \left. - \underbrace{\frac{1}{R^4}\frac{\partial^3 v^0}{\partial \theta^3}}_{ter(28)} + \underbrace{\frac{1}{R^4}\frac{\partial^4 w^0}{\partial \theta^4}}_{ter(29)} + \underbrace{\frac{1-\nu}{2}\frac{1}{R^3}\frac{\partial^3 u^0}{\partial x \partial \theta^2}}_{ter(30)}\right] - \underbrace{p_w}_{ter(31)} = 0\end{aligned} \tag{3.33}$$

Applying the method to all the identified terms, simplifying, integrating by parts, and changing the integration domain we get:

$$\begin{aligned}\text{ter}(1) :& \rho h \int_0^{2\pi}\int_0^l f^u_{rx} f^u_{s\theta} \cdot \left(f^u_{ix} f^u_{j\theta}\right) \mathrm{d}x R \, \mathrm{d}\theta \ddot{q}^u_{ij} \\ =& \rho h R \frac{l}{2} \int_0^{2\pi} f^u_{s\theta} f^u_{j\theta} \, \mathrm{d}\theta \int_{-1}^{1} f^u_{r\xi} f^u_{i\xi} \, \mathrm{d}\xi \ddot{q}^u_{ij}(t)\end{aligned} \tag{3.34}$$

$$\begin{aligned}\text{ter}(2) :& -\frac{Eh}{1-\nu^2}\int_0^{2\pi}\int_0^l f^u_{rx} f^u_{s\theta} \cdot \frac{\partial^2}{\partial x^2}\left(f^u_{ix} f^u_{j\theta}\right) \mathrm{d}x R \, \mathrm{d}\theta q^u_{ij}(t) \\ =& \frac{2}{l}\frac{EhR}{1-\nu^2}\int_0^{2\pi} f^u_{s\theta} f^u_{j\theta} \, \mathrm{d}\theta \int_{-1}^{1} \frac{\mathrm{d}f^u_{r\xi}}{\mathrm{d}\xi}\frac{\mathrm{d}f^u_{i\xi}}{\mathrm{d}\xi}\mathrm{d}\xi q^u_{ij}(t)\end{aligned} \tag{3.35}$$

$$\begin{aligned}\text{ter}(3) :& -\frac{Eh}{1-\nu^2}\frac{1-\nu}{2R^2}\int_0^{2\pi}\int_0^l f^u_{rx} f^u_{s\theta} \cdot \frac{\partial^2}{\partial \theta^2}\left(f^u_{ix} f^u_{j\theta}\right) \mathrm{d}x R \, \mathrm{d}\theta q^u_{ij}(t) \\ =& \frac{Ehl(1-\nu)}{4(1-\nu^2)R}\int_0^{2\pi}\frac{\mathrm{d}f^u_{s\theta}}{\mathrm{d}\theta}\frac{\mathrm{d}f^u_{j\theta}}{\mathrm{d}\theta}\mathrm{d}\theta \int_{-1}^{1} f^u_{r\xi} f^u_{i\xi} \, \mathrm{d}\xi q^u_{ij}(t)\end{aligned} \tag{3.36}$$

$$\begin{aligned}\mathrm{ter}(4) &: -\frac{Eh\nu}{(1-\nu^2)R}\int_0^{2\pi}\int_0^{l} f^u_{rx}f^u_{s\theta}\cdot\frac{\partial}{\partial x}\left(f^w_{ix}f^w_{j\theta}\right)\mathrm{d}xR\,\mathrm{d}\theta q^w_{ij}(t)\\ &= -\frac{Eh\nu}{1-\nu^2}\int_0^{2\pi} f^u_{s\theta}f^w_{j\theta}\,\mathrm{d}\theta\int_{-1}^{1} f^u_{r\xi}\frac{\mathrm{d}f^w_{i\xi}}{\mathrm{d}\xi}\mathrm{d}\xi q^w_{ij}(t)\end{aligned} \tag{3.37}$$

$$\begin{aligned}\mathrm{ter}(5) &: -\frac{Eh}{1-\nu^2}\frac{1+\nu}{2R}\int_0^{2\pi}\int_0^{l} f^u_{rx}f^u_{s\theta}\cdot\frac{\partial^2}{\partial x\partial\theta}\left(f^v_{ix}f^v_{j\theta}\right)\mathrm{d}xR\,\mathrm{d}\theta q^v_{ij}(t)\\ &= -\frac{Eh}{1-\nu^2}\frac{1+\nu}{2}\int_0^{2\pi} f^u_{s\theta}\frac{\mathrm{d}f^v_{j\theta}}{\mathrm{d}\theta}\mathrm{d}\theta\int_{-1}^{1} f^u_{r\xi}\frac{\mathrm{d}f^v_{i\xi}}{\mathrm{d}\xi}\mathrm{d}\xi q^v_{ij}(t)\end{aligned} \tag{3.38}$$

$$\begin{aligned}\mathrm{ter}(6) &: -\frac{Eh^3}{24(1+\nu)R^3}\int_0^{2\pi}\int_0^{l} f^u_{rx}f^u_{s\theta}\cdot\frac{\partial^3}{\partial x\partial\theta^2}\left(f^w_{ix}f^w_{j\theta}\right)\mathrm{d}xR\,\mathrm{d}\theta q^w_{ij}(t)\\ &= \frac{Eh^3}{24(1+\nu)R^2}\int_0^{2\pi}\frac{\mathrm{d}f^u_{s\theta}}{\mathrm{d}\theta}\frac{\mathrm{d}f^w_{j\theta}}{\mathrm{d}\theta}\mathrm{d}\theta\int_{-1}^{1} f^u_{r\xi}\frac{\mathrm{d}f^w_{i\xi}}{\mathrm{d}\xi}\mathrm{d}\xi q^w_{ij}(t)\end{aligned} \tag{3.39}$$

$$\begin{aligned}\mathrm{ter}(7) &: \frac{3}{4}\frac{Eh^3}{24(1+\nu)R^3}\int_0^{2\pi}\int_0^{l} f^u_{rx}f^u_{s\theta}\cdot\frac{\partial^2}{\partial x\partial\theta}\left(f^v_{ix}f^v_{j\theta}\right)\mathrm{d}xR\,\mathrm{d}\theta q^v_{ij}(t)\\ &= \frac{Eh^3}{32(1+\nu)R^2}\int_0^{2\pi} f^u_{s\theta}\frac{\mathrm{d}f^v_{j\theta}}{\mathrm{d}\theta}\mathrm{d}\theta\int_{-1}^{1} f^u_{r\xi}\frac{\mathrm{d}f^v_{i\xi}}{\mathrm{d}\xi}\mathrm{d}\xi q^v_{ij}(t)\end{aligned} \tag{3.40}$$

$$\begin{aligned}\mathrm{ter}(8) &: -\frac{Eh^3}{24(1+\nu)R^3}\frac{1}{4R}\int_0^{2\pi}\int_0^{l} f^u_{rx}f^u_{s\theta}\cdot\frac{\partial^2}{\partial\theta^2}\left(f^u_{ix}f^u_{j\theta}\right)\mathrm{d}xR\,\mathrm{d}\theta q^u_{ij}(t)\\ &= \frac{Eh^3l}{192(1+\nu)R^3}\int_0^{2\pi}\frac{\mathrm{d}f^u_{s\theta}}{\mathrm{d}\theta}\frac{\mathrm{d}f^u_{j\theta}}{\mathrm{d}\theta}\mathrm{d}\theta\int_{-1}^{1} f^u_{r\xi}f^u_{i\xi}\,\mathrm{d}\xi q^u_{ij}(t)\end{aligned} \tag{3.41}$$

$$\begin{aligned}\mathrm{ter}(9) &: \int_0^{2\pi}\int_0^{l} f^u_{rx}f^u_{s\theta}\cdot p_u\mathrm{d}xR\,\mathrm{d}\theta\\ &= \frac{l}{2}\int_0^{2\pi}\int_{-1}^{1} f^u_{r\xi}f^u_{s\theta}\cdot p_uR\cdot\mathrm{d}\xi\,\mathrm{d}\theta\end{aligned} \tag{3.42}$$

$$\begin{aligned}\mathrm{ter}(10) &: \rho h\int_0^{2\pi}\int_0^{l} f^v_{rx}f^v_{s\theta}\cdot\left(f^v_{ix}f^v_{j\theta}\right)\mathrm{d}xR\,\mathrm{d}\theta\ddot{q}^v_{ij}(t)\\ &= \rho hR\frac{l}{2}\int_0^{2\pi} f^v_{s\theta}f^v_{j\theta}\,\mathrm{d}\theta\int_{-1}^{1} f^v_{r\xi}f^v_{i\xi}\,\mathrm{d}\xi\ddot{q}^v_{ij}(t)\end{aligned} \tag{3.43}$$

$$\begin{aligned}\mathrm{ter}(11) &: -\frac{Eh}{1-\nu^2}\frac{1}{R^2}\int_0^{2\pi}\int_0^{l} f^v_{rx}f^v_{s\theta}\cdot\frac{\partial^2}{\partial\theta^2}\left(f^v_{ix}f^v_{j\theta}\right)\mathrm{d}xR\,\mathrm{d}\theta q^v_{ij}(t)\\ &= \frac{Ehl}{(1-\nu^2)2R}\int_0^{2\pi}\frac{\mathrm{d}f^v_{s\theta}}{\mathrm{d}\theta}\frac{\mathrm{d}f^v_{j\theta}}{\mathrm{d}\theta}\mathrm{d}\theta\int_{-1}^{1} f^v_{r\xi}f^v_{i\xi}\,\mathrm{d}\xi q^v_{ij}(t)\end{aligned} \tag{3.44}$$

$$\begin{aligned}\mathrm{ter}(12) &: -\frac{Eh}{1-\nu^2}\frac{1}{R^2}\int_0^{2\pi}\int_0^{l} f^v_{rx}f^v_{s\theta}\cdot\frac{\partial}{\partial\theta}\left(f^w_{ix}f^w_{j\theta}\right)\mathrm{d}xR\,\mathrm{d}\theta q^w_{ij}(t)\\ &= -\frac{Ehl}{(1-\nu^2)2R}\int_0^{2\pi} f^v_{s\theta}\frac{\mathrm{d}f^w_{j\theta}}{\mathrm{d}\theta}\mathrm{d}\theta\int_{-1}^{1} f^v_{r\xi}f^w_{i\xi}\,\mathrm{d}\xi q^w_{ij}(t)\end{aligned} \tag{3.45}$$

$$\begin{aligned}\mathrm{ter}(13) &: -\frac{Eh}{1-\nu^2}\frac{1+\nu}{2}\frac{1}{R}\int_0^{2\pi}\int_0^{l} f^v_{rx}f^v_{s\theta}\cdot\frac{\partial^2}{\partial x\partial\theta}\left(f^u_{ix}f^u_{j\theta}\right)\mathrm{d}xR\,\mathrm{d}\theta q^u_{ij}(t)\\ &= -\frac{Eh}{1-\nu^2}\frac{1+\nu}{2}\int_0^{2\pi} f^v_{s\theta}\frac{\mathrm{d}f^u_{j\theta}}{\mathrm{d}\theta}\mathrm{d}\theta\int_{-1}^{1} f^v_{r\xi}\frac{\mathrm{d}f^u_{i\xi}}{\mathrm{d}\xi}\mathrm{d}\xi q^u_{ij}(t)\end{aligned} \tag{3.46}$$

$$\begin{aligned}\mathrm{ter}(14) &: -\frac{Eh}{1-\nu^2}\frac{1-\nu}{2}\int_0^{2\pi}\int_0^{l} f_{rx}^{v} f_{s\theta}^{v}\cdot\frac{\partial^2}{\partial x^2}\left(f_{ix}^{v} f_{j\theta}^{v}\right)\mathrm{d}xR\,\mathrm{d}\theta q_{ij}^{v}(t)\\ &= \frac{Eh(1-\nu)R}{(1-\nu^2)\,l}\int_0^{2\pi} f_{s\theta}^{v} f_{j\theta}^{v}\,\mathrm{d}\theta\int_{-1}^{1}\frac{\mathrm{d}f_{r\xi}^{v}}{\mathrm{d}\xi}\frac{\mathrm{d}f_{i\xi}^{v}}{\mathrm{d}\xi}\mathrm{d}\xi q_{ij}^{v}(t)\end{aligned} \tag{3.47}$$

$$\begin{aligned}\mathrm{ter}(15) &: -\frac{Eh^3}{12\,(1-\nu^2)}\frac{1}{R^4}\int_0^{2\pi}\int_0^{l} f_{rx}^{v} f_{s\theta}^{v}\cdot\frac{\partial^2}{\partial\theta^2}\left(f_{ix}^{v} f_{j\theta}^{v}\right)\mathrm{d}xR\,\mathrm{d}\theta q_{ij}^{v}(t)\\ &= \frac{Eh^3 l}{24\,(1-\nu^2)\,R^3}\int_0^{2\pi}\frac{\mathrm{d}f_{s\theta}^{v}}{\mathrm{d}\theta}\frac{\mathrm{d}f_{j\theta}^{v}}{\mathrm{d}\theta}\mathrm{d}\theta\int_{-1}^{1} f_{r\xi}^{v} f_{i\xi}^{v}\,\mathrm{d}\xi q_{ij}^{v}(t)\end{aligned} \tag{3.48}$$

$$\begin{aligned}\mathrm{ter}(16) &: \frac{Eh^3}{12\,(1-\nu^2)}\frac{1}{R^4}\int_0^{2\pi}\int_0^{l} f_{rx}^{v} f_{s\theta}^{v}\cdot\frac{\partial^3}{\partial\theta^3}\left(f_{ix}^{w} f_{j\theta}^{w}\right)\mathrm{d}xR\,\mathrm{d}\theta q_{ij}^{w}(t)\\ &= -\frac{Eh^3 l}{24\,(1-\nu^2)\,R^3}\int_0^{2\pi}\frac{\mathrm{d}f_{s\theta}^{v}}{\mathrm{d}\theta}\frac{\mathrm{d}^2 f_{j\theta}^{w}}{\mathrm{d}\theta^2}\,\mathrm{d}\theta\int_{-1}^{1} f_{r\xi}^{v} f_{i\xi}^{w}\,\mathrm{d}\xi q_{ij}^{w}(t)\end{aligned} \tag{3.49}$$

$$\begin{aligned}\mathrm{ter}(17) &: \frac{Eh^3(3-\nu)}{24\,(1-\nu^2)\,R^2}\int_0^{2\pi}\int_0^{l} f_{rx}^{v} f_{s\theta}^{v}\cdot\frac{\partial^3}{\partial x^2\partial\theta}\left(f_{ix}^{w} f_{j\theta}^{w}\right)\mathrm{d}xR\,\mathrm{d}\theta q_{ij}^{w}(t)\\ &= -\frac{Eh^3(3-\nu)}{12\,(1-\nu^2)\,lR}\int_0^{2\pi} f_{s\theta}^{v}\frac{\mathrm{d}f_{j\theta}^{w}}{\mathrm{d}\theta}\mathrm{d}\theta\int_{-1}^{1}\frac{\mathrm{d}f_{r\xi}^{v}}{\mathrm{d}\xi}\frac{\mathrm{d}f_{i\xi}^{w}}{\mathrm{d}\xi}\mathrm{d}\xi q_{ij}^{w}(t)\end{aligned} \tag{3.50}$$

$$\begin{aligned}\mathrm{ter}(18) &: -\frac{Eh^3}{12\,(1-\nu^2)}\frac{9(1-\nu)}{8R^2}\int_0^{2\pi}\int_0^{l} f_{rx}^{v} f_{s\theta}^{v}\cdot\frac{\partial^2}{\partial x^2}\left(f_{ix}^{v} f_{j\theta}^{v}\right)\mathrm{d}xR\,\mathrm{d}\theta q_{ij}^{v}(t)\\ &= \frac{9Eh^3(1-\nu)}{48\,(1-\nu^2)\,lR}\int_0^{2\pi} f_{s\theta}^{v} f_{j\theta}^{v}\,\mathrm{d}\theta\int_{-1}^{1}\frac{\mathrm{d}f_{r\xi}^{v}}{\mathrm{d}\xi}\frac{\mathrm{d}f_{i\xi}^{v}}{\mathrm{d}\xi}\mathrm{d}\xi q_{ij}^{v}(t)\end{aligned} \tag{3.51}$$

$$\begin{aligned}\mathrm{ter}(19) &: \frac{Eh^3}{12\,(1-\nu^2}\frac{3(1-\nu}{8R^3}\int_0^{2\pi}\int_0^{l} f_{rx}^{v} f_{s\theta}^{v}\cdot\frac{\partial^2}{\partial x\partial\theta}\left(f_{ix}^{u} f_{j\theta}^{u}\right)\mathrm{d}xR\,\mathrm{d}\theta q_{ij}^{u}(t)\\ &= \frac{Eh^3(1-\nu)}{32\,(1-\nu^2)\,R^2}\int_0^{2\pi} f_{s\theta}^{v}\frac{\mathrm{d}f_{j\theta}^{u}}{\mathrm{d}\theta}\mathrm{d}\theta\int_{-1}^{1} f_{r\xi}^{v}\frac{\mathrm{d}f_{i\xi}^{u}}{\mathrm{d}\xi}\mathrm{d}\xi q_{ij}^{u}(t)\end{aligned} \tag{3.52}$$

$$\begin{aligned}\mathrm{ter}(20) &: \int_0^{2\pi}\int_0^{l} f_{rx}^{v} f_{s\theta}^{v}\cdot p_v\mathrm{d}xR\,\mathrm{d}\theta\\ &= \frac{l}{2}\int_0^{2\pi}\int_{-1}^{1} f_{r\xi}^{v} f_{s\theta}^{v}\cdot p_v R\cdot\mathrm{d}\xi\,\mathrm{d}\theta\end{aligned} \tag{3.53}$$

$$\begin{aligned}\mathrm{ter}(21) &: \rho h\int_0^{2\pi}\int_0^{l} f_{rx}^{w} f_{s\theta}^{w}\cdot\left(f_{ix}^{w} f_{j\theta}^{w}\right)\mathrm{d}xR\,\mathrm{d}\theta\ddot{q}_{ij}^{w}(t)\\ &= \rho hR\frac{l}{2}\int_0^{2\pi} f_{s\theta}^{w} f_{j\theta}^{w}\,\mathrm{d}\theta\int_{-1}^{1} f_{r\xi}^{w} f_{i\xi}^{w}\,\mathrm{d}\xi\ddot{q}_{ij}^{w}(t)\end{aligned} \tag{3.54}$$

$$\begin{aligned}\mathrm{ter}(22) &: \frac{Eh}{1-\nu^2}\frac{1}{R^2}\int_0^{2\pi}\int_0^{l} f_{rx}^{w} f_{s\theta}^{w}\cdot\frac{\partial}{\partial\theta}\left(f_{ix}^{v} f_{j\theta}^{v}\right)\mathrm{d}xR\,\mathrm{d}\theta q_{ij}^{v}(t)\\ &= \frac{Ehl}{(1-\nu^2)\,2R}\int_0^{2\pi} f_{s\theta}^{w}\frac{\mathrm{d}f_{j\theta}^{v}}{\mathrm{d}\theta}\mathrm{d}\theta\int_{-1}^{1} f_{r\xi}^{w} f_{i\xi}^{v}\,\mathrm{d}\xi q_{ij}^{v}(t)\end{aligned} \tag{3.55}$$

$$\begin{aligned}\text{ter}(23) &: \frac{Eh}{1-\nu^2}\frac{1}{R^2}\int_0^{2\pi}\int_0^{l} f^w_{rx}f^w_{s\theta}\cdot\left(f^w_{ix}f^w_{j\theta}\right)\mathrm{d}xR\,\mathrm{d}\theta q^w_{ij}(t)\\ &= \frac{Eh}{1-\nu^2}\frac{1}{R}\frac{l}{2}\int_0^{2\pi} f^w_{s\theta}f^w_{j\theta}\,\mathrm{d}\theta\int_{-1}^{1} f^w_{r\xi}f^w_{i\xi}\,\mathrm{d}\xi\, q^w_{ij}(t)\end{aligned} \tag{3.56}$$

$$\begin{aligned}\text{ter}(24) &: \frac{Eh\nu}{(1-\nu^2)R}\int_0^{2\pi}\int_0^{l} f^w_{rx}f^w_{s\theta}\cdot\frac{\partial}{\partial x}\left(f^u_{ix}f^u_{j\theta}\right)\mathrm{d}xR\,\mathrm{d}\theta q^u_{ij}(t)\\ &= \frac{Eh\nu}{1-\nu^2}\int_0^{2\pi} f^w_{s\theta}f^u_{j\theta}\,\mathrm{d}\theta\int_{-1}^{1} f^w_{r\xi}\frac{\mathrm{d}f^u_{i\xi}}{\mathrm{d}\xi}\mathrm{d}\xi q^u_{ij}(t)\end{aligned} \tag{3.57}$$

$$\begin{aligned}\text{ter}(25) &: \frac{Eh^3}{12\,(1-\nu^2}\int_0^{2\pi}\int_0^{l} f^w_{rx}f^w_{s\theta}\cdot\frac{\partial^4}{\partial x^4}\left(f^w_{ix}f^w_{j\theta}\right)\mathrm{d}xR\,\mathrm{d}\theta q^w_{ij}(t)\\ &= \frac{2Eh^3R}{3\,(1-\nu^2)\,l^3}\int_0^{2\pi} f^w_{s\theta}f^w_{j\theta}\,\mathrm{d}\theta\int_{-1}^{1}\frac{\mathrm{d}^2f^w_{r\xi}}{\mathrm{d}\xi^2}\frac{\mathrm{d}^2f^w_{i\xi}}{\mathrm{d}\xi^2}\,\mathrm{d}\xi\, q^w_{ij}(t)\end{aligned} \tag{3.58}$$

$$\begin{aligned}\text{ter}(26) &: -\frac{Eh^3(3-\nu)}{24\,(1-\nu^2)R^2}\int_0^{2\pi}\int_0^{l} f^w_{rx}f^w_{s\theta}\cdot\frac{\partial^3}{\partial x^2\partial\theta}\left(f^v_{ix}f^v_{j\theta}\right)\mathrm{d}xR\,\mathrm{d}\theta q^v_{ij}(t)\\ &= \frac{Eh^3(3-\nu)}{12\,(1-\nu^2)\,lR}\int_0^{2\pi} f^w_{s\theta}\frac{\mathrm{d}f^v_{j\theta}}{\mathrm{d}\theta}\mathrm{d}\theta\int_{-1}^{1}\frac{\mathrm{d}f^w_{r\xi}}{\mathrm{d}\xi}\frac{\mathrm{d}f^v_{i\xi}}{\mathrm{d}\xi}\mathrm{d}\xi q^v_{ij}(t)\end{aligned} \tag{3.59}$$

$$\begin{aligned}\text{ter}(27) &: \frac{Eh^3}{12\,(1-\nu^2)}\frac{2}{R^2}\int_0^{2\pi}\int_0^{l} f^w_{rx}f^w_{s\theta}\cdot\frac{\partial^4}{\partial x^2\partial\theta^2}\left(f^w_{ix}f^w_{j\theta}\right)\mathrm{d}xR\,\mathrm{d}\theta q^w_{ij}(t)\\ &= \frac{Eh^3}{3\,(1-\nu^2)\,lR}\int_0^{2\pi}\frac{\mathrm{d}f^w_{s\theta}}{\mathrm{d}\theta}\frac{\mathrm{d}f^w_{j\theta}}{\mathrm{d}\theta}\mathrm{d}\theta\int_{-1}^{1}\frac{\mathrm{d}f^w_{r\xi}}{\mathrm{d}\xi}\frac{\mathrm{d}f^w_{i\xi}}{\mathrm{d}\xi}\mathrm{d}\xi q^w_{ij}(t)\end{aligned} \tag{3.60}$$

$$\begin{aligned}\text{ter}(28) &: -\frac{Eh^3}{12\,(1-\nu^2)}\frac{1}{R^4}\int_0^{2\pi}\int_0^{l} f^w_{rx}f^w_{s\theta}\cdot\frac{\partial^3}{\partial\theta^3}\left(f^v_{ix}f^v_{j\theta}\right)\mathrm{d}xR\,\mathrm{d}\theta q^v_{ij}(t)\\ &= \frac{Eh^3l}{24\,(1-\nu^2)R^3}\int_0^{2\pi}\frac{\mathrm{d}f^w_{s\theta}}{\mathrm{d}\theta}\frac{\mathrm{d}^2f^v_{j\theta}}{\mathrm{d}\theta^2}\,\mathrm{d}\theta\int_{-1}^{1} f^w_{r\xi}f^v_{i\xi}\,\mathrm{d}\xi\, q^v_{ij}(t)\end{aligned} \tag{3.61}$$

$$\begin{aligned}\text{ter}(29) &: \frac{Eh^3}{12\,(1-\nu^2}\frac{1}{R^4}\int_0^{2\pi}\int_0^{l} f^w_{rx}f^w_{s\theta}\cdot\frac{\partial^4}{\partial\theta^4}\left(f^w_{ix}f^w_{j\theta}\right)\mathrm{d}xR\,\mathrm{d}\theta q^w_{ij}(t)\\ &= \frac{Eh^3l}{24\,(1-\nu^2)R^3}\int_0^{2\pi}\frac{\mathrm{d}^2f^w_{s\theta}}{\mathrm{d}\theta^2}\frac{\mathrm{d}^2f^w_{j\theta}}{\mathrm{d}\theta^2}\,\mathrm{d}\theta\int_{-1}^{1} f^w_{r\xi}f^w_{i\xi}\,\mathrm{d}\xi q^w_{ij}(t)\end{aligned} \tag{3.62}$$

$$\begin{aligned}\text{ter}(30) &: \frac{Eh^3}{12\,(1-\nu^2)}\frac{1-\nu}{2R^3}\int_0^{2\pi}\int_0^{l} f^w_{rx}f^w_{s\theta}\cdot\frac{\partial^3}{\partial x\partial\theta^2}\left(f^u_{ix}f^u_{j\theta}\right)\mathrm{d}xR\,\mathrm{d}\theta q^u_{ij}(t)\\ &= -\frac{Eh^3}{24(1+\nu)R^2}\int_0^{2\pi}\frac{\mathrm{d}f^w_{s\theta}}{\mathrm{d}\theta}\frac{\mathrm{d}f^u_{j\theta}}{\mathrm{d}\theta}\mathrm{d}\theta\int_{-1}^{1} f^w_{r\xi}\frac{\mathrm{d}f^u_{i\xi}}{\mathrm{d}\xi}\mathrm{d}\xi q^u_{ij}(t)\end{aligned} \tag{3.63}$$

$$\begin{aligned}\text{ter}(31) &: \int_0^{2\pi}\int_0^{l} f^w_{rx}f^w_{s\theta}\cdot p_w\mathrm{d}xR\,\mathrm{d}\theta\\ &= \frac{l}{2}\int_0^{2\pi}\int_{-1}^{1} f^w_{r\xi}f^w_{s\theta}\cdot p_wR\cdot\mathrm{d}\xi\,\mathrm{d}\theta\end{aligned} \tag{3.64}$$

Presenting the problem in its matrix formulation, and in order to the generalized displacements, it comes:

$$\begin{bmatrix} [M_{uu}] & 0 & 0 \\ 0 & [M_{vv}] & 0 \\ 0 & 0 & [M_{ww}] \end{bmatrix} \begin{Bmatrix} \{\ddot{q}_u(t)\} \\ \{\ddot{q}_v(t)\} \\ \{\ddot{q}_w(t)\} \end{Bmatrix} + \begin{bmatrix} [K_{uu}] & [K_{uv}] & [K_{uw}] \\ [K_{vu}] & [K_{vv}] & [K_{vw}] \\ [K_{wu}] & [K_{wv}] & [K_{ww}] \end{bmatrix} \begin{Bmatrix} \{q_u(t)\} \\ \{q_v(t)\} \\ \{q_w(t)\} \end{Bmatrix} = \begin{Bmatrix} \{P_u\} \\ \{P_v\} \\ \{P_w\} \end{Bmatrix} \tag{3.65}$$

where the submatrices may be written as:

- $[M_{uu}] \leftarrow \text{ter}(1)$
- $[M_{vv}] \leftarrow \text{ter}(10)$
- $[M_{ww}] \leftarrow \text{ter}(21)$
- $[K_{uu}] \leftarrow \text{ter}(2) + \text{ter}(3) + \text{ter}(8)$
- $[K_{uv}] \leftarrow \text{ter}(5) + \text{ter}(7)$
- $[K_{uw}] \leftarrow \text{ter}(4) + \text{ter}(6)$
- $[K_{vu}] \leftarrow \text{ter}(13) + \text{ter}(19)$
- $[K_{vv}] \leftarrow \text{ter}(11) + \text{ter}(14) + \text{ter}(15) + \text{ter}(18)$
- $[K_{vw}] \leftarrow \text{ter}(12) + \text{ter}(16) + \text{ter}(17)$
- $[K_{wu}] \leftarrow \text{ter}(24) + \text{ter}(30)$
- $[K_{wv}] \leftarrow \text{ter}(22) + \text{ter}(26) + \text{ter}(28)$
- $[K_{ww}] \leftarrow \text{ter}(23) + \text{ter}(25) + \text{ter}(27) + \text{ter}(29)$
- $\{P_u\} \leftarrow \text{ter}(9)$
- $\{P_v\} \leftarrow \text{ter}(20)$
- $\{P_w\} \leftarrow \text{ter}(31)$

3.5. Reduced Model

For certain problems, it is a good approximation to disregard membrane inertia. The benefits of this simplification are clear since this would reduce the number of equations of the problem to a third of the full model. It is important not to confuse this approach with the omission of the membrane displacement components, u and v. Neglecting these displacements would destroy the shell model essence since all displacements are coupled.

In [114], Ribeiro studied the influence of the membrane inertia of a shallow shell under periodic linear behavior. It was concluded that membrane inertia forces were not

significant and so could be neglected. It was also observed that neglecting membrane inertia could lead to a totally different result under nonlinear vibrations.

The consequences of neglecting membrane inertia for a cylindrical shell have already been studied by Forsberg [115]. He concluded that the primary effects of neglecting membrane inertia terms are the omission of two higher frequencies for each nodal pattern, and the remaining frequency value is increased. Disregarding membrane inertia the lower frequency mode shapes and modal forces were not significantly affected [115].

Furthermore, the formulation of models neglecting membrane inertia will be presented starting from the matrix form of the Equation (3.65). First, just the longitudinal membrane inertia will be disregarded. After, both longitudinal $[M_{uu}]$ and tangential membrane inertia $[M_{vv}]$ will be disregarded.

3.5.1 Neglecting Longitudinal Inertia

Neglecting longitudinal membrane inertia, $[M_{uu}]$:

$$\begin{gathered}\begin{bmatrix} 0 & 0 & 0 \\ 0 & [M_{vv}] & 0 \\ 0 & 0 & [M_{ww}] \end{bmatrix} \begin{Bmatrix} \{\ddot{q}_u(t)\} \\ \{\ddot{q}_v(t)\} \\ \{\ddot{q}_w(t)\} \end{Bmatrix} \\ + \begin{bmatrix} [K_{uu}] & [K_{uv}] & [K_{uw}] \\ [K_{vu}] & [K_{vv}] & [K_{vw}] \\ [K_{wu}] & [K_{wv}] & [K_{ww}] \end{bmatrix} \begin{Bmatrix} \{q_u(t)\} \\ \{q_v(t)\} \\ \{q_w(t)\} \end{Bmatrix} = \begin{Bmatrix} \{P_u(t)\} \\ \{P_v(t)\} \\ \{P_w(t)\} \end{Bmatrix}\end{gathered} \tag{3.66}$$

It is possible to separate the problem into two distinct equations, Equation (3.67) and Equation (3.68):

$$\begin{gathered}\begin{bmatrix} [M_{vv}] & 0 \\ 0 & [M_{ww}] \end{bmatrix} \begin{Bmatrix} \{\ddot{q}_v(t)\} \\ \{\ddot{q}_w(t)\} \end{Bmatrix} \\ + \begin{bmatrix} [K_{vu}] & [K_{vv}] & [K_{vw}] \\ [K_{wu}] & [K_{wv}] & [K_{ww}] \end{bmatrix} \begin{Bmatrix} \{q_u(t)\} \\ \{q_v(t)\} \\ \{q_w(t)\} \end{Bmatrix} = \begin{Bmatrix} \{P_v(t)\} \\ \{P_w(t)\} \end{Bmatrix}\end{gathered} \tag{3.67}$$

$$\begin{bmatrix} [K_{uu}] & [K_{uv}] & [K_{uw}] \end{bmatrix} \begin{Bmatrix} \{q_u(t)\} \\ \{q_v(t)\} \\ \{q_w(t)\} \end{Bmatrix} = \{P_u(t)\} \tag{3.68}$$

Simplifying Equation (3.68) and isolating the term $\{q_u(t)\}$:

$$[K_{uu}]\{q_u(t)\} + [K_{uv}]\{q_v(t)\} + [K_{uw}]\{q_w(t)\} = \{P_u(t)\} \tag{3.69}$$

$$\{q_u(t)\} = [K_{uu}]^{-1} \left(\{P_u(t)\} - \begin{bmatrix} [K_{uv}] [K_{uw}] \end{bmatrix} \begin{Bmatrix} \{q_v(t)\} \\ \{q_w(t)\} \end{Bmatrix} \right) \tag{3.70}$$

Simplifying Equation (3.67) and substituting $\{q_u(t)\}$ as calculated in Equation (3.70)

$$\begin{gathered}\begin{bmatrix} [M_{vv}] & 0 \\ 0 & [M_{ww}] \end{bmatrix} \begin{Bmatrix} \{\ddot{q}_v(t)\} \\ \{\ddot{q}_w(t)\} \end{Bmatrix} \\ + \begin{bmatrix} [K_{vu}] \\ [K_{wu}] \end{bmatrix} \{q_u(t)\} + \begin{bmatrix} [K_{vv}] & [K_{vw}] \\ [K_{wv}] & [K_{ww}] \end{bmatrix} \begin{Bmatrix} \{q_v(t)\} \\ \{q_w(t)\} \end{Bmatrix} = \begin{Bmatrix} \{P_v(t)\} \\ \{P_w(t)\} \end{Bmatrix}\end{gathered} \tag{3.71}$$

$$\begin{gathered}\begin{bmatrix} [M_{vv}] & 0 \\ 0 & [M_{ww}] \end{bmatrix} \begin{Bmatrix} \{\ddot{q}_v(t)\} \\ \{\ddot{q}_w(t)\} \end{Bmatrix} \\ + \begin{bmatrix} [K_{vu}] \\ [K_{wu}] \end{bmatrix} [K_{uu}]^{-1} \left(\{P_u(t)\} - \begin{bmatrix} [K_{uv}] [K_{uw}] \end{bmatrix} \begin{Bmatrix} \{q_v(t)\} \\ \{q_w(t)\} \end{Bmatrix} \right) \\ + \begin{bmatrix} [K_{vv}] & [K_{vw}] \\ [K_{wv}] & [K_{ww}] \end{bmatrix} \begin{Bmatrix} \{q_v(t)\} \\ \{q_w(t)\} \end{Bmatrix} = \begin{Bmatrix} \{P_v(t)\} \\ \{P_w(t)\} \end{Bmatrix}\end{gathered} \tag{3.72}$$

Finally, since the external pressure only acts in the w direction, it is possible to write:

$$\begin{gathered}\begin{bmatrix} [M_{vv}] & 0 \\ 0 & [M_{ww}] \end{bmatrix} \begin{Bmatrix} \{\ddot{q}_v(t)\} \\ \{\ddot{q}_w(t)\} \end{Bmatrix} \\ - \begin{bmatrix} [K_{vu}] \\ [K_{wu}] \end{bmatrix} [K_{uu}]^{-1} \begin{bmatrix} [K_{uv}] [K_{uw}] \end{bmatrix} \begin{Bmatrix} \{q_v(t)\} \\ \{q_w(t)\} \end{Bmatrix} \\ + \begin{bmatrix} [K_{vv}] & [K_{vw}] \\ [K_{wv}] & [K_{ww}] \end{bmatrix} \begin{Bmatrix} \{q_v(t)\} \\ \{q_w(t)\} \end{Bmatrix} = \begin{Bmatrix} 0 \\ \{P_w(t)\} \end{Bmatrix}\end{gathered} \tag{3.73}$$

3.5.2 Neglecting Membrane Inertia

Neglecting longitudinal, $[M_{uu}]$, and tangential , $[M_{vv}]$, components of inertia:

$$\begin{gathered}\begin{bmatrix} 0 & 0 & 0 \\ 0 & 0 & 0 \\ 0 & 0 & [M_{ww}] \end{bmatrix} \begin{Bmatrix} \{\ddot{q}_u(t)\} \\ \{\ddot{q}_v(t)\} \\ \{\ddot{q}_w(t)\} \end{Bmatrix} \\ + \begin{bmatrix} [K_{uu}] & [K_{uv}] & [K_{uw}] \\ [K_{vu}] & [K_{vv}] & [K_{vw}] \\ [K_{wu}] & [K_{wv}] & [K_{ww}] \end{bmatrix} \begin{Bmatrix} \{q_u(t)\} \\ \{q_v(t)\} \\ \{q_w(t)\} \end{Bmatrix} = \begin{Bmatrix} \{P_u(t)\} \\ \{P_v(t)\} \\ \{P_w(t)\} \end{Bmatrix}\end{gathered} \tag{3.74}$$

It is possible to separate the problem into two distinct equations, Equation (3.75) and Equation (3.76):

$$\begin{gathered}[M_{ww}] \{\ddot{q}_w(t)\} + \begin{bmatrix} [K_{wu}] [K_{wv}] \end{bmatrix} \begin{Bmatrix} \{q_u(t)\} \\ \{q_v(t)\} \end{Bmatrix} \\ + [K_{ww}] \{q_w(t)\} = \{P_w(t)\}\end{gathered} \tag{3.75}$$

$$\begin{bmatrix} [K_{uu}] & [K_{uv}] \\ [K_{vu}] & [K_{vv}] \end{bmatrix} \begin{Bmatrix} \{q_u(t)\} \\ \{q_v(t)\} \end{Bmatrix} + \begin{bmatrix} [K_{uw}] \\ [K_{vw}] \end{bmatrix} \{q_w(t)\} = \begin{Bmatrix} \{P_u(t)\} \\ \{P_v(t)\} \end{Bmatrix} \tag{3.76}$$

Isolating the terms $\{q_u(t)\}$ and $\{q_v(t)\}$:

$$\left\{ \begin{array}{c} \{q_u(t)\} \\ \{q_v(t)\} \end{array} \right\} = \left[\begin{array}{cc} [K_{uu}] & [K_{uv}] \\ [K_{vu}] & [K_{vv}] \end{array} \right]^{-1} \left(\left\{ \begin{array}{c} \{P_u(t)\} \\ \{P_v(t)\} \end{array} \right\} - \left[\begin{array}{c} [K_{uw}] \\ [K_{vw}] \end{array} \right] \{q_w(t)\} \right) \tag{3.77}$$

Recalling the Equation (3.75), substituting $\{q_u(t)\}$ and $\{q_v(t)\}$:

$$\begin{array}{c} [M_{ww}]\{\ddot{q}_w(t)\} \\ + \left[\begin{array}{cc} [K_{wu}] & [K_{wv}] \end{array} \right] \left[\begin{array}{cc} [K_{uu}] & [K_{uv}] \\ [K_{vu}] & [K_{vv}] \end{array} \right]^{-1} \left(\left\{ \begin{array}{c} \{P_u(t)\} \\ \{P_v(t)\} \end{array} \right\} - \left[\begin{array}{c} [K_{uw}] \\ [K_{vw}] \end{array} \right] \{q_w(t)\} \right) \\ + [K_{ww}]\{q_w(t)\} = \{P_w(t)\} \end{array} \tag{3.78}$$

Finally, since the external pressure only acts in the w direction, it is possible to write:

$$\begin{array}{c} [M_{ww}]\{\ddot{q}_w(t)\} - \left[\begin{array}{cc} [K_{wu}] & [K_{wv}] \end{array} \right] \left[\begin{array}{cc} [K_{uu}] & [K_{uv}] \\ [K_{vu}] & [K_{vv}] \end{array} \right]^{-1} \left[\begin{array}{c} [K_{uw}] \\ [K_{vw}] \end{array} \right] \{q_w(t)\} \\ + [K_{ww}]\{q_w(t)\} = \{P_w(t)\} \end{array} \tag{3.79}$$

3.6. Force Modelling

The electrostatic interaction between the CNT and the gate beneath often acts as the actuator for CNT-based resonators (as presented in Figure 3.1). The CNT is specifically subjected to an applied biased voltage (with respect to the gate), which produces extra charges on the CNT and results in an electrostatic attraction between the CNT and the gate. The static and dynamic responses of the CNT are represented by the DC and AC components of the applied voltage, respectively.

To compute the electrostatic forces acting on the CNT, a capacitance model was used [116]. Approximating the nanotube to a perfect cylindrical conductor it is possible to assume that the voltage is a constant along its length. The capacitance for two parallel cylinders with opposite charges is given in [117]. This problem has the same electric field as a cylinder over a ground plane because the existence of the ground plane is equivalent to the existence of a fictitious cylinder with an opposing charge reflected in the plane. Then, the capacitance per unit length for the cylinder over the conductive ground plane is given by:

$$C(b) = \frac{\pi\varepsilon_0}{\log\left[1 + \frac{b}{R} + \sqrt{\left(\frac{b}{R}+1\right)^2 - 1}\right]} \tag{3.80}$$

where R corresponds to the radius of the cylinder/conductor b is the gap between the conductor and the ground plane and ε_0 is the permittivity of vacuum.

The electrostatic energy per unit length is given by:

$$\frac{E_{elec}}{l} = \frac{CV^2}{2} \tag{3.81}$$

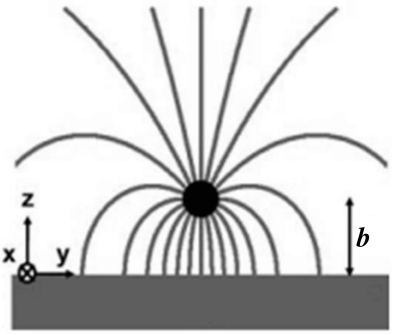

Fig. 3.3. Schematic of the field lines of electrostatic potential induced in the CNT by the gate; reprinted from [118] with permission from John Wiley and Sons

where V is the voltage applied to the cylinder. This way, the electrostatic force per unit length is given by:

$$F_{elec} = \frac{\mathrm{d}\left(\frac{E_{elec}}{l}\right)}{\mathrm{d}b} = -\frac{\pi\varepsilon_0 V^2}{R\sqrt{\frac{b(b+2R)}{R^2}}\log^2\left[1+\frac{b}{R}+\sqrt{\frac{b(b+2R)}{R^2}}\right]}. \tag{3.82}$$

This approach results in a simplified model for the electrostatic forces per unit length of the tube. However, when using this force expression in a shell model it is necessary to distribute the force through the circumferential direction.

The electrostatic force is a pressure field resultant of an electric field (Figure 3.3) existing between two different charges. These fields are proportional to each other, having the same direction at the same point. An electric field is always perpendicular to the charges, so, it is possible to conclude that the electrostatic force acting on the CNT shell will always be perpendicular to the surface of the tube. This way, the electrostatic force will contribute only to the radial direction of the external pressures applied to the cylinder (p_w). This radial pressure is not uniform in a section of the CNT. The closest the charge is to the ground plane, the greatest will be the attracting force. Considering a uniform charge distribution throughout the cylinder, it can be inferred that the infinitesimal force acting on a tiny area element of the shell will increase as the distance between the element and the ground plane decreases. The exact circumferential distribution depends on the proximity of each section to the ground plane and the way it is deformed. It would be necessary to solve Maxwell's Equations each timestep to solve this dependency.

F_{elec} is the resultant component of the force of each section of the shell, being perpendicular to the gate. Taking this into account, and considering the Equation (3.82) it is possible to write:

$$F_{elec} = \int_0^{2\pi} p_w R d\theta \tag{3.83}$$

To satisfy all the previous statements a simplified expression for the pressure field on the shell is proposed:

$$p_w = -\frac{\sin(\theta/2)\pi\varepsilon_0 V^2}{4R^2\sqrt{\frac{b(b+2R)}{R^2}}\log^2\left[1+\frac{b}{R}+\sqrt{\frac{b(b+2R)}{R^2}}\right]} \tag{3.84}$$

and, considering that the voltage applied V is a sum of a constant component, V_{DC}, and an alternating voltage whose amplitude is V_{AC} and frequency ω_{AC}

$$V(t) = V_{DC} + V_{AC}sin(\omega_{AC}t) \tag{3.85}$$

we can finally write:

$$p_w(t,\theta,b) = -\frac{\sin(\theta/2)\pi\varepsilon_0(V_{DC}+V_{AC}sin(\omega_{AC}t))^2}{4R^2\sqrt{\frac{b(b+2R)}{R^2}}\log^2\left[1+\frac{b}{R}+\sqrt{\frac{b(b+2R)}{R^2}}\right]} \tag{3.86}$$

The DC voltage functions as a tuning parameter, controlling the CNT resonators' static deflection's amplitude, which affects the system's natural frequency [67]. By applying a harmonic component of voltage the system will oscillate around a central deflected position.

The expression presented represents a first approach for modeling the electrostatic interaction between nanotubes and a flat rigid electrode. This approach must be improved in the future.

3.7. Time Integration: Algorithm

To integrate the equations of motion in time, Newmark's method ($\gamma = 1/2$ and $\beta = 1/4$) was used. Being an implicit integration method it facilitated the implementation of the nonlinear electrostatic force. Its unconditional stability and second-order accuracy were also characteristics that helped with the choice.

The inputs of the algorithm are the generalized mass, stiffness, and damping matrix. The system's initial conditions are also required. Regarding the force, the first approach was to integrate and write a generalized vector which would just depend on the generalized displacement vector and time. However, due to its complex relation to displacement, this was not possible to implement. So, for each different time, and displacement input, the generalized force vector is numerically integrated and assembled. This approach revealed to have a lot of computational load associated.

Algorithm 1 Newmark's Method - Part 1

INPUT:

- Mechanical Properties; compute $[M], [K]$ and $[C]$
- Initial Conditions at $(t = 0)$: $\{q\}^0$ and $\{\dot{q}\}^0$
- Pressure Expression (3.86): $p_w(t, \theta, b)$

OUTPUT:

- Displacement, Velocity, Acceleration in time: $\{q\}^t$, $\{\dot{q}\}^t$ and $\{\ddot{q}\}^t$

Preliminary calculations:

$$\{\ddot{q}\}^0 \leftarrow [M]^{-1}\left(\{f\}^0 - [C]\{\dot{q}\}^0 - [K]\{q\}^0\right) \tag{3.87}$$

▷ Calculate acceleration at the instant $t = 0$

$$\begin{gathered}\gamma \leftarrow \frac{1}{2}, \quad \beta \leftarrow \frac{1}{4} \\ a_0 \leftarrow \frac{1}{\beta(\Delta t)^2}, \quad a_1 \leftarrow \frac{\gamma}{\beta \Delta t}, \quad a_2 \leftarrow \frac{1}{\beta \Delta t}, \quad a_3 \leftarrow \frac{1}{2\beta} - 1 \\ a_4 \leftarrow \frac{\gamma}{\beta} - 1, \quad a_5 \leftarrow \frac{\Delta t}{2}\left(\frac{\gamma}{\beta} - 2\right), \quad a_6 \leftarrow \Delta t(1-\gamma), \quad a_7 \leftarrow \gamma \Delta t\end{gathered} \tag{3.88}$$

▷ Determine the time step and constants

$$[K]_{eff} \leftarrow [K] + a_0[M] + a_1[C] \tag{3.89}$$

▷ Compute effective stiffness matrix

$\{\Delta q\} \leftarrow 0$

3.8. Final Remarks

In the current chapter, a model for a clamped-clamped single-wall carbon nanotube under electrostatic actuation was developed. This is based on the thin shell theory of Sanders-Koiter, which lays in the principles of Kirchhoff-Love.

After deducing the strong form of the equations of motion for a thin shell (using the Galerkin method), a p-version finite element method was applied to discretize the domain. Starting with Hamilton's principle, and then integrating by parts, the weak formulation was achieved. Then the FEM matrices were assembled and the problem was written in its matrix form. Aiming to reduce computational efforts, two models that neglect different components of the membrane inertia were derived.

Following, the focus was to model the electrostatic interaction between the charged

Algorithm 2 Newmark's Method - Part 2

For each time increment:

$\{q\}^{t+\Delta t} \leftarrow \{q\}^t + \{\Delta q\}$

▷ Estimate Displacement at $t+\Delta t$

while Convergence of $\{q\}^{t+\Delta t}$ is not achieved **do**

$$\begin{aligned}\{P\}^{t+\Delta t}{}_{eff} \leftarrow \{P\}^{t+\Delta t} &+ [M]\left(a_0\{q\}^t + a_2\{\dot{q}\}^t + a_3\{\ddot{q}\}^t\right) \\ &+ [C]\left(a_1\{q\}^t + a_4\{\dot{q}\}^t + a_5\{\ddot{q}\}^t\right)\end{aligned} \tag{3.90}$$

▷ Effective load at $t+\Delta t$

$$\{q\}^{t+\Delta t} \leftarrow [K]_{eff}{}^{-1}\{P\}^{t+\Delta t}{}_{eff} \tag{3.91}$$

▷ Displacement at $t+\Delta t$

end while

$\{\ddot{q}\}^{t+\Delta t} \leftarrow a_0\left(\{q\}^{t+\Delta t} - \{q\}^t\right) - a_2\{\dot{q}\}^t - a_3\{\dot{q}\}^t$
$\{\dot{q}\}^{t+\Delta t} \leftarrow \{\dot{q}\}^t + a_6\{\ddot{q}\}^t + a_7\{\ddot{q}\}^{t+\Delta t}$

▷ Acceleration and velocity at $t+\Delta t$

$\{\Delta q\} \leftarrow \{q\}^{t+\Delta t} - \{q\}^t$

Next Time-step

CNT and a ground gate. For that, a simplified, capacitive-based model was used. Finally, the time integration algorithm used is presented.

It is important, before validation and implementation of the model to recall its limitations and assumptions. The CNT material is assumed to be homogeneous and isotropic and even though it is a common practice in the literature this may induce errors in certain analyses, mainly in higher modes. Neglecting the non-linear terms in the formulation of the shell model comes with the cost of incapability to model high displacement deformations. Another existing limitation is the simplified model of the force and its distribution through the shell. Taking all of these statements into consideration, in the next chapter, we will try to validate the model using small deformations, choosing lower values of voltage, and always being aware of the limitations of the model.

Chapter 4

Model Validation and Results

4.1. Introduction

In this chapter, the previously formulated model will be tested and compared to data presented in the literature.

First, a convergence analysis will take place, to analyze and decide the number of shape functions needed to reliably compute natural frequencies and modes shapes, for all full and reduced models developed. Then a comparison between natural frequency values obtained through the developed models will be done as well as a validation using the literature data. Finally, a wide range of mode shapes obtained using the developed shell model is documented. This variability demonstrates the versatility of using a shell model instead of a beam model, still needing less computational resources, and being much simpler than a molecular dynamic approach.

4.2. Numerical Results: Natural Frequencies Convergence

It is crucial to define the material's properties before validating the model. As already stated the CNT will be considered isotropic and elastic in exchange for simplicity of the model. That being said, it will be necessary to deduce the equivalent material's properties.

Different authors worked both with molecular dynamics and experiments with CNTs and documented different isolated "effective" elastic properties of these structures, not defining a specific set of parameters. When using an isotropic and uniform shell model these "effective" properties can't be directly used in the developed model and "equivalent" elastic properties must be deduced. Such a procedure was done by Yakobson et al. in [103], from the principle that the elastic properties of a two-dimensional hexagonal structure are isotropic. This led to the approximation that a uniform shell can be characterized by two elastic parameters: flexural rigidity (D) and resistance to membrane stretching (C).

Semi-empirical methods are used to establish flexural rigidity and resistance to membrane stretching in a way that the behavior obtained with the continuum model under strain matches the molecular dynamics experiments [103].

All parameters used to parameterize the CNT for the following subsections are presented in Table 4.1.

Table 4.1. Equivalent elastic properties of a SWCNT [103]

Equivalent thickness h [nm]	0.066
Equivalent Young's modulus E [TPa]	5.5
Equivalent Poisson's ratio ν	0.19
Equivalent mass density ρ [Kg/m^3]	11.7

The present section intends to: first, analyze the convergence of natural frequencies of a clamped-clamped SWCNT using the developed shell model with the increase of the number of shape functions; second, repeat this process for the reduced models (neglecting membrane and longitudinal inertia); third, compare the calculated values of natural frequencies and conclude about the influence of membrane inertia on the proposed problem. The same values will finally be compared to a MD solution. For the present study, an armchair SWCNT with a chirality of (r,s)=(5, 5) and a length-to-diameter ratio of $\chi = l/D$ =10.34 was used.

Different numbers of shape functions are employed. In p-version finite element method with a hierarchic set of shape functions, the eigenvalues converge to the exact solution from above, as the number of shape functions is increased. Relying on this statement, the number of shape functions was increased to achieve convergence. The number of shape functions considered for each degree of freedom (u, v, and w) was the same and is represented below as N.

4.2.1 Full Model

Considering the full model (with membrane inertia), presented in the Equation (3.65), the natural frequencies and natural modes of vibration of the system were computed following an eigenvalue approach. The first four beam-like natural modes and corresponding frequencies were then selected for further analysis.

The evolution of the value of the natural frequency (ω) of the first four beam-like modes is represented in Figure 4.1, against the number of shape functions used (N). The convergence of the four natural frequencies is evident. Table 4.2 presents the values of natural frequencies of the same four modes for different values of N, as well as a column with the error evolution with the increase of the number of N.

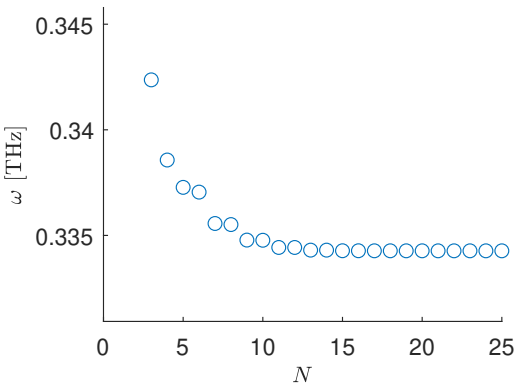

(a) First beam-like mode

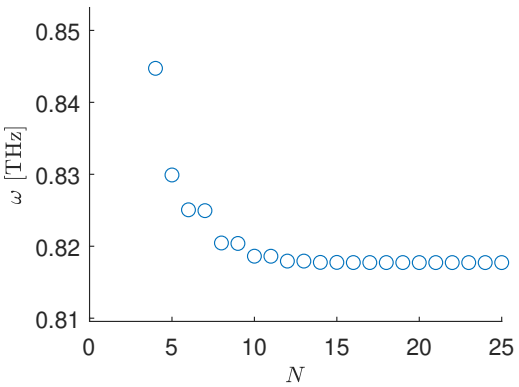

(b) Second beam-like mode

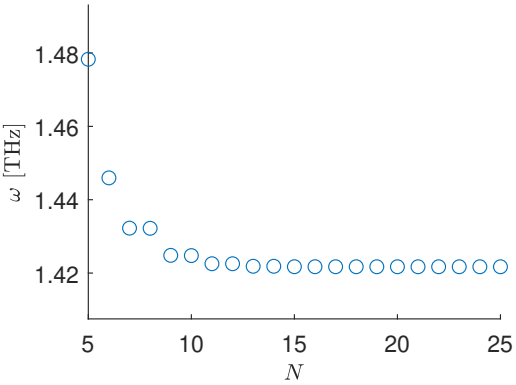

(c) Third beam-like mode

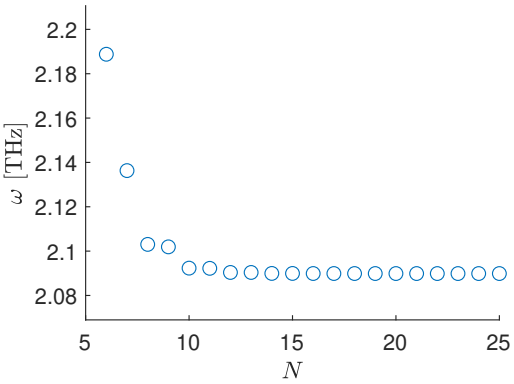

(d) Fourth beam-like mode

Fig. 4.1. Convergence study of beam-like modes' frequencies - full model

Table 4.2. Relative error progression in the convergence study of natural frequencies [THz] of beam-like modes - full model

N	First	Diff.(%)	Second	Diff.(%)	Third	Diff.(%)	Fourth	Diff.(%)
3	0.3424	2.42 %	-	-	-	-	-	-
4	0.3386	1.29 %	0.8447	3.30 %	-	-	-	-
5	0.3373	0.90 %	0.8299	1.49 %	1.4783	3.98 %	-	-
6	0.3371	0.83 %	0.8251	0.90 %	1.4460	1.70 %	2.1888	4.73 %
7	0.3356	0.39 %	0.8249	0.88 %	1.4322	0.74 %	2.1363	2.22 %
8	0.3355	0.37 %	0.8205	0.33 %	1.4322	0.74 %	2.1030	0.63 %
9	0.3348	0.15 %	0.8204	0.33 %	1.4248	0.22 %	2.1019	0.58 %
10	0.3348	0.15 %	0.8186	0.11 %	1.4248	0.21 %	2.0923	0.12 %
11	0.3344	0.05 %	0.8186	0.11 %	1.4225	0.06 %	2.0922	0.11 %
12	0.3344	0.05 %	0.8179	0.03 %	1.4225	0.06 %	2.0904	0.02 %
13	0.3343	0.01 %	0.8179	0.03 %	1.4219	0.01 %	2.0904	0.02 %
14	0.3343	0.01 %	0.8178	0.00 %	1.4218	0.01 %	2.0899	0.00 %
15	0.3343	0.00 %	0.8178	0.00 %	1.4217	0.00 %	2.0899	0.00 %

Relying on the fact that increasing the number of shape functions in a p-version finite element approach will eventually lead to the exact solution, the convergence of the natural frequencies' values is analyzed. The frequency values computed with $N = 25$ were used as a reference to calculate the error in the following analysis. It can be observed that the model regularly converges. The model has an error lower than 0.2% in the value of the natural frequency of the first four beam-like modes starting at the value of $N = 11$ and forward.

4.2.2 Reduced Model - Neglecting Longitudinal Inertia

Considering the reduced model in which the longitudinal inertia is neglected, presented in the Equation (3.73), the natural frequencies and natural modes of vibration of the system were computed following an eigenvalue approach. The first four beam-like natural modes

and corresponding frequencies were then selected for further analysis.

The evolution of the value of the natural frequency of the first four beam-like modes is represented in Figure 4.2, against the number of shape functions used (N). The convergence of the four natural frequencies is evident. Table 4.3 presents the values of natural frequencies of the same four modes for different values of N, as well as a column with the error evolution with the increase of the number of N.

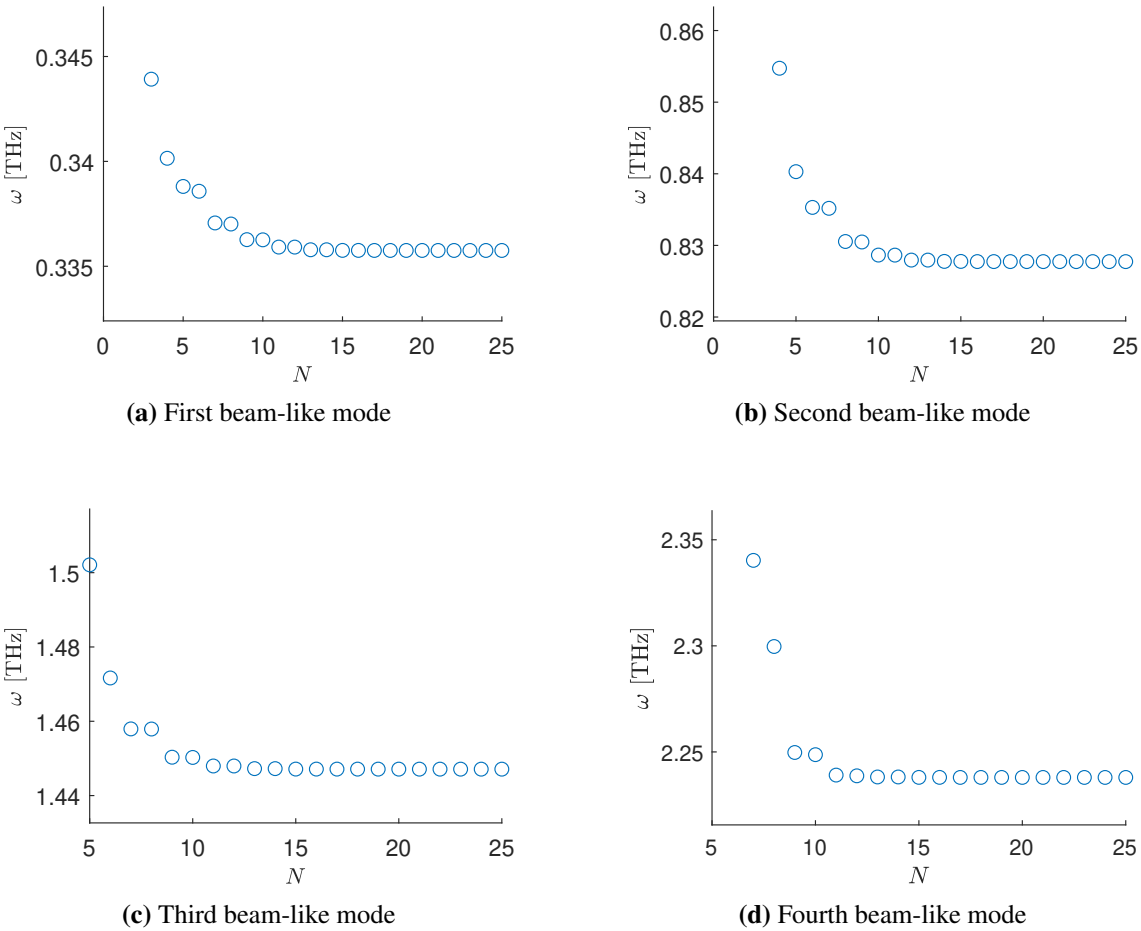

(a) First beam-like mode

(b) Second beam-like mode

(c) Third beam-like mode

(d) Fourth beam-like mode

Fig. 4.2. Convergence study of beam-like modes' frequencies - reduced model neglecting longitudinal inertia

As already performed before, the convergence was analyzed relying on the fact that increasing the number of shape functions in a p-version finite element approach will eventually lead to the exact solution. The frequency values computed with $N = 25$ were used as a reference to calculate the error. Similar results were obtained. It can be observed that the model regularly converges. The model has an error lower than 0.2% in the value of the natural frequency of the first four beam-like modes starting at the value of $N = 11$ and forward.

Table 4.3. Relative error progression in the convergence study of natural frequencies [THz] of beam-like modes - reduced model neglecting longitudinal inertia

N	First	Diff.(%)	Second	Diff.(%)	Third	Diff.(%)	Fourth	Diff.(%)
3	0.3439	2.43 %	-	-	-	-	-	-
4	0.3401	1.31 %	0.8547	3.26 %	-	-	-	-
5	0.3388	0.91 %	0.8403	1.52 %	1.5021	3.80 %	-	-
6	0.3386	0.84 %	0.8353	0.91 %	1.4717	1.70 %	-	-
7	0.3371	0.39 %	0.8352	0.90 %	1.4579	0.75 %	2.3403	4.57 %
8	0.3370	0.38 %	0.8305	0.34 %	1.4579	0.75 %	2.2997	2.76 %
9	0.3363	0.15 %	0.8305	0.33 %	1.4503	0.22 %	2.2497	0.53 %
10	0.3363	0.15 %	0.8286	0.11 %	1.4503	0.22 %	2.2487	0.48 %
11	0.3359	0.05 %	0.8286	0.11 %	1.4480	0.06 %	2.2391	0.05 %
12	0.3359	0.05 %	0.8279	0.03 %	1.4480	0.06 %	2.2387	0.03 %
13	0.3358	0.01 %	0.8279	0.03 %	1.4473	0.01 %	2.2382	0.01 %
14	0.3358	0.01 %	0.8278	0.00 %	1.4473	0.01 %	2.2382	0.01 %
15	0.3358	0.00 %	0.8278	0.00 %	1.4471	0.00 %	2.2380	0.00 %

4.2.3 Reduced Model - Neglecting Membrane Inertia

Considering the reduced model in which all the membrane components of inertia are neglected, presented in the Equation (3.79), the natural frequencies and natural modes of vibration of the system were computed following an eigenvalue approach. The first four beam-like natural modes and corresponding frequencies were then selected for further analysis.

The evolution of the value of the natural frequency of the first four beam-like modes is represented in Figure 4.3, against the number of shape functions used (N). The convergence of the four natural frequencies is evident. Table 4.4 presents the values of natural frequencies of the same four modes for different values of N, as well as a column with the error evolution with the increase of the number of N.

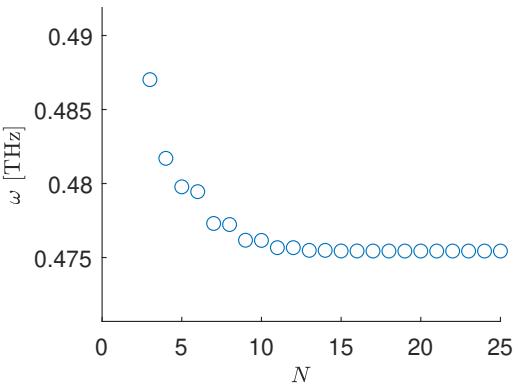

(a) First beam-like mode

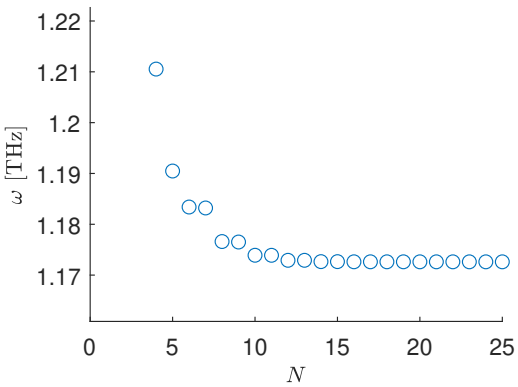

(b) Second beam-like mode

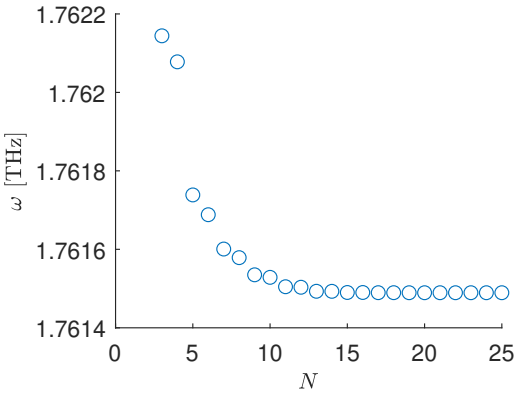

(c) Third beam-like mode

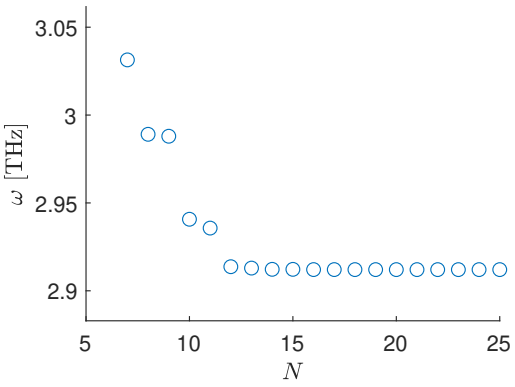

(d) Fourth beam-like mode

Fig. 4.3. Convergence study of beam-like modes' frequencies - reduced model neglecting membrane inertia

Table 4.4. Relative error progression in the convergence study of natural frequencies [THz] of beam-like modes - reduced model neglecting membrane inertia

N	First	Diff.(%)	Second	Diff.(%)	Third	Diff.(%)	Fourth	Diff.(%)
3	0.4870	2.44 %	-	-	-	-	-	-
4	0.4817	1.32 %	1.2105	3.23 %	-	-	-	-
5	0.4798	0.91 %	1.1905	1.52 %	1.7617	0.01 %	-	-
6	0.4795	0.84 %	1.1834	0.92 %	1.7617	0.01 %	-	-
7	0.4773	0.39 %	1.1832	0.90 %	1.7616	0.01 %	3.0314	3.03 %
8	0.4772	0.38 %	1.1766	0.34 %	1.7616	0.01 %	2.9891	2.99 %
9	0.4762	0.15 %	1.1765	0.33 %	1.7615	0.00 %	2.9880	2.99 %
10	0.4762	0.15 %	1.1739	0.11 %	1.7615	0.00 %	2.9407	2.94 %
11	0.4757	0.05 %	1.1739	0.11 %	1.7615	0.00 %	2.9357	2.94 %
12	0.4757	0.05 %	1.1729	0.03 %	1.7615	0.00 %	2.9137	2.91 %
13	0.4755	0.01 %	1.1729	0.03 %	1.7615	0.00 %	2.9129	2.91 %
14	0.4755	0.01 %	1.1727	0.00 %	1.7615	0.00 %	2.9122	2.91 %
15	0.4754	0.00 %	1.1727	0.00 %	1.7615	0.00 %	2.9122	2.91 %

Once again, relying on the fact that increasing the number of shape functions in a p-version finite element approach will eventually lead to the exact solution, the convergence of the natural frequencies' values was analyzed. The frequency values computed with $N = 25$ were used as a reference to calculate the error. Similar results as before were obtained and the model regularly converged. The model has an error lower than 0.2% in the value of the natural frequency of the first four beam-like modes starting at the value of $N = 11$ and forward.

4.2.4 Validation of the Models: Natural Frequencies Validation

To analyze the influence of neglecting membrane inertia and study the viability of using such models to predict the behavior of a CNT-resonator in a bridge configuration, the natural frequency values obtained before will be compared. The values are gathered in Table 4.5, as well as MD results from Duan et al. [5], for the same CNT configuration ((5, 5) armchair SWCNT doubly clamped and $\chi = l/D = 10.34$).

Table 4.5. Comparison of natural frequencies of beam-like modes of full model and reduced models with molecular dynamics results

	MD [5]	Full	Diff.(%)	No $[M_{uu}]$	Diff.(%)	No $[M_{uu}]$ and $[M_{vv}]$	Diff.(%)
ω_{b1}	0.336	0.3343	0.51 %	0.3358	0.07 %	0.4754	41.50 %
ω_{b2}	0.818	0.8177	0.03 %	0.8277	1.19 %	1.1726	43.35 %
ω_{b3}	1.417	1.4217	0.33 %	1.4471	2.13 %	1.7615	24.31 %
ω_{b4}	2.079	2.0899	0.52 %	2.2380	7.65 %	2.9121	40.07 %

These comparisons show that the developed model achieves excellent results in terms of natural frequencies (under 0.6% of error when compared to MD). Neglecting, totally the membrane inertia, the model becomes unreliable when calculating natural frequencies. For the same mode of vibration, we generally get 40% higher values of natural frequency (complying with [115]). That being said, this approach will not be further employed.

When just the longitudinal inertia is neglected, the results obtained are more interesting. In the first 4 modes, the error is no higher than 10% and the error of the frequency corresponding to the first mode is less than 0.5%. With this comparison, it is possible to validate the proposed model and the usage of a reduced model to represent the same behaviour.

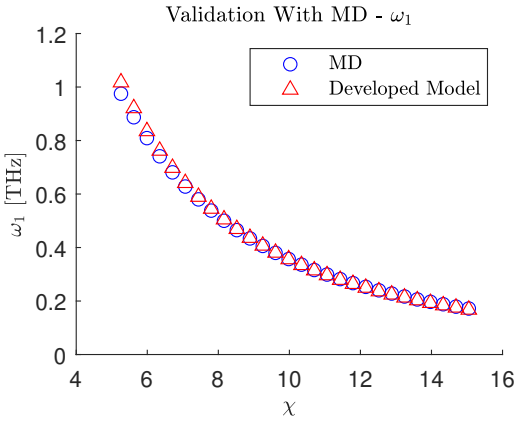

(a) First beam-like mode

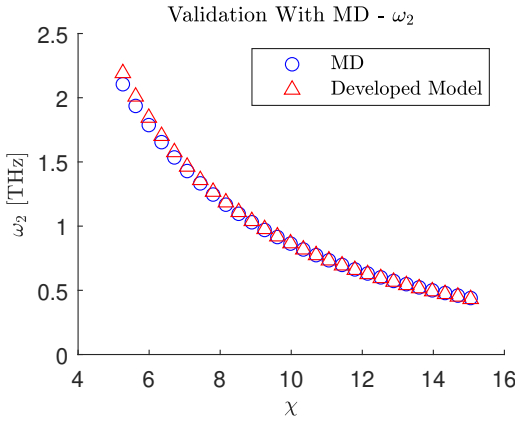

(b) Second beam-like mode

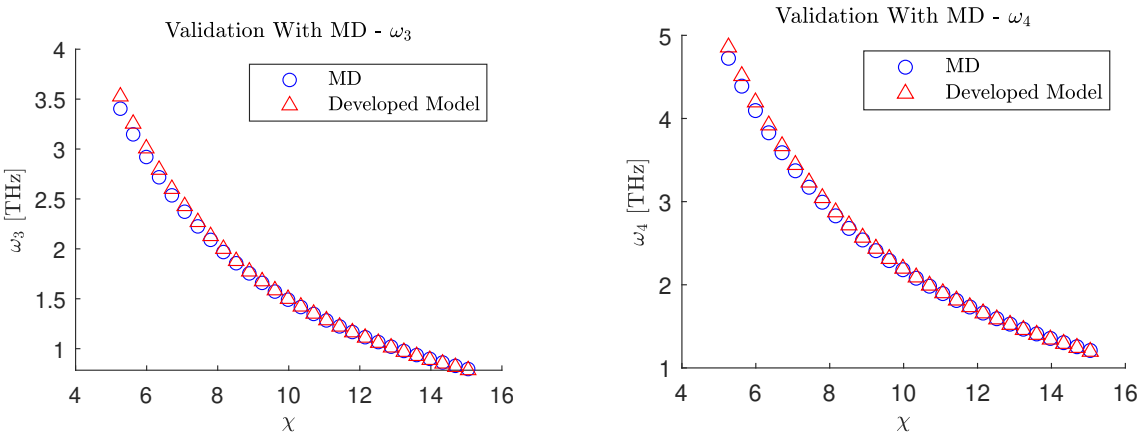

(c) Third beam-like mode

(d) Fourth beam-like mode

Fig. 4.4. Comparison with MD [5] of beam-like modes' natural frequency - full model

As the next step to validate the elastic model, the natural frequencies corresponding to the first four beam-like modes were extensively compared with Molecular Dynamics calculations performed by Duan [5] for a (5, 5) armchair doubly clamped SWCNT. The results are presented in Figure 4.4.

The results from the developed model are noticeably close to the ones proposed by Duan. It is possible to observe in the graphs that with the decrease in the aspect ratio (χ), the natural frequencies for all the analyzed modes tend to increase for both the shell model and MD results. The difference between both and so, the error of the model, decreases with the growth of the aspect ratio. This way, the error of the model is lower for higher aspect ratios. The maximum relative error in the fundamental natural frequency occurs for the minimum aspect ratio and it is 4%

For lower aspect ratios, the natural frequencies computed through the shell model are higher than the ones obtained with the Molecular Dynamics approach. There is a break-even point (defined by a specific value of aspect ratio) when this effect is reversed and the results from MD become greater than the proposed model. To improve the results of the model for lower aspect ratios, a nonlocal elasticity theory could be used with the compromise of increasing the complexity of the problem [119].

4.3. Natural Modes Shapes

Solving the eigenvalue problem we compute the natural frequencies of the CNT as well as the corresponding natural mode shape of vibration. The mode shapes presented in this section were calculated considering a doubly clamped armchair SWCNT with a chirality of (r,s)=(5, 5) and a length-to-diameter ratio of χ =10.34. The nomenclature based on the nodal arrangement of the mode of vibration as described in the work of [115] will be used to identify specific modes of vibration. In Appendix A a scheme explaining the used nomenclature is included, as well as a more extensive selection of natural mode shapes for the same CNT configuration.

Figure 4.5 the first four beam-like modes ($n = 1$) are presented. They consist of bending modes that present sine curves shape, similar to the deformed shape of a beam. The raising

of the natural frequency value with the increase of longitudinal wave number is an expected behavior and it is observed.

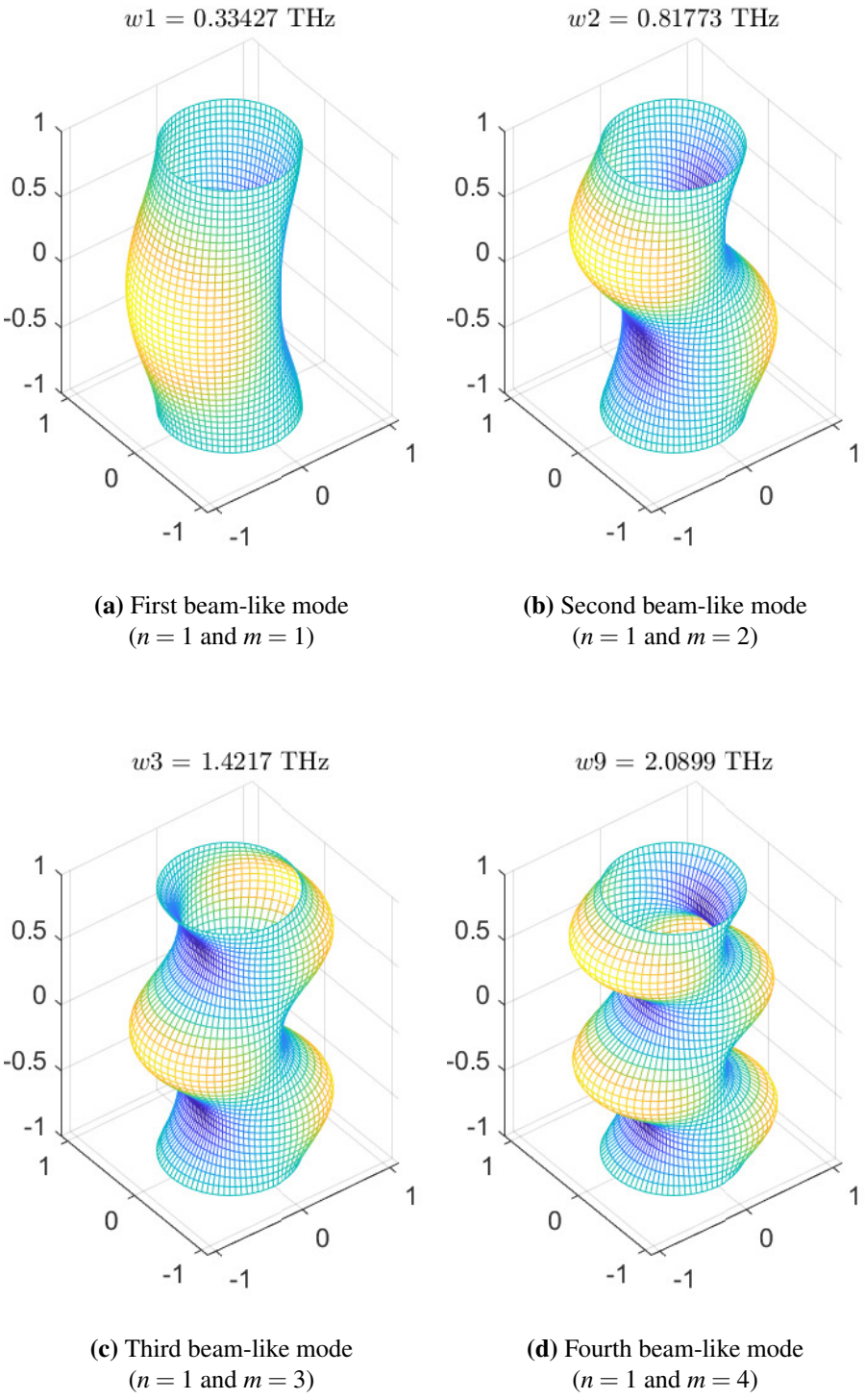

(a) First beam-like mode ($n = 1$ and $m = 1$)

(b) Second beam-like mode ($n = 1$ and $m = 2$)

(c) Third beam-like mode ($n = 1$ and $m = 3$)

(d) Fourth beam-like mode ($n = 1$ and $m = 4$)

Fig. 4.5. Beam-like mode shapes of a doubly clamped nanotube

The differentiating value of shell theory compared to a beam one is the circumferential behavior that the first one permits. For different circumferential nodal patterns, 4 radial

breathing models for $m = 1$ and $n > 0$ are represented in Figure 4.6. These modes were compared to the work of Georgantzinos et al. [120].

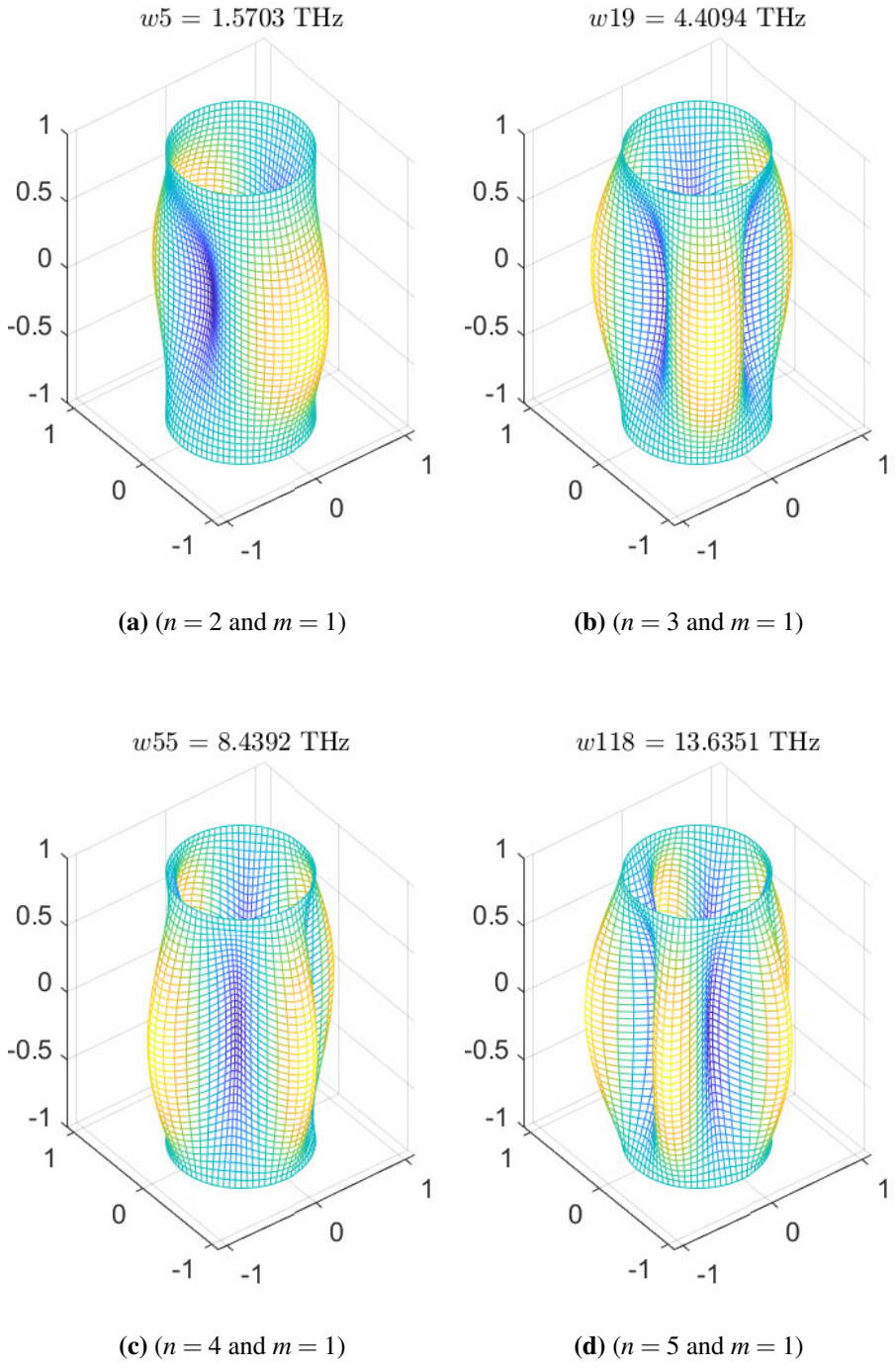

(a) ($n = 2$ and $m = 1$)

(b) ($n = 3$ and $m = 1$)

(c) ($n = 4$ and $m = 1$)

(d) ($n = 5$ and $m = 1$)

Fig. 4.6. Radial breathing mode shapes of a doubly clamped nanotube

4.4. Numerical Results: Steady State Response

Validation

The developed equations of motion were integrated in time using Newmak's method, thus obtaining the system's dynamic response. Small DC and AC voltage values were used to avoid large displacements, none covered by the thin shell theory employed. The study of the response to small amplitude voltages, and consequentially, low amplitude forces is important since it enables precise prediction of the resonance frequency in the linear regime. The resonance frequency is usually measured experimentally for CNTs driven by AC and DC loads [121].

To validate the results of the response in time, comparisons were done with the work developed in [72]. Farokhi presents a non-linear, size-dependent beam model to solve the problem analyzed in this thesis.

The dynamic behavior of the CNT oscillator under both DC and AC actuation was then analyzed.

The numerical results are obtained for the CNT resonator with $l = 3000$ [nm], $R = 1.0$ [nm], and $b = 300$ [nm]. The elastic properties and shell thickness used were the ones presented in Table 4.1 Regarding the damping of the system, a linear combination between the mass and stiffness matrix was considered - Rayleigh damping.

$$[C] = \alpha_c [M] + \beta_c [K] \tag{4.1}$$

In his work, Farokhi defines modal damping rations ($\zeta_n = \zeta_m = \zeta = 0.03$) based on the fundamental beam mode and the fundamental longitudinal mode of a rod with the same geometry. The Rayleigh damping constants were calculated in a way that modal damping ratios of the equivalent modes in the shell model are the same as in [72]. That being said, the constants were calculated using the following expressions [122]:

$$\alpha_c = \frac{2\zeta\omega_n\omega_m}{\omega_n + \omega_m} \tag{4.2}$$

$$\beta_c = \frac{2\zeta}{\omega_n + \omega_m} \tag{4.3}$$

where ω_n and ω_m correspond to the natural frequencies of the fundamental beam-like natural mode and the fundamental longitudinal natural mode of the shell. It is important to clarify that, although in the remainder of this dissertation, the frequency ω is presented in multiples of [Hz], in this case, the frequencies must be written in [rad/s]

The CNT was charged with $V_{DC} = 0.125$ [V] and $V_{AC} = 0.018$ [V] at a frequency ratio, $\Omega_{AC} = 1.15$, defined by ω_{AC}/ω_1. The computed position of the midpoint of the central section of the CNT ($\xi = 0$) is plotted in Figure 4.7. The displacement of this section's central point was computed as an average of the displacements of the extreme points of the section ($\theta = 0$ and $\theta = \pi$). In the first place, the DC voltage was applied and the system reached a non-trivial equilibrium configuration. The system begins its harmonic behavior and reaches a steady state of periodic vibration after a certain time. The maximum and minimum values of displacement in steady-state behavior were recorded and are presented in the graph. For the present case, and as a way to try validating the developed model,

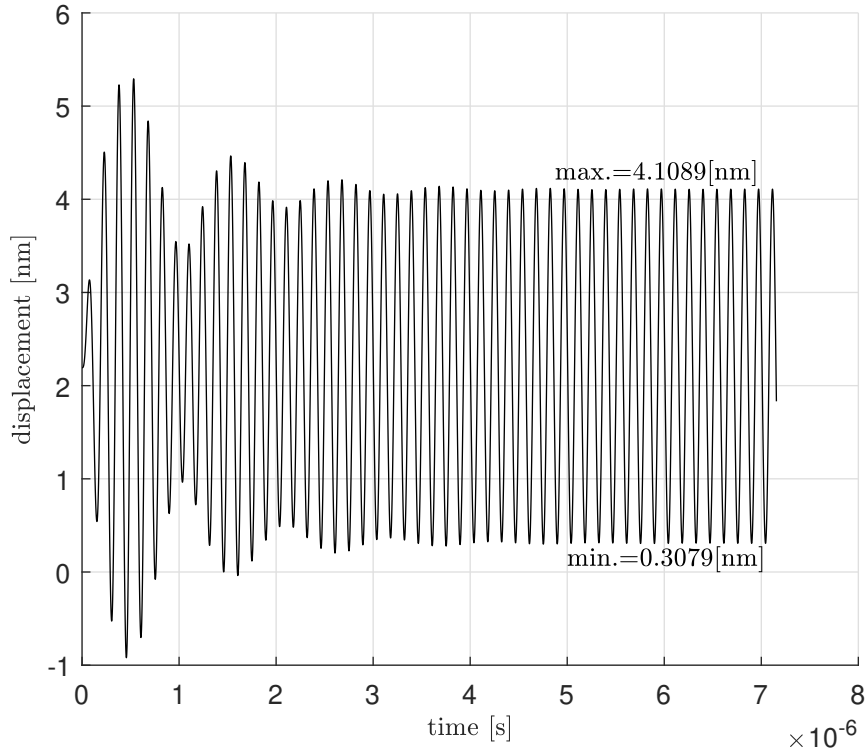

Fig. 4.7. Plot of the displacement in time of the midpoint of the section of the CNT under electrostatic actuation at $\xi = 0$ - obtained with the full model; $V_{DC} = 0.125$ [V], $V_{AC} = 0.018$ [V] and $\Omega_{AC} = 1.15$

the value of maximum displacement was compared with Farokhi's work. Compared to its non-local, non-linear beam model, the relative error was 6.8%.

Figure 4.8 represents the deformed shape of the analyzed CNT oscillator configuration. This deformed shape was obtained at the time in which the displacement of the central point of the CNT was maximum in steady-state conditions. The similarities of this deformed shape with the first beam-like mode shape are clear. However, according to the developed model, radial expansion also occurs under electrostatic actuation. This effect is disregarded when using a beam model. In Figure 4.9 a plot of the generalized velocity against the generalized coordinate number fifty-five (generalized coordinate related to a symmetrical shape function of the displacement *w*) is presented. The closed loop indicates that the system reached steady-state conditions.

The model was tested for more values of Ω_{AC} and the results were collected and compared in Table 4.6. The graphs of time response where this data was collected from are presented in Appendix B.

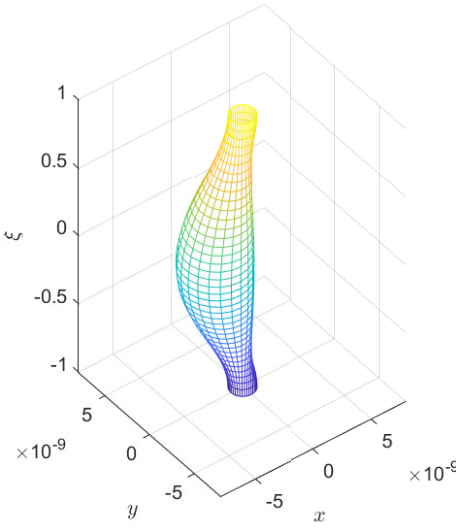

Fig. 4.8. Deformed shape of the CNT under electrostatic actuation at - obtained with the full model; $V_{DC} = 0.125$ [V], $V_{AC} = 0.018$ [V] and $\Omega_{AC} = 1.15$

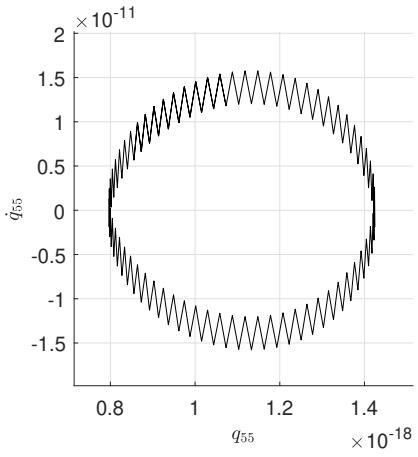

Fig. 4.9. Phase plot - generalized coordinate q_{55} - obtained with the full model; $V_{DC} = 0.125$ [V], $V_{AC} = 0.018$ [V] and $\Omega_{AC} = 1.15$

Table 4.6. Maximum value of displacement [nm] of the midpoint of the section of the CNT at $\xi = 0$ - Comparison between full model, the model neglecting $[M_{uu}]$ and the work of Farokhi. $V_{DC} = 0.125$ [V] and $V_{AC} = 0.018$ [V]

Ω_{AC}	Farokhi [72]	Full	Diff.(%)	No $[M_{uu}]$	Diff.(%)
0.75	4.35	3.67	15.6 %	3.68	15.4 %
0.80	4.63	3.99	13.8 %	3.99	13.8 %
1.10	4.65	5.02	7.96 %	5.02	7.96 %
1.15	4.41	4.11	6.80 %	4.11	6.80 %
1.20	4.21	3.63	13.8 %	3.62	14.0 %

Even though some differences are registered, the error that both proposed models present is reduced. The discrepancies may be justified because the model we are comparing with, is a non-linear size-dependent beam model. For the present geometry and loads the model of Farokhi displays a highly nonlinear resonant response encompassing both softening and hardening-type behaviours.

Number of shape functions

Due to excessive time of computation, the number of shape functions used in time integration had to be reduced to $N = 5$. Five shape functions were used instead of 11 as concluded in section 4.2. An analysis was done to evaluate the impact of this shape function reduction. Using the reduced model, for the same CNT oscillator configuration, time integration

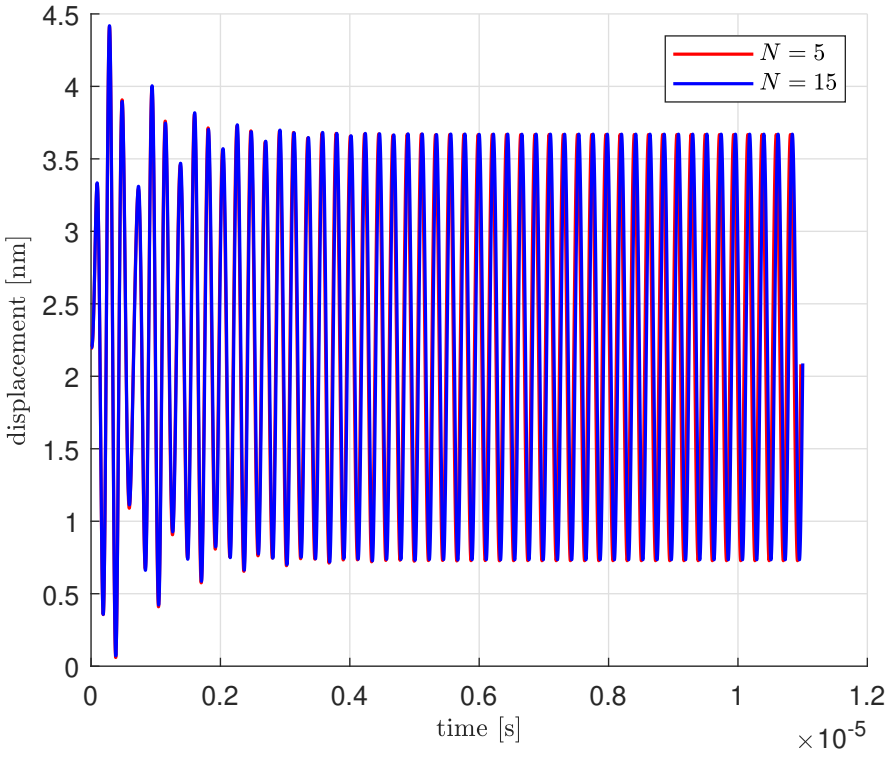

Fig. 4.10. Comparison between $N = 5$ and $N = 15$; plot of the displacement in time of the midpoint of the section of the CNT under electrostatic actuation at $\xi = 0$ - obtained with the full model; $V_{DC} = 0.125$ [V], $V_{AC} = 0.018$ [V] and $\Omega_{AC} = 0.75$

parameters, and actuation voltage and frequency, a comparison was performed. The results are presented in Figure 4.10 and more detailed, under steady-state conditions in Figure 4.11. By only changing the number of shape functions used in the model for both simulations it is possible to conclude on the influence of this number on the results.

Analysing both graphs it is clear that the differences between both responses in time are almost nonexistent. A small negative phase is introduced in the response of the model using five shape functions. This effect is more evident in Figure 4.11. The error in the amplitude of the movement is under 0.1%. That being said, we can conclude that the error committed by using five shape functions instead of a higher number is minute.

4.5. Final Remarks

The current chapter started with a convergence study. Its objective was to define the proper number of shape functions to use to perform a modal analysis for all three models developed in the previous chapter. After that, the models were compared to MD analysis and revealed promising results. The model that neglected membrane inertia was not considered reliable for the following studies. The full model and the model that neglected the longitudinal inertia were distinctly close to the MD simulations, mainly representing CNTs with high chirality. After that, the main relevant computed mode shapes were

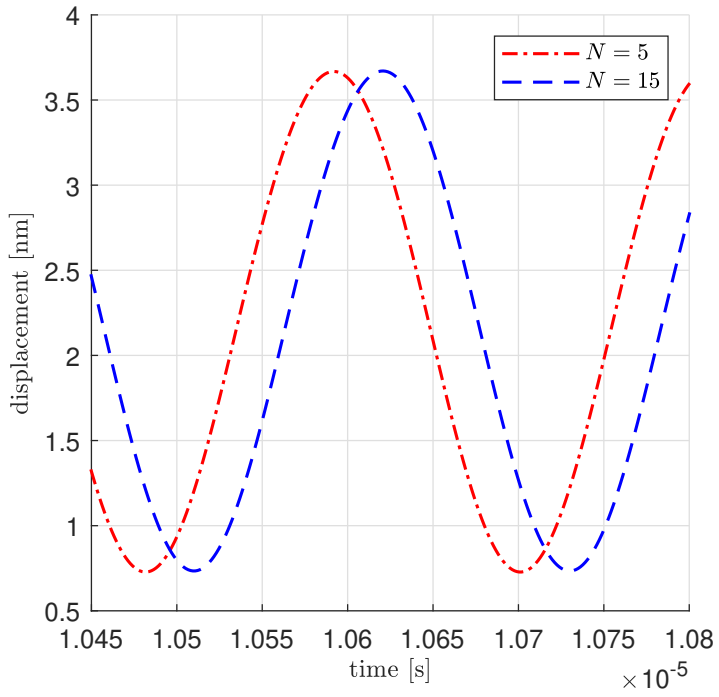

Fig. 4.11. Comparison between $N = 5$ and $N = 15$; Plot of the displacement in time of the midpoint of the section of the CNT under electrostatic actuation at $\xi = 0$ - obtained with the full model; $V_{DC} = 0.125$ [V], $V_{AC} = 0.018$ [V] and $\Omega_{AC} = 0.75$ - Steady-state regime

computed and compared to the literature. Finally, the electrostatic actuation was included. For a certain actuation, the amplitude results are compared to published works, and the model is validated. A study of the effect of using a reduced number of shape functions on the dynamic response was also done. This need emerged due to the high computational cost of the integrating approach.

Chapter 5

Study Of A CNT Resonator With An Attached Mass

5.1. Introduction

This Chapter is dedicated to the study of a CNT resonator with an attached concentrated mass (Figure 5.1). The objective is to model the behavior of a CNT resonator being used as a mass sensor.

As already presented in Chapter 2 different approaches can be used to detect the presence of an attached mass to a CNT.

One already applied method relies on the frequency shift that occurs to the value of the fundamental mode of vibration when a mass is attached to the CNT. This effect will be analyzed in this chapter. Comparisons between the response of the CNT to the same excitation will be performed.

We will start with the mathematical formulation of the problem, complementing the already determined equations of motion for a SWCNT to consider the concentrated mass. A p-version FEM approach will again be employed. The same methodology will be applied. Using the Galerkin method and then, integrating by parts the weak form of the equations of motion of the problem will be derived. The FEM matrices will then be assembled and the problem will be written in its matrix form. After that, the model will be compared to MD results presented in the literature, and mode shapes will be computed. Finally, the results of natural frequency and frequency shift will be analyzed as well as its steady-state response under capacitive actuation.

5.2. Model Development

Recalling the system of Equations (3.17) and introducing the term related to the concentrated mass using the Dirac delta function, as in [124], we get:

$$\begin{aligned} &\rho h\ddot{u}^0 + \frac{m_x}{R}\delta\left(x-x^p\right)\delta\left(\theta-\theta^p\right)\ddot{u}^0 \\ &-\frac{\partial N_{xx}}{\partial x} - \frac{1}{R}\frac{\partial N_{x\theta}}{\partial \theta} + \frac{1}{2R^2}\frac{\partial M_{x\theta}}{\partial \theta} = p_u \end{aligned} \tag{5.1}$$

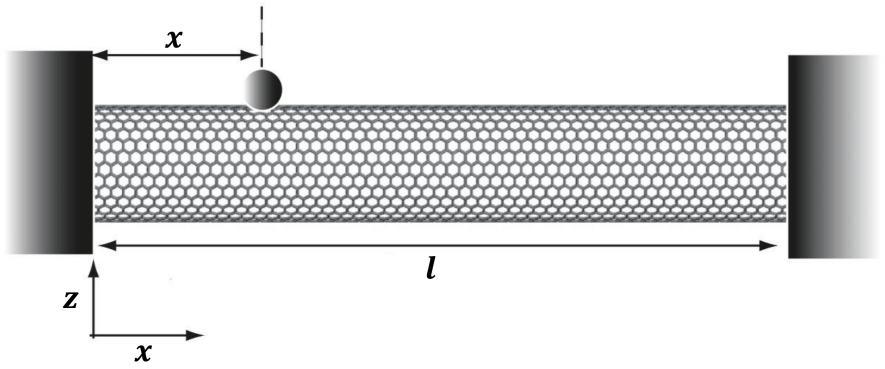

Fig. 5.1. Simplified schematic of a doubly clamped CNT-based resonator with an attached mass [123].

$$\begin{aligned}&\rho h\ddot{v}^0+\frac{m_x}{R}\delta\left(x-x^p\right)\delta\left(\theta-\theta^p\right)\ddot{v}^0\\&-\frac{1}{R}\frac{\partial N_{\theta\theta}}{\partial\theta}-\frac{\partial N_{x\theta}}{\partial x}-\frac{1}{R^2}\frac{\partial M_{\theta\theta}}{\partial\theta}-\frac{3}{2R}\frac{\partial M_{x\theta}}{\partial x}=p_v\end{aligned}\tag{5.2}$$

$$\begin{aligned}&\rho h\ddot{w}^0+\frac{m_x}{R}\delta\left(x-x^p\right)\delta\left(\theta-\theta^p\right)\ddot{w}^0\\&+\frac{N_{\theta\theta}}{R}-\frac{\partial^2 M_{xx}}{\partial x^2}-\frac{1}{R^2}\frac{\partial M_{\theta\theta}}{\partial\theta}-\frac{2}{R}\frac{\partial^2 M_{x\theta}}{\partial x\partial\theta}=p_w\end{aligned}\tag{5.3}$$

where $\frac{m_x}{R}$ corresponds to a mass per unit area referring to the attached mass. Dirac delta function is used to locally apply this mass. After integrating the term $\frac{m_x}{R}\delta\left(x-x^p\right)\delta\left(\theta-\theta^p\right)$ in the shell domain we obtain M_{conc}, the value of the concentrated mass. (x^p,θ^p) is the coordinate pair that defines the position of the concentrated mass on the shell domain. After changing the domain of integration from the variable x to ξ, (ξ^p,θ^p) defines the position of the mass in the new domain. The relation between x and ξ is recalled as:

$$\xi=\frac{2x-l}{l}\tag{5.4}$$

Applying Galerkin's Method we obtain:

$$\begin{aligned}&\int_0^{2\pi}\int_0^l f_r^u(x)f_s^u(\theta)\mathscr{L}_u^{CM}(x,\theta,t)\mathrm{d}xR\,\mathrm{d}\theta\\&\int_0^{2\pi}\int_0^l f_r^v(x)f_s^v(\theta)\mathscr{L}_v^{CM}(x,\theta,t)\mathrm{d}xR\,\mathrm{d}\theta\\&\int_0^{2\pi}\int_0^l f_r^w(x)f_s^w(\theta)\mathscr{L}_w^{CM}(x,\theta,t)\mathrm{d}xR\,\mathrm{d}\theta\end{aligned}\tag{5.5}$$

With, $\mathscr{L}_u^{CM}(x,\theta,t)$, $\mathscr{L}_u^{CM}(x,\theta,t)$ and $\mathscr{L}_u^{CM}(x,\theta,t)$ representing the equations of motion of the system:

$$\begin{aligned}\mathscr{L}_u^{CM}(x,\theta,t) =& \rho h \underbrace{\frac{\partial^2 u^0}{\partial t^2}}_{ter(1)} + \frac{m_x}{R}\delta(x-x^p)\,\delta(\theta-\theta^p)\,\underbrace{\frac{\partial^2 u^0}{\partial t^2}}_{ter(111)} \\ & - \frac{Eh}{1-\nu^2}\left[\underbrace{\frac{\partial^2 u^0}{\partial x^2}}_{ter(2)} + \underbrace{\frac{1-\nu}{2}\frac{1}{R^2}\frac{\partial^2 u^0}{\partial \theta^2}}_{ter(3)} + \underbrace{\nu\frac{1}{R}\frac{\partial w^0}{\partial x}}_{ter(4)} + \underbrace{\frac{1+\nu}{2}\frac{1}{R}\frac{\partial^2 v^0}{\partial x\partial\theta}}_{ter(5)}\right] \\ & + \frac{Eh^3}{24(1+\nu)R^3}\left[\underbrace{\frac{\partial^3 w^0}{\partial x\partial\theta^2}}_{ter(6)} - \underbrace{\frac{3}{4}\frac{\partial^2 v^0}{\partial x\partial\theta}}_{ter(7)} + \underbrace{\frac{1}{4R}\frac{\partial^2 u^0}{\partial\theta^2}}_{ter(8)}\right] - \underbrace{p_u}_{ter(9)} = 0\end{aligned} \tag{5.6}$$

$$\begin{aligned}\mathscr{L}_v^{CM}(x,\theta,t) =& \rho h \underbrace{\frac{\partial^2 v^0}{\partial t^2}}_{ter(10)} + \frac{m_x}{R}\delta(x-x^p)\,\delta(\theta-\theta^p)\,\underbrace{\frac{\partial^2 v^0}{\partial t^2}}_{ter(112)} \\ & - \frac{Eh}{1-\nu^2}\left[\underbrace{\frac{1}{R^2}\frac{\partial^2 v^0}{\partial\theta^2}}_{ter(11)} + \underbrace{\frac{1}{R^2}\frac{\partial w^0}{\partial\theta}}_{ter(12)} + \underbrace{\frac{1+\nu}{2}\frac{1}{R}\frac{\partial^2 u^0}{\partial x\partial\theta}}_{ter(13)} + \underbrace{\frac{1-\nu}{2}\frac{\partial^2 v^0}{\partial x^2}}_{\text{ter}(14)}\right] \\ & - \frac{Eh^3}{12(1-\nu^2)}\left[\underbrace{\frac{1}{R^4}\frac{\partial^2 v^0}{\partial\theta^2}}_{ter(15)} - \underbrace{\frac{1}{R^4}\frac{\partial^3 w^0}{\partial\theta^3}}_{ter(16)} - \underbrace{\frac{3-\nu}{2}\frac{1}{R^2}\frac{\partial^3 w^0}{\partial x^2\partial\theta}}_{ter(17)}\right. \\ & \left. + \underbrace{\frac{9(1-\nu)}{8R^2}\frac{\partial^2 v^0}{\partial x^2}}_{ter(18)} - \underbrace{\frac{3(1-\nu)}{8R^3}\frac{\partial^2 u^0}{\partial x\partial\theta}}_{ter(19)}\right] - \underbrace{p_w}_{ter(20)} = 0\end{aligned} \tag{5.7}$$

$$\begin{aligned}\mathscr{L}_w^{CM}(x,\theta,t) =& \rho h \underbrace{\frac{\partial^2 w^0}{\partial t^2}}_{ter(21)} + \frac{m_x}{R}\delta(x-x^p)\,\delta(\theta-\theta^p)\,\underbrace{\frac{\partial^2 w^0}{\partial t^2}}_{\text{ter}(113)} \\ & + \frac{Eh}{1-\nu^2}\left[\underbrace{\frac{1}{R^2}\frac{\partial v^0}{\partial\theta}}_{ter(22)} + \underbrace{\frac{w^0}{R^2}}_{ter(23)} + \underbrace{\nu\frac{1}{R}\frac{\partial u^0}{\partial x}}_{ter(24)}\right] \\ & + \frac{Eh^3}{12(1-\nu^2)}\left[\underbrace{\frac{\partial^4 w^0}{\partial x^4}}_{ter(25)} - \underbrace{\frac{3-\nu}{2R^2}\frac{\partial^3 v^0}{\partial x^2\partial\theta}}_{ter(26)} + \underbrace{\frac{2}{R^2}\frac{\partial^4 w^0}{\partial x^2\partial\theta^2}}_{ter(27)}\right. \\ & \left. - \underbrace{\frac{1}{R^4}\frac{\partial^3 v^0}{\partial\theta^3}}_{ter(28)} + \underbrace{\frac{1}{R^4}\frac{\partial^4 w^0}{\partial\theta^4}}_{ter(29)} + \underbrace{\frac{1-\nu}{2}\frac{1}{R^3}\frac{\partial^3 u^0}{\partial x\partial\theta^2}}_{ter(30)}\right] - \underbrace{p_w}_{ter(31)} = 0\end{aligned} \tag{5.8}$$

After applying Galerkin's method and integrating by parts, the extra terms we get due to the concentrated mass will only affect the mass matrix and are written as:

$$\begin{aligned}\text{ter}(111): &\int_0^{2\pi}\int_0^{l}\frac{m_x}{R}f^u_{rx}f^u_{s\theta}\cdot\left(f^u_{ix}f^u_{j\theta}\right)\delta\left(x-x^p\right)\delta\left(\theta-\theta^p\right)\mathrm{d}xR\,\mathrm{d}\theta\ddot{q}^u_{ij}(t)\\ &= M_{\text{conc}}\,f^u_{s\theta}\left(\theta^p\right)f^u_{j\theta}\left(\theta^p\right)f^u_{r\xi}\left(\xi^p\right)f^u_{i\xi}\left(\xi^p\right)\ddot{q}^u_{ij}(t)\end{aligned} \tag{5.9}$$

$$\begin{aligned}\text{ter}(112): &\int_0^{2\pi}\int_0^{l}\frac{m_x}{R}f^v_{rx}f^v_{s\theta}\cdot\left(f^v_{ix}f^v_{j\theta}\right)\delta\left(x-x^p\right)\delta\left(\theta-\theta^p\right)\mathrm{d}xR\,\mathrm{d}\theta\ddot{q}^v_{ij}(t)\\ &= M_{\text{conc}}\,f^v_{s\theta}\left(\theta^p\right)f^v_{j\theta}\left(\theta^p\right)f^v_{r\xi}\left(\xi^p\right)f^v_{i\xi}\left(\xi^p\right)\ddot{q}^v_{ij}(t)\end{aligned} \tag{5.10}$$

$$\begin{aligned}\text{ter}(113): &\int_0^{2\pi}\int_0^{l}\frac{m_x}{R}f^w_{rx}f^w_{s\theta}\cdot\left(f^w_{ix}f^w_{j\theta}\right)\delta\left(x-x^p\right)\delta\left(\theta-\theta^p\right)\mathrm{d}xR\,\mathrm{d}\theta\ddot{q}^w_{ij}(t)\\ &= M_{\text{conc}}\,f^w_{s\theta}\left(\theta^p\right)f^w_{j\theta}\left(\theta^p\right)f^w_{r\xi}\left(\xi^p\right)f^w_{i\xi}\left(\xi^p\right)\ddot{q}^w_{ij}(t)\end{aligned} \tag{5.11}$$

In its matrix form, the algebraic system of equations comes as:

$$\begin{aligned}&\begin{bmatrix}\left[M^{CM}_{uu}\right] & 0 & 0\\ 0 & \left[M^{CM}_{vv}\right] & 0\\ 0 & 0 & \left[M^{CM}_{ww}\right]\end{bmatrix}+\begin{Bmatrix}\{\ddot{q}_u(t)\}\\ \{\ddot{q}_v(t)\}\\ \{\ddot{q}_w(t)\}\end{Bmatrix}\\ &+\begin{bmatrix}[K_{uu}] & [K_{uv}] & [K_{uw}]\\ [K_{vu}] & [K_{vv}] & [K_{vw}]\\ [K_{wu}] & [K_{wv}] & [K_{ww}]\end{bmatrix}\begin{Bmatrix}\{q_u(t)\}\\ \{q_v(t)\}\\ \{q_w(t)\}\end{Bmatrix}=\begin{Bmatrix}\{P_u(t)\}\\ \{P_v(t)\}\\ \{P_w(t)\}\end{Bmatrix}\end{aligned} \tag{5.12}$$

Where the submatrices of the mass matrix may be written as:

- $\left[M^{CM}_{uu}\right] \leftarrow \text{ter}(1)+\text{ter}(111)$
- $\left[M^{CM}_{vv}\right] \leftarrow \text{ter}(10)+\text{ter}(112)$
- $\left[M^{CM}_{ww}\right] \leftarrow \text{ter}(21)+\text{ter}(113)$

5.3. Validation

To validate the developed elastic shell model, the results of the natural frequency of the first natural mode of vibration are compared to values collected from the bibliography. In Table 5.1 a comparison of the fundamental natural frequency [GHz] of a doubly clamped SWCNT with an attached mass in the middle of the CNT ($\xi^p = 0$) is presented. The values obtained through the developed shell model are compared to the results written by Li et al. [89] whose results were obtained using molecular dynamics. The elastic properties and thickness of the CNT used were the ones already presented in Table 4.1. The values presented were calculated considering a position of the mass of $(\xi^p, \theta^p) = (0,0)$. The CNT in the study has a diameter of $d = 0.8$ [nm]. A wide range of mass values, M_{conc}, was tested - from 10^{-8} [fg] to 10^{-1} [fg] (1 femtogram = 10^{-15} gram). Frequencies were computed for discreet values of the length of the CNT (l).

The third column of the Table presents the relative error of the values calculated using the developed model when compared to MD. From these results, we can say that the shell model is in agreement with the MD model proposed in [89].

5.4. Natural Mode Shapes

Attaching a concentrated mass to the CNT it is expected for the natural frequencies and the mode shapes to be affected. In the position of the concentrated mass, we expect higher relative displacements. Solving the eigenvalue problem, the natural frequencies and natural mode shapes were computed for a clamped-clamped SWCNT with a diameter of $d = 0.8$ [nm] and a total length of $l = 10$ [nm]. A total mass of 10^{-1} [fg] was considered to be attached at the middle of the CNT - $(\xi^p, \theta^p) = (0,0)$. The first four natural mode shapes of the system are presented in Figure 5.2

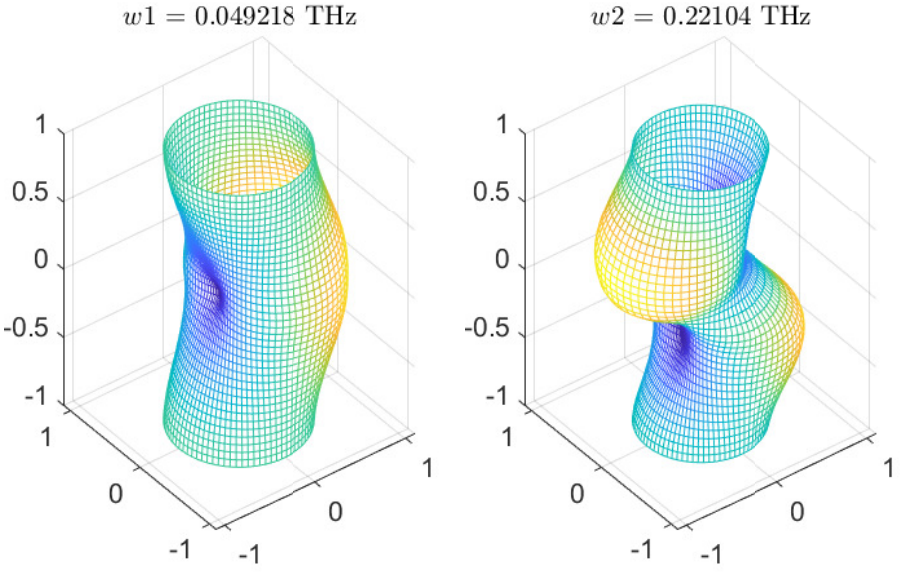

(a) First natural mode shape

(b) Second natural mode shape

Table 5.1. Comparison between the fundamental natural frequency [GHz] of a doubly clamped SWCNT with an attached mass in the middle of the CNT obtained through the developed shell model and MD simulations - Variation of the first 3 natural frequencies with attached mass value - $d = 0.8$ [nm] [89]

M_{conc} [fg]	Shell Model	MD [89]	Error
$l = 6$ [nm]			
10^{-8}	491.9	474.9	3.5 %
10^{-7}	487.5	474.8	2.6 %
10^{-6}	442.1	437.5	1.0 %
10^{-5}	230.6	248.2	7.6 %
10^{-4}	77.7	82.6	6.3 %
10^{-3}	24.7	27.9	13.0 %
10^{-2}	7.8	8.7	11.5 %
10^{-1}	2.5	2.9	16.0 %
$l = 8$ [nm]			
10^{-8}	300.2	291.3	3.0 %
10^{-7}	298.1	288.3	3.3 %
10^{-6}	278.4	274.9	1.3 %
10^{-5}	172.3	173.9	0.9 %
10^{-4}	62.2	64.6	3.9 %
10^{-3}	19.9	20.9	5.0 %
10^{-2}	6.3	6.8	7.9 %
10^{-1}	2.0	2.1	5.0 %
$l = 10$ [nm]			
10^{-8}	200.5	191.5	4.5 %
10^{-7}	199.4	191.4	4.0 %
10^{-6}	188.8	178	5.7 %
10^{-5}	128.3	120.1	6.4 %
10^{-4}	49.2	47.9	2.6 %
10^{-3}	15.9	15.7	1.3 %
10^{-2}	5.0	5.0	0.0 %
10^{-1}	1.6	1.6	0.0 %

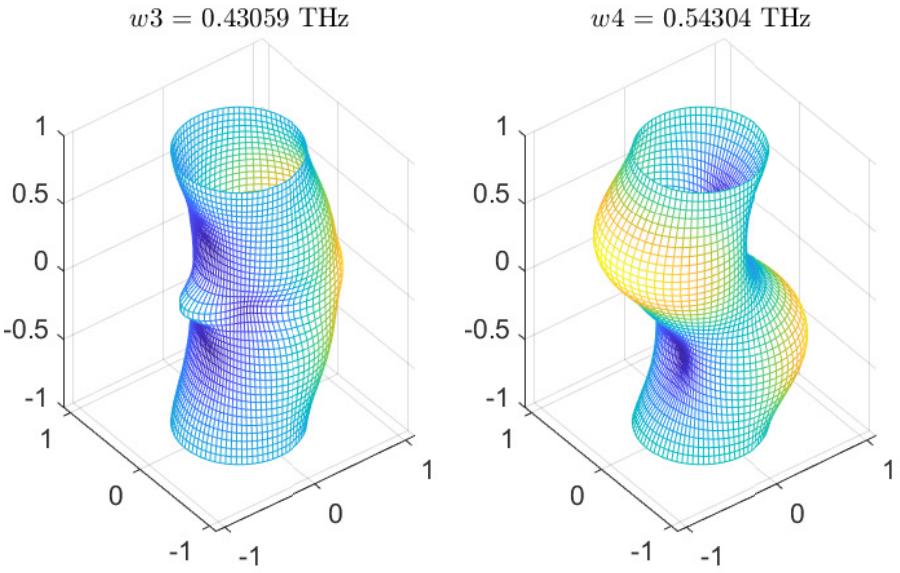

(c) Third natural mode shape **(d)** Fourth natural mode shape

Fig. 5.2. Natural mode shapes of a doubly clamped nanotube with a concentrated mass at $(\xi^p, \theta^p) = (0,0)$

5.5. Frequency-Shift

A study was performed to analyze the dependency of the natural frequency values of different natural modes on the attached mass value (Figure 5.3). For a certain CNT geometry, with the increase of the mass attached, the natural frequencies tend to decrease. For masses smaller than 10^{-7} [fg] this frequency shift is not as evident as for masses higher than this value. It can be seen that for masses higher than 10^{-5} [fg] the functional relation between the logarithm of the value of natural frequencies and the logarithm of the value of the attached mass is close to linear. This effect was also seen in the work of Li et al. [89].

Based on this effect of frequency shifting, and knowing how different values of mass affect the fundamental natural frequency of a certain CNT geometry, it is possible to quantify the mass attached to a nanotube. This is the most used way to transduce mass with a CNT oscillator. To ease the mass detection and calculation, the CNT oscillator can be used in this characteristical range.

A linear regression was fitted to the plot of the fundamental natural frequency in relation to the attached mass (Figure 5.4) in this region. In this region, the transfer function of the proposed NEM may be written as:

$$log(\omega_1) = \alpha_{conc} log(M_{conc}) + \beta_{conc} \tag{5.13}$$

where ω_1 is the fundamental natural frequency of the resonator with the attached mass and α_{conc} and β_{conc} are constants. The geometry of the CNT will influence this relation. Different values of α_{conc} and β_{conc} may be computed to characterize the behavior of different CNTs' geometries.

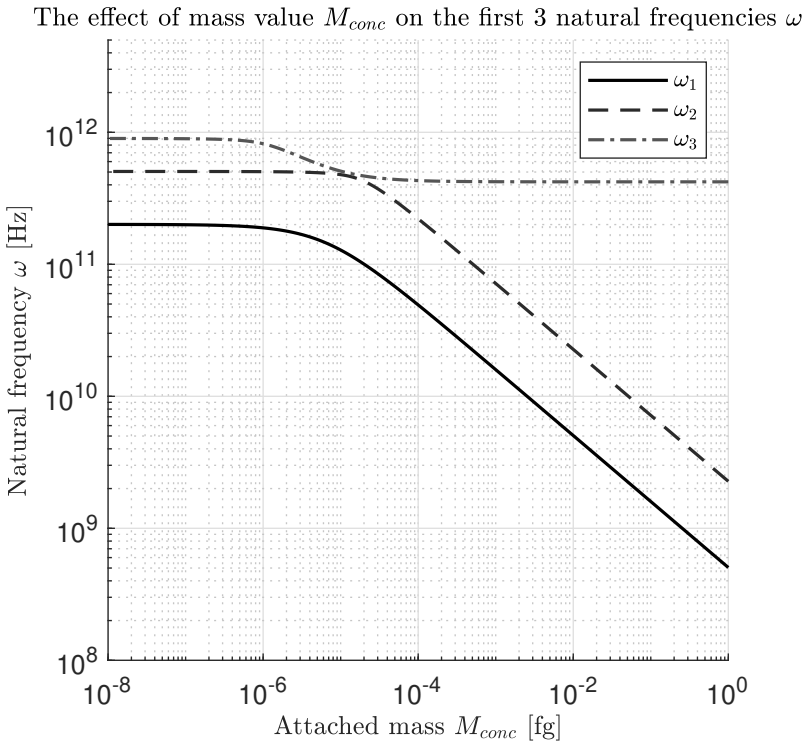

Fig. 5.3. Variation of the first 3 natural frequencies with attached mass value - $d = 0.8$ [nm]; $l = 10$ [nm]

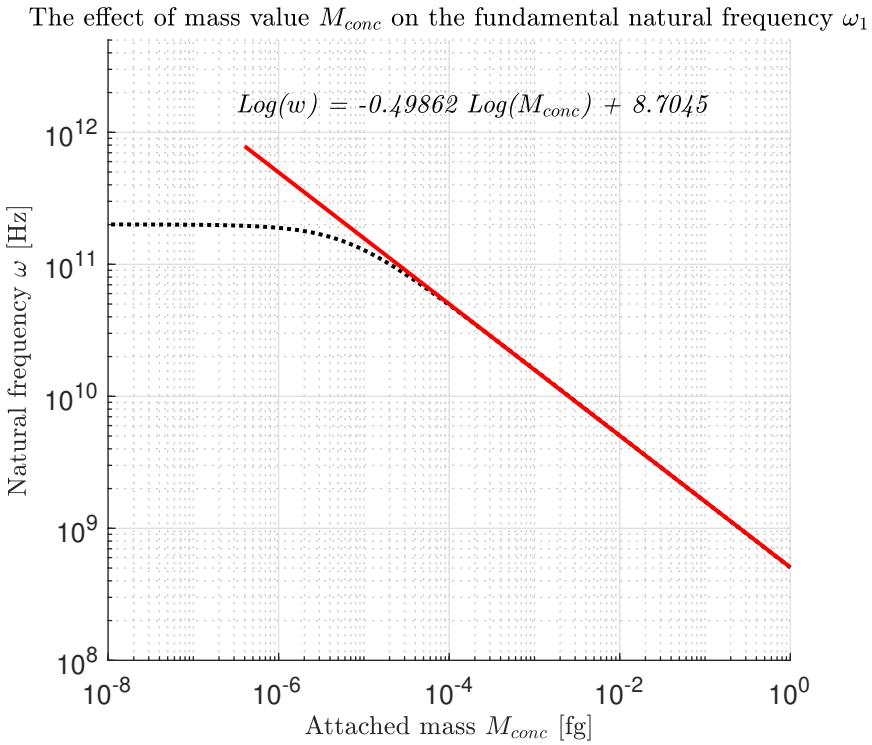

Fig. 5.4. Variation of the fundamental natural frequency with attached mass value and linear approximation - $d = 0.8$ [nm]; $l = 10$ [nm]

This methodology was replicated for different values of CNT's length and diameter suitable for such mass sensing applications. The constants α_{conc} and β_{conc} were obtained by fitting a linear regression to the logarithmic representation of the fundamental natural frequency against the localized mass value. The results are presented in graphs in Appendix C.

Influence of CNT geometry

To further understand the dependency of this natural frequency variation on the geometry of the CNT, the following study was performed. The frequency shift is defined as the difference between the fundamental frequencies of a nanotube with and without attached mass. In a range of attached mass values between 10^{-8} and 10^{0} [fg], for different values of CNT diameter (d) and length (l), the frequency shift presented by the oscillator is plotted in Figures 5.5 to 5.7.

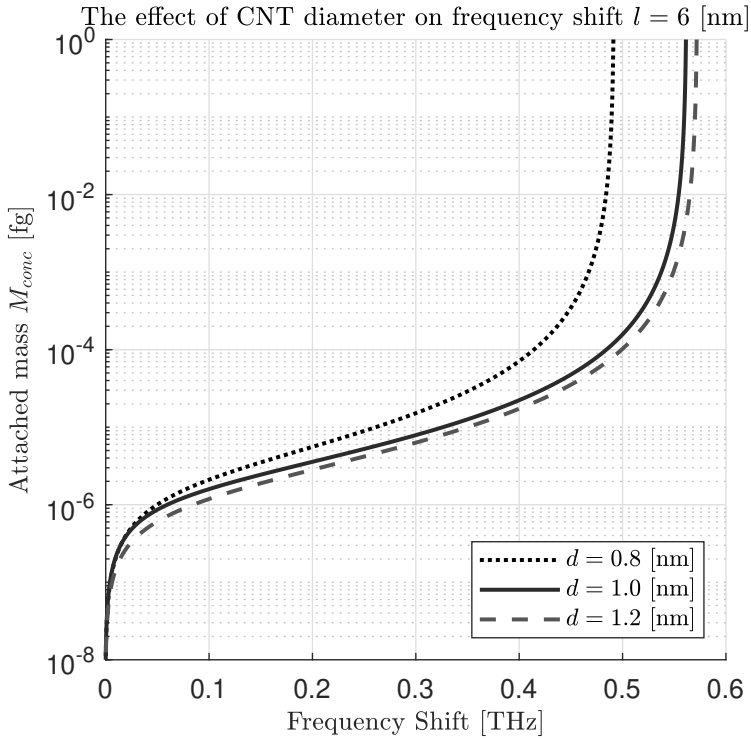

Fig. 5.5. Resonant frequency shifts of fully clamped nanotube resonator of $l = 6$ [nm] with different tube diameters compared to the value of attached mass

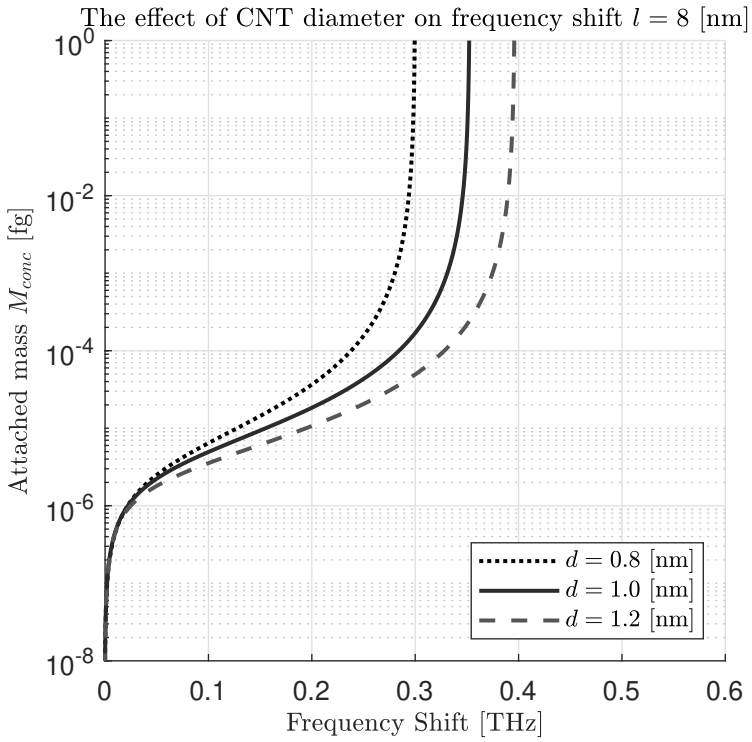

Fig. 5.6. Resonant frequency shifts of fully clamped nanotube resonator of $l = 8$ [nm] with different tube diameters compared to the value of attached mass

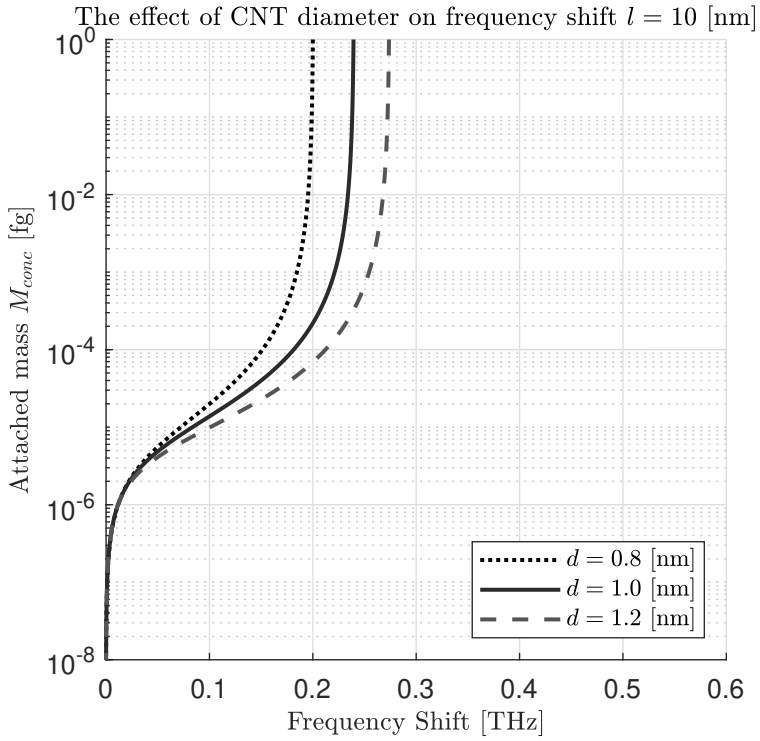

Fig. 5.7. Resonant frequency shifts of fully clamped nanotube resonator of $l = 10$ [nm] with different tube diameters compared to the value of attached mass

Analysing the results it is clear that the frequency shift is higher for higher values of mass. This means that higher values of attached masses will produce higher changes in the CNT fundamental natural frequency. It is also possible to conclude that bigger diameter CNTs will have higher frequency shifts for the same value of attached mass and tube length. The reverse effect is observed with CNT's length since the observed shift is higher the shortest the CNT is. For the range of diameter and length presented, the length of the tube has more impact on the variation of the frequency shift than the diameter. With this in mind, it is possible to conclude that higher diameter and shorter resonators will be more sensible for transducing the value of attached masses since they will have higher frequency shifts.

Influence of mass position

When building a CNT oscillator and positioning a mass in the center of the tube, imperfections may occur. Some experimental works with CNT resonators already covered the study of some usual imperfections and tried to quantify how these imperfections influence the mass readings.

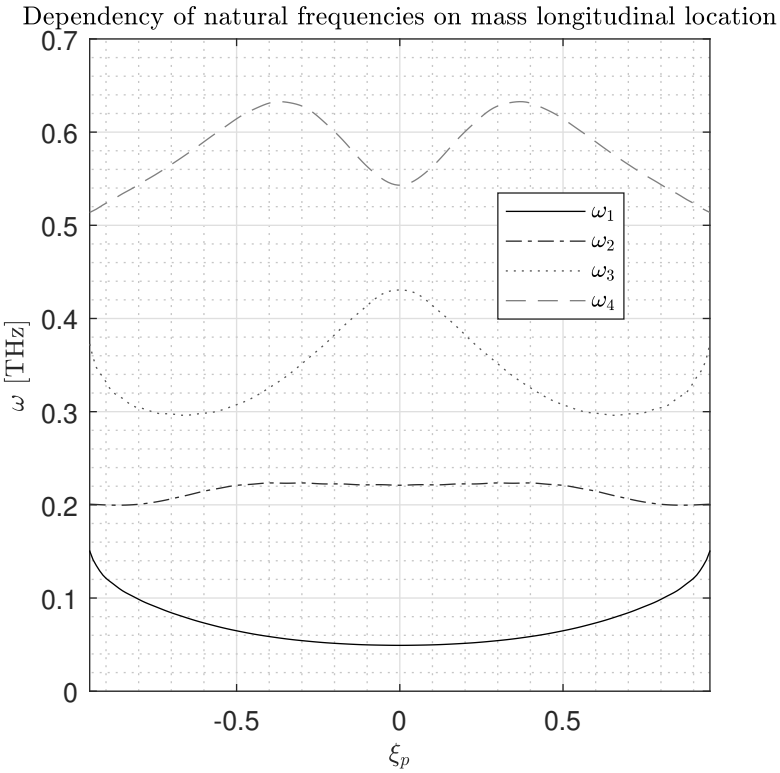

Fig. 5.8. Variation of the value of the first 4 natural frequencies (ω) with the longitudinal position of the concentrated mass (ξ_p)

To quantify how the positing of the concentrated mass may affect the CNT's fundamental natural frequency, and consequently, the mass measuring, the developed model was employed. In Figure 5.8 the dependency of the frequency of the first four natural modes

on the longitudinal position of the concentrated mass (ξ_p) is presented. The results were obtained using the geometry that was previously introduced ($d = 0.8$ [nm], $l = 10$ [nm]) and a concentrated mass value of 10^{-4} [fg].

All the presented modes' frequencies are significantly affected by the mass longitudinal position. The value of the fundamental natural frequency when the mass is located near the end of the CNT is roughly three times higher than the value in the middle of the tube. The second mode natural frequency is the one that is less affected by mass position. The third and fourth modes' natural frequencies are highly affected by ξ_p presenting a behavior similar to a sine curve.

Assuming that the concentrated mass has an offset from the center of the CNT of 1 [nm] (10% of the length), we can calculate the system's fundamental natural frequency as 51.418 [GHz]. Compared to the case when the mass is perfectly positioned in the middle of the tube (ω_1=49.230 [GHz]) this represents an increase of 4.4% of the fundamental natural frequency value which corresponds to a difference of 5% in the mass measurement if we consider the equation presented in Figure 5.4.

5.6. Forced Regime - Dynamic Response

This section is dedicated to studying the behavior of a CNT with an attached mass. The objective is to identify changes induced in the CNT-forced regime by the presence of a concentrated mass. We will focus on small displacement oscillations and relate the obtained amplitude of motion with the suspended mass.

Different approaches may be used to capture, in time, the displacement of a CNT oscillator such as a scanning electron microscope (SEM) or a transmission electron microscope (TEM), and directly observe the vibrations of the structure [119]. Analyzing reflected laser beams in the structure is another precise and well-established method used to measure displacement in NEMS [66].

Measuring the amplitude of movement of the CNT, with an attached mass, under electrostatic actuation and being able to relate this amplitude with the value of the attached mass, may be a different method to measure small masses using a CNT oscillator. Using the developed model, fixing the characteristics of the oscillator and its actuation, and just changing the value of the attached mass, a study was performed in order to understand this dependency. For this study, the mass was considered to be positioned in the middle of the CNT at the closest point to the gate. $(\xi^p, \theta^p) = (0, \pi)$. The CNT geometry and elastic properties used were the same as in Section 4.4.

Regarding the electrostatic actuation, the same $V_{DC} = 0.125$ [V] and $V_{AC} = 0.018$ [V] were used as before. The frequency of the AC component, ω_{AC} was set to a constant. Its value was calculated considering $\Omega_{AC} = 1.2$ for the system without a concentrated mass. The dependency of the amplitude of movement of the central point of the CNT after achieving steady-state conditions on the value of the attached mass is presented in Figure 5.9.

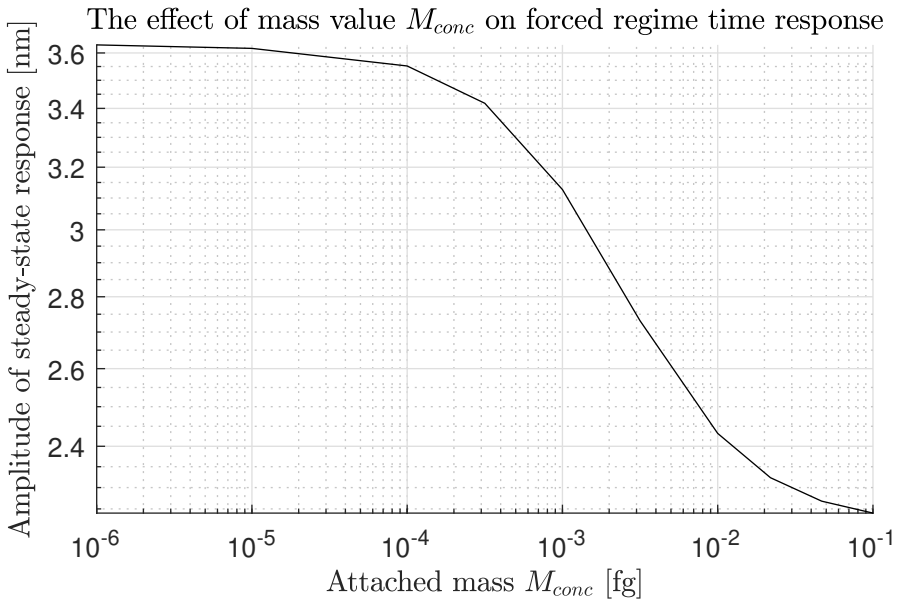

Fig. 5.9. Dependency of the amplitude of the steady-state response of a CNT under non-linear electrostatic actuation with the magnitude of a concentrated attached mass.

Analyzing the results, we can say that the value of the amplitude of the steady-state response decreases with the growth of the value of the concentrated mass. This conclusion is supported by the previous section's statements. In this case, an increase in the attached mass would lead to a decrease in the system's natural frequencies leading to an increase in the system's frequency ratio, shifting it to a point further from the resonance, and so, with a lower amplification factor. This variation is more pronounced for mass values higher than 10^{-4} [fg]. For values of mass lower than 10^{-5} the change in amplitude displacement is residual. Finally, we can conclude that for masses higher than 10^{-4}, measurable changes in the amplitude are caused by the introduction of a concentrated mass in the CNT resonator. This mechanism may be used to transduce mass in displacement, with the goal of measuring the value of the attached mass.

5.7. Final Remarks

In the present chapter, a concentrated mass is included in the previously developed shell model. Fundamental natural frequencies are compared with molecular dynamics models to validate the formulation. Satisfactory results are obtained. Further, the effect of frequency shift is introduced, and the way this phenomenon can be used to transduce mass is explored. A simplistic equation is proposed to relate the value of the attached mass and the variation of the fundamental frequency. With this, by measuring the fundamental frequency of a CNT oscillator with an attached mass, we can indirectly measure the value of the mass. Then, the influence of mass location in the system's fundamental frequency is studied, trying to quantify possible errors that may emerge due to misalignment in the concentrated mass position. Finally, the influence of the presence of different values of concentrated mass on the dynamic behavior of the system is studied under electrostatic actuation.

Chapter 6

Closure

6.1. Conclusions

CNTs have emerged as a focal point of scientific inquiry due to their exceptional mechanical, electrical, and thermal properties. These nanostructures are ideal for various applications because of their exceptional strength, electrical conductivity, and thermal stability. From nanoelectronics to drug delivery systems, CNTs have demonstrated their versatility and potential across diverse scientific disciplines.

The investigation into CNT oscillators is of particular significance due to their role as fundamental building blocks in various nanoscale systems. The use of CNT oscillators as mass sensors is a reality and several are the experiments reporting this. A deep understanding of CNT-oscillator behavior is vital for predicting and manipulating their responses under different conditions. This knowledge is pivotal for the development of highly sensitive mass sensors, enabling the detection of minute quantities with remarkable precision.

Regarding the modeling method, shell models strike a balance between continuum beam models, which simplify structures into continuous beams, and atomistic models, which simulate individual atoms. This bridge allows researchers to capture some nano effects while maintaining a level of computational efficiency and simplicity that is often missing in atomistic approaches.

The current work presented a model based on Sander-Koiter's thin shell theory to simulate the behavior of a carbon nanotube resonator. Sanders-Koiter's theory is chosen since it presents opportunities for nonlinear field growth in the future. A p-version finite element approach was used, and the CNT was modeled with just one element. Following the Galerkin method and then, integrating by parts, the weak form of the equations of motion was written. After that, the problem was written in its matrix form and the generalized matrices were assembled. Two simplified models, neglecting longitudinal inertia and neglecting membrane inertia were formulated, with the intention of reducing computational costs.

A validation process of the elastic models was elaborated considering molecular dynamics solutions. The natural frequency results of the full model and the model that neglected longitudinal inertia were remarkable for CNTs with high aspect ratios. For low aspect ratios errors no higher than 4% occur in the calculation of the first four beam-like

modes' frequencies. The model that neglected membrane inertia was not further considered since for low-frequency modes it presented high errors. Characteristical and already studied mode shapes of CNT's were also identified (some of them impossible to get with a beam model). After that, by integrating the equations of motion in time, and applying Newmak's method, the dynamic behavior of the CNT under electrostatic actuation was analyzed. The results of both, full and simplified models were validated with results from a non-linear beam model. Some differences mainly for higher displacements were observed.

After that, a concentrated mass was added to the surface of the CNT, and after validation of the fundamental frequencies, for different geometries, a modal study took place. The effect of frequency shift was analyzed and identified as a mechanism possible to transduce mass by stating the relationship between the value of attached mass and the change in the fundamental frequency of certain geometry CNT. Possible errors in mass measurements due to misalignment of the mass from the center of the nanotube were quantified by analyzing the variation of the fundamental natural frequency of the oscillator with the change in mass position. For the used geometry, the fundamental natural frequency could be three times higher if the mass was positioned nearby the end of the tube.

Finally, the variation with mass value of the amplitude of the system's steady-state response under electrostatic actuation is predicted using the developed model.

6.2. Future Works

The present work considers a capacitive approach to represent the electrostatic behavior between the charged CNT and the gate, as it is widely used in several literature studies based on beam models. The way the electrostatic forces are spread along the shell depends not only on the geometry of the oscillator but also on the deformed shape of the CNT. A further study should be done to improve the representation of the electrostatic behavior.

Another path for future research would be to develop a MD model. With this (after validation with experimental works) it would be possible to clarify the variance that exists in the definition of equivalent material properties when applying continuum models. A further step in the validation of the developed shell model would be taken.

Being aware of the increase in complexity, the advantages of including a non-local theory could be studied in the future. This may bring advantages mainly when modeling shorter CNTs as was seen in this work. It would also be interesting not to disregard non-linear terms in the shell theory formulation, so the model could be used under high deformation conditions. The possibility of predicting higher displacement dynamic behavior of CNTs would allow the creation of a more versatile model. At first, it would be interesting to analyze its behavior as a mass sensor, working closer to the resonance, and producing higher displacements, increasing the resonator sensibility. In second hand, different phenomena could be explored with the shell model e.g., the pull-in voltage of a CNT. Taking into account geometric and damping non-linearity would mean a further step toward a more reliable model since these effects were experimentally verified.

Another interesting future research would be to implement electrostatics fundamental equations and parallel to the shell elastic equations solve them by applying a finite element approach. This model would allow a precise prediction of the system's behavior as well as validations of simpler analytical expressions for the electrostatic load.

References

[1] Sumio Iijima. “Helical microtubules of graphitic carbon”. In: *Nature* 354.6348 (Nov. 1991), pp. 56–58. ISSN: 1476-4687. DOI: 10.1038/354056a0. URL: https://doi.org/10.1038/354056a0.

[2] Ronald F. Gibson, Emmanuel O. Ayorinde, and Yuan-Feng Wen. “Vibrations of carbon nanotubes and their composites: A review”. In: *Composites Science and Technology* 67.1 (2007), pp. 1–28. ISSN: 0266-3538. DOI: https://doi.org/10.1016/j.compscitech.2006.03.031. URL: https://www.sciencedirect.com/science/article/pii/S026635380600131X.

[3] A. K. Naik et al. “Towards single-molecule nanomechanical mass spectrometry”. In: *Nature Nanotechnology* 4.7 (July 2009), pp. 445–450. ISSN: 1748-3395. DOI: 10.1038/nnano.2009.152. URL: https://doi.org/10.1038/nnano.2009.152.

[4] Farzad Khademolhosseini et al. “Nonlocal Continuum Modeling and Molecular Dynamics Simulation of Torsional Vibration of Carbon Nanotubes”. In: *IEEE Transactions on Nanotechnology* 11.1 (2012), pp. 34–43. DOI: 10.1109/TNANO.2011.2111380.

[5] Wenhui Duan, Chien Ming Wang, and Y Y Zhang. “Calibration of nonlocal scaling effect parameter for free vibration of carbon nanotubes by molecular dynamics”. English. In: *Journal of Applied Physics* 101.2 (2007), pp. 1–7. ISSN: 0021-8979.

[6] R. Ansari, H. Rouhi, and S. Sahmani. “Calibration of the analytical nonlocal shell model for vibrations of double-walled carbon nanotubes with arbitrary boundary conditions using molecular dynamics”. In: *International Journal of Mechanical Sciences* 53.9 (2011), pp. 786–792. ISSN: 0020-7403. DOI: https://doi.org/10.1016/j.ijmecsci.2011.06.010. URL: https://www.sciencedirect.com/science/article/pii/S0020740311001299.

[7] Rumeng Liu and Lifeng Wang. “Vibration of Cantilevered Double-Walled Carbon Nanotubes Predicted by Timoshenko Beam Model and Molecular Dynamics”. In: *International Journal of Computational Methods* 12 (2015), p. 1540017. URL: https://api.semanticscholar.org/CorpusID:125039042.

[8] Matteo Strozzi et al. “Nonlinear vibrations and energy exchange of single-walled carbon nanotubes. Circumferential flexural modes”. In: *Journal of Sound and Vibration* 381 (2016), pp. 156–178. ISSN: 0022-460X. DOI: https://doi.org/10.1016/j.jsv.2016.06.013. URL: https://www.sciencedirect.com/science/article/pii/S0022460X16302358.

[9] Matteo Strozzi et al. “Low-frequency linear vibrations of single-walled carbon nanotubes: Analytical and numerical models”. In: *Journal of Sound and Vibration* 333.13 (2014), pp. 2936–2957. ISSN: 0022-460X. DOI: https://doi.org/10.1016/j.jsv.2014.01.016. URL: https://www.sciencedirect.com/science/article/pii/S0022460X14000601.

[10] Reza Ansari, Hessam Rouhi, and Saeid Sahmani. “Free vibration analysis of single- and double-walled carbon nanotubes based on nonlocal elastic shell models”. In: *Journal of Vibration and Control* 20.5 (2014), pp. 670–678. DOI: 10.1177/1077546312463750. eprint: https://doi.org/10.1177/1077546312463750. URL: https://doi.org/10.1177/1077546312463750.

[11] K.V. Avramov. “Nonlinear vibrations characteristics of single-walled carbon nanotubes by nonlocal elastic shell model”. In: *International Journal of Non-Linear Mechanics* 107 (2018), pp. 149–160. ISSN: 0020-7462. DOI: https://doi.org/10.1016/j.ijnonlinmec.2018.08.017. URL: https://www.sciencedirect.com/science/article/pii/S0020746218303238.

[12] Erik T Thostenson, Zhifeng Ren, and Tsu-Wei Chou. “Advances in the science and technology of carbon nanotubes and their composites: a review”. In: *Composites Science and Technology* 61.13 (2001), pp. 1899–1912. ISSN: 0266-3538. DOI: https://doi.org/10.1016/S0266-3538(01)00094-X. URL: https://www.sciencedirect.com/science/article/pii/S026635380100094X.

[13] Chunyu Li and Tsu-Wei Chou. “A structural mechanics approach for the analysis of carbon nanotubes”. In: *International Journal of Solids and Structures* 40 (May 2003), pp. 2487–2499. DOI: 10.1016/S0020-7683(03)00056-8.

[14] D. S. Bethune et al. “Cobalt-catalysed growth of carbon nanotubes with single-atomic-layer walls”. In: 363.6430 (June 1993), pp. 605–607. DOI: 10.1038/363605a0.

[15] C. Journet et al. “Large-scale production of single-walled carbon nanotubes by the electric-arc technique”. In: *Nature* 388.6644 (Aug. 1997), pp. 756–758. ISSN: 1476-4687. DOI: 10.1038/41972. URL: https://doi.org/10.1038/41972.

[16] Hongjie Dai et al. “Single-wall nanotubes produced by metal-catalyzed disproportionation of carbon monoxide”. In: *Chemical Physics Letters* 260.3 (1996), pp. 471–475. ISSN: 0009-2614. DOI: https://doi.org/10.1016/0009-2614(96)00862-7. URL: https://www.sciencedirect.com/science/article/pii/0009261496008627.

[17] Pavel Nikolaev et al. “Gas-phase catalytic growth of single-walled carbon nanotubes from carbon monoxide”. In: *Chemical Physics Letters* 313.1 (1999), pp. 91–97. ISSN: 0009-2614. DOI: https://doi.org/10.1016/S0009-2614(99)01029-5. URL: https://www.sciencedirect.com/science/article/pii/S0009261499010295.

[18] Z F Ren et al. “Synthesis of large arrays of well-aligned carbon nanotubes on glass”. en. In: *Science* 282.5391 (Nov. 1998), pp. 1105–1107.

[19] Z. F. Ren et al. “Growth of a single freestanding multiwall carbon nanotube on each nanonickel dot”. In: *Applied Physics Letters* 75.8 (Aug. 1999), pp. 1086–1088. ISSN: 0003-6951. DOI: 10.1063/1.124605. eprint: https://pubs.aip.org/aip/apl/article-pdf/75/8/1086/7813695/1086_1_online.pdf. URL: https://doi.org/10.1063/1.124605.

[20] Z. P. Huang et al. “Growth of highly oriented carbon nanotubes by plasma-enhanced hot filament chemical vapor deposition”. In: *Applied Physics Letters* 73.26 (Dec. 1998), pp. 3845–3847. ISSN: 0003-6951. DOI: 10.1063/1.122912. eprint: https://pubs.aip.org/aip/apl/article-pdf/73/26/3845/10178651/3845_1_online.pdf. URL: https://doi.org/10.1063/1.122912.

[21] Olga Zaytseva and Günter Neumann. “Carbon nanomaterials: Production, impact on plant development, agricultural and environmental applications”. In: *Chemical and Biological Technologies in Agriculture* 3 (July 2016). DOI: 10.1186/s40538-016-0070-8.

[22] Maohui Ge and Klaus Sattler. “Bundles of carbon nanotubes generated by vapor-phase growth”. In: *Applied Physics Letters* 64.6 (Feb. 1994), pp. 710–711. ISSN: 0003-6951. DOI: 10.1063/1.111042. eprint: https://pubs.aip.org/aip/apl/article-pdf/64/6/710/7799730/710_1_online.pdf. URL: https://doi.org/10.1063/1.111042.

[23] Lian-Mao Peng, Zhiyong Zhang, and Sheng Wang. “Carbon nanotube electronics: recent advances”. In: *Materials Today* 17.9 (2014), pp. 433–442. ISSN: 1369-7021. DOI: https://doi.org/10.1016/j.mattod.2014.07.008. URL: https://www.sciencedirect.com/science/article/pii/S1369702114002582.

[24] Shashi Bala and Mamta Khosla. “Design and analysis of electrostatic doped tunnel CNTFET for various process parameters variation”. In: *Superlattices and Microstructures* 124 (2018), pp. 160–167. ISSN: 0749-6036. DOI: https://doi.org/10.1016/j.spmi.2018.10.007. URL: https://www.sciencedirect.com/science/article/pii/S0749603618317397.

[25] Lian-Mao Peng, Zhiyong Zhang, and Chenguang Qiu. “Carbon nanotube digital electronics”. In: *Nature Electronics* 2.11 (Nov. 2019), pp. 499–505. ISSN: 2520-1131. DOI: 10.1038/s41928-019-0330-2. URL: https://doi.org/10.1038/s41928-019-0330-2.

[26] Sourabh Kumar Soni, Benedict Thomas, and Vishesh Ranjan Kar. “A Comprehensive Review on CNTs and CNT-Reinforced Composites: Syntheses, Characteristics and Applications”. In: *Materials Today Communications* 25 (2020), p. 101546. ISSN: 2352-4928. DOI: https://doi.org/10.1016/j.mtcomm.2020.101546. URL: https://www.sciencedirect.com/science/article/pii/S2352492820325575.

[27] Mohammad Hamidul Islam et al. “Graphene and CNT-Based Smart Fiber-Reinforced Composites: A Review”. In: *Advanced Functional Materials* 32.40 (2022), p. 2205723. DOI: https://doi.org/10.1002/adfm.202205723. eprint: https://onlinelibrary.wiley.com/doi/pdf/10.1002/adfm.202205723. URL: https://onlinelibrary.wiley.com/doi/abs/10.1002/adfm.202205723.

[28] Bogumiła Kumanek and Dawid Janas. “Thermal conductivity of carbon nanotube networks: a review”. In: *Journal of Materials Science* 54.10 (May 2019), pp. 7397–7427. ISSN: 1573-4803. DOI: 10.1007/s10853-019-03368-0. URL: https://doi.org/10.1007/s10853-019-03368-0.

[29] André Schlott et al. “Heat Exchange Structures Based on Copper/CNT Composite”. In: *22nd Symposium on Composites*. Vol. 809. Key Engineering Materials. Trans Tech Publications Ltd, Aug. 2019, pp. 106–114. DOI: 10.4028/www.scientific.net/KEM.809.106.

[30] Seyed Yazdan Madani et al. “A new era of cancer treatment: carbon nanotubes as drug delivery tools”. In: *International Journal of Nanomedicine* 6 (2011). PMID: 22162655, pp. 2963–2979. DOI: 10.2147/IJN.S16923. eprint: https://www.tandfonline.com/doi/pdf/10.2147/IJN.S16923. URL: https://www.tandfonline.com/doi/abs/10.2147/IJN.S16923.

[31] Dheeraj S. Randive et al. “Colon targeted dosage form of Capecitabine using folic acid anchored modified carbon nanotube: in vitro cytotoxicity, apoptosis and in vivo roentgenographic study”. In: *Drug Development and Industrial Pharmacy* 47.9 (2021). PMID: 34663149, pp. 1401–1412. DOI: 10.1080/03639045.2021.1994988. eprint: https://doi.org/10.1080/03639045.2021.1994988. URL: https://doi.org/10.1080/03639045.2021.1994988.

[32] Ali Hassan et al. “Applications and hazards associated with carbon nanotubes in biomedical sciences”. In: *Inorganic and Nano-Metal Chemistry* 50.9 (2020), pp. 741–752. DOI: 10.1080/24701556.2020.1724151. eprint: https://doi.org/10.1080/24701556.2020.1724151. URL: https://doi.org/10.1080/24701556.2020.1724151.

[33] Z. Lee et al. “Metallic NEMS components fabricated from nanocomposite Al–Mo films”. In: *Nanotechnology* 17 (2006), pp. 3063–3070. URL: https://api.semanticscholar.org/CorpusID:137293017.

[34] Parmanand Sharma et al. “Nano-fabrication with metallic glass—an exotic material for nano-electromechanical systems”. In: *Nanotechnology* 18.3 (Jan. 2007), p. 035302. DOI: 10.1088/0957-4484/18/3/035302. URL: https://dx.doi.org/10.1088/0957-4484/18/3/035302.

[35] C. Stampfer et al. “Fabrication of Single-Walled Carbon-Nanotube-Based Pressure Sensors”. In: *Nano Letters* 6.2 (2006). PMID: 16464041, pp. 233–237. DOI: 10.1021/nl052171d. eprint: https://doi.org/10.1021/nl052171d. URL: https://doi.org/10.1021/nl052171d.

[36] Andreas K. Hüttel et al. “Carbon Nanotubes as Ultrahigh Quality Factor Mechanical Resonators”. In: *Nano Letters* 9.7 (2009). PMID: 19492820, pp. 2547–2552. DOI: 10.1021/nl900612h. eprint: https://doi.org/10.1021/nl900612h. URL: https://doi.org/10.1021/nl900612h.

[37] Sun-Bae Kim and Ji-Hwan Kim. “Quality factors for the nano-mechanical tubes with thermoelastic damping and initial stress”. In: *Journal of Sound and Vibration* 330.7 (2011), pp. 1393–1402. ISSN: 0022-460X. DOI: https://doi.org/10.1016/j.jsv.2010.10.015. URL: https://www.sciencedirect.com/science/article/pii/S0022460X10006760.

[38] Edward A. Laird et al. “A High Quality Factor Carbon Nanotube Mechanical Resonator at 39 GHz”. In: *Nano Letters* 12.1 (2012). PMID: 22111547, pp. 193–197. DOI: 10.1021/nl203279v. eprint: https://doi.org/10.1021/nl203279v. URL: https://doi.org/10.1021/nl203279v.

[39] Quan Wang and Behrouz Arash. “A review on applications of carbon nanotubes and graphenes as nano-resonator sensors”. In: *Computational Materials Science* 82 (2014), pp. 350–360. ISSN: 0927-0256. DOI: https://doi.org/10.1016/j.commatsci.2013.10.010. URL: https://www.sciencedirect.com/science/article/pii/S0927025613006113.

[40] J. Chaste et al. “A nanomechanical mass sensor with yoctogram resolution”. In: *Nature Nanotechnology* 7.5 (May 2012), pp. 301–304. ISSN: 1748-3395. DOI: 10.1038/nnano.2012.42. URL: https://doi.org/10.1038/nnano.2012.42.

[41] Changyao Chen et al. “Performance of monolayer graphene nanomechanical resonators with electrical readout”. In: *Nature Nanotechnology* 4.12 (Sept. 2009), pp. 861–867. DOI: 10.1038/nnano.2009.267. URL: https://doi.org/10.1038%2Fnnano.2009.267.

[42] Pengfei Qi et al. “Toward Large Arrays of Multiplex Functionalized Carbon Nanotube Sensors for Highly Sensitive and Selective Molecular Detection”. In: *Nano Letters* 3.3 (Mar. 2003), pp. 347–351. ISSN: 1530-6984. DOI: 10.1021/nl034010k. URL: https://doi.org/10.1021/nl034010k.

[43] J. Moser et al. “Ultrasensitive force detection with a nanotube mechanical resonator”. In: *Nature Nanotechnology* 8.7 (July 2013), pp. 493–496. ISSN: 1748-3395. DOI: 10.1038/nnano.2013.97. URL: https://doi.org/10.1038/nnano.2013.97.

[44] M. D. LaHaye et al. “Approaching the Quantum Limit of a Nanomechanical Resonator”. In: *Science* 304.5667 (2004), pp. 74–77. DOI: 10.1126/science.1094419. eprint: https://www.science.org/doi/pdf/10.1126/science.1094419. URL: https://www.science.org/doi/abs/10.1126/science.1094419.

[45] Robert L. Badzey and Pritiraj Mohanty. “Coherent signal amplification in bistable nanomechanical oscillators by stochastic resonance”. In: *Nature* 437.7061 (Oct. 2005), pp. 995–998. ISSN: 1476-4687. DOI: 10.1038/nature04124. URL: https://doi.org/10.1038/nature04124.

[46] Phillip W Snyder et al. “A stochastic, cantilever approach to the evaluation of solution phase thermodynamic quantities”. In: *Proceedings of the National Academy of Sciences of the United States of America* 104.8 (Feb. 2007), pp. 2579–2584. ISSN: 0027-8424. DOI: 10.1073/pnas.0606604104. URL: https://europepmc.org/articles/PMC1815225.

[47] J. Tamayo et al. “Underlying mechanisms of the self-sustained oscillation of a nanomechanical stochastic resonator in a liquid”. In: *Phys. Rev. B* 76 (18 Nov. 2007), p. 180201. DOI: 10.1103/PhysRevB.76.180201. URL: https://link.aps.org/doi/10.1103/PhysRevB.76.180201.

[48] M R Paul, M T Clark, and M C Cross. “The stochastic dynamics of micron and nanoscale elastic cantilevers in fluid: fluctuations from dissipation”. In: *Nanotechnology* 17.17 (Aug. 2006), p. 4502. DOI: 10.1088/0957-4484/17/17/037. URL: https://dx.doi.org/10.1088/0957-4484/17/17/037.

[49] Somenath Roy and Zhiqiang Gao. “Nanostructure-based electrical biosensors”. In: *Nano Today* 4.4 (2009), pp. 318–334. ISSN: 1748-0132. DOI: https://doi.org/10.1016/j.nantod.2009.06.003. URL: https://www.sciencedirect.com/science/article/pii/S1748013209000607.

[50] Rajib Chowdhury, Sondipon Adhikari, and John C Mitchell. “Vibrating carbon nanotube based bio-sensors”. In: *Physica E-low-dimensional Systems & Nanostructures* 42 (2009), pp. 104–109. URL: https://api.semanticscholar.org/CorpusID:55582382.

[51] Seung-Bo Shim, Matthias Imboden, and Pritiraj Mohanty. “Synchronized Oscillation in Coupled Nanomechanical Oscillators”. In: *Science* 316.5821 (2007), pp. 95–99. DOI: 10.1126/science.1137307. eprint: https://www.science.org/doi/pdf/10.1126/science.1137307. URL: https://www.science.org/doi/abs/10.1126/science.1137307.

[52] Taeyun Kwon et al. “Nanomechanical In Situ Monitoring of Proteolysis of Peptide by Cathepsin B”. In: *PLOS ONE* 4.7 (July 2009), pp. 1–8. DOI: 10.1371/journal.pone.0006248. URL: https://doi.org/10.1371/journal.pone.0006248.

[53] Thomas P. Burg et al. “Weighing of biomolecules, single cells and single nanoparticles in fluid”. In: *Nature* 446.7139 (Apr. 2007), pp. 1066–1069. ISSN: 1476-4687. DOI: 10.1038/nature05741. URL: https://doi.org/10.1038/nature05741.

[54] Y Arntz et al. “Label-free protein assay based on a nanomechanical cantilever array”. In: *Nanotechnology* 14.1 (Dec. 2002), p. 86. DOI: 10.1088/0957-4484/14/1/319. URL: https://dx.doi.org/10.1088/0957-4484/14/1/319.

[55] Kyo Seon Hwang et al. “In-situ quantitative analysis of a prostate-specific antigen (PSA) using a nanomechanical PZT cantilever”. In: *Lab Chip* 4 (6 2004), pp. 547–552. DOI: 10.1039/B410905H. URL: http://dx.doi.org/10.1039/B410905H.

[56] YeoHeung Yun et al. “Nanotube electrodes and biosensors”. In: *Nano Today* 2.6 (2007), pp. 30–37. ISSN: 1748-0132. DOI: https://doi.org/10.1016/S1748-0132(07)70171-8. URL: https://www.sciencedirect.com/science/article/pii/S1748013207701718.

[57] Philip S. Waggoner and Harold G. Craighead. “Micro- and nanomechanical sensors for environmental, chemical, and biological detection”. In: *Lab Chip* 7 (10 2007), pp. 1238–1255. DOI: 10.1039/B707401H. URL: http://dx.doi.org/10.1039/B707401H.

[58] Branimir Ilic et al. “Single cell detection with micromechanical oscillators”. In: *Journal of Vacuum Science & Technology B: Microelectronics and Nanometer Structures* 19 (Nov. 2001), pp. 2825–2828. DOI: 10.1116/1.1421572.

[59] Guanghua Wu et al. “Origin of nanomechanical cantilever motion generated from biomolecular interactions”. In: *Proceedings of the National Academy of Sciences* 98.4 (2001), pp. 1560–1564. DOI: 10.1073/pnas.98.4.1560. eprint: https://www.pnas.org/doi/pdf/10.1073/pnas.98.4.1560. URL: https://www.pnas.org/doi/abs/10.1073/pnas.98.4.1560.

[60] James A. Sioss et al. “Nanoresonator chip-based RNA sensor strategy for detection of circulating tumor cells: response using PCA3 as a prostate cancer marker”. In: *Nanomedicine: Nanotechnology, Biology and Medicine* 8.6 (2012), pp. 1017–1025. ISSN: 1549-9634. DOI: https://doi.org/10.1016/j.nano.2011.11.009. URL: https://www.sciencedirect.com/science/article/pii/S1549963411005302.

[61] Jeffrey Rhoads, Steven Shaw, and Kimberly Foster. “Nonlinear dynamics and its applications in micro- and nano-resonators”. In: *J. Dyn. Syst., Meas., Control* 132.3 (May 2010). DOI: 10.1115/1.4001333.

[62] Arthur W. Barnard et al. “Fluctuation broadening in carbon nanotube resonators”. In: *Proceedings of the National Academy of Sciences* 109.47 (2012), pp. 19093–19096. DOI: 10.1073/pnas.1216407109. eprint: https://www.pnas.org/doi/pdf/10.1073/pnas.1216407109. URL: https://www.pnas.org/doi/abs/10.1073/pnas.1216407109.

[63] Benjamin Lassagne et al. “Ultrasensitive mass sensing with a nanotube electromechanical resonator.” In: *Nano letters* 8 11 (2008), pp. 3735–8. URL: https://api.semanticscholar.org/CorpusID:12437852.

[64] Shunichi Sawano, Takayuki Arie, and Seiji Akita. “Carbon Nanotube Resonator in Liquid”. In: *Nano Letters* 10.9 (Sept. 2010), pp. 3395–3398. ISSN: 1530-6984. DOI: 10.1021/nl101292b. URL: https://doi.org/10.1021/nl101292b.

[65] Benoit Witkamp, Menno Poot, and Herre S. J. van der Zant. “Bending-Mode Vibration of a Suspended Nanotube Resonator”. In: *Nano Letters* 6.12 (Dec. 2006), pp. 2904–2908. ISSN: 1530-6984. DOI: 10.1021/nl062206p. URL: https://doi.org/10.1021/nl062206p.

[66] Vera A. Sazonova. “A tunable carbon nanotube resonator”. PhD thesis. Cornell University, 2006.

[67] Hamed Farokhi. *Nonlinear behaviour of carbon nanotube resonators with applications in mass-sensors*. McGill University (Canada), 2017.

[68] Y.M. Fu, J.W. Hong, and X.Q. Wang. “Analysis of nonlinear vibration for embedded carbon nanotubes”. In: *Journal of Sound and Vibration* 296.4 (2006), pp. 746–756. ISSN: 0022-460X. DOI: https://doi.org/10.1016/j.jsv.2006.02.024. URL: https://www.sciencedirect.com/science/article/pii/S0022460X06002513.

[69] B. Arash and Q. Wang. “A review on the application of nonlocal elastic models in modeling of carbon nanotubes and graphenes”. In: *Computational Materials Science* 51.1 (2012), pp. 303–313. ISSN: 0927-0256. DOI: https://doi.org/10.1016/j.commatsci.2011.07.040. URL: https://www.sciencedirect.com/science/article/pii/S0927025611004320.

[70] E. Hernández et al. “Elastic Properties of C and $B_xC_yN_z$ Composite Nanotubes”. In: *Phys. Rev. Lett.* 80 (20 May 1998), pp. 4502–4505. DOI: 10.1103/PhysRevLett.80.4502. URL: https://link.aps.org/doi/10.1103/PhysRevLett.80.4502.

[71] Daniel Sánchez-Portal et al. “Ab initio structural, elastic, and vibrational properties of carbon nanotubes”. In: *Phys. Rev. B* 59 (19 May 1999), pp. 12678–12688. DOI: 10.1103/PhysRevB.59.12678. URL: https://link.aps.org/doi/10.1103/PhysRevB.59.12678.

[72] Hamed Farokhi, Michael P. Païdoussis, and Arun K. Misra. “A new nonlinear model for analyzing the behaviour of carbon nanotube-based resonators”. In: *Journal of Sound and Vibration* 378 (2016), pp. 56–75. ISSN: 0022-460X. DOI: https://doi.org/10.1016/j.jsv.2016.05.008. URL: https://www.sciencedirect.com/science/article/pii/S0022460X16301018.

[73] Brandon Bodily and C. Sun. “Structural and equivalent continuum properties of single-walled carbon nanotubes”. In: *Int. J. of Materials and Product Technology* 18 (Jan. 2003), pp. 381–397. DOI: 10.1504/IJMPT.2003.002498.

[74] B.I. Yakobson et al. “High strain rate fracture and C-chain unraveling in carbon nanotubes”. In: *Computational Materials Science* 8.4 (1997), pp. 341–348. ISSN: 0927-0256. DOI: https://doi.org/10.1016/S0927-0256(97)00047-5. URL: https://www.sciencedirect.com/science/article/pii/S0927025697000475.

[75] Jaroaw Meller. “Molecular Dynamics”. In: *Encyclopedia of Life Sciences*. John Wiley & Sons, Ltd, 2001. ISBN: 9780470015902. DOI: https://doi.org/10.1038/npg.els.0003048. eprint: https://onlinelibrary.wiley.com/doi/pdf/10.1038/npg.els.0003048. URL: https://onlinelibrary.wiley.com/doi/abs/10.1038/npg.els.0003048.

[76] Ajit K. Vallabhaneni et al. “A band-pass filter approach within molecular dynamics for the prediction of intrinsic quality factors of nanoresonators”. In: *Journal of Applied Physics* 112.7 (Oct. 2012), p. 074301. ISSN: 0021-8979. DOI: 10.1063/1.4754450. eprint: https://pubs.aip.org/aip/jap/article-pdf/doi/10.1063/1.4754450/15099233/074301_1_online.pdf. URL: https://doi.org/10.1063/1.4754450.

[77] Sung Youb Kim and Harold S. Park. “Utilizing Mechanical Strain to Mitigate the Intrinsic Loss Mechanisms in Oscillating Metal Nanowires”. In: *Phys. Rev. Lett.* 101 (21 Nov. 2008), p. 215502. DOI: 10.1103/PhysRevLett.101.215502. URL: https://link.aps.org/doi/10.1103/PhysRevLett.101.215502.

[78] Ajit K. Vallabhaneni et al. “Observation of nonclassical scaling laws in the quality factors of cantilevered carbon nanotube resonators”. In: *Journal of Applied Physics* 110.3 (Aug. 2011), p. 034312. ISSN: 0021-8979. DOI: 10.1063/1.3611396. eprint: https://pubs.aip.org/aip/jap/article-pdf/doi/10.1063/1.3611396/14064953/034312_1_online.pdf. URL: https://doi.org/10.1063/1.3611396.

[79] Jong Won Yoon and Ho Jung Hwang. “Molecular dynamics modeling and simulations of a single-walled carbon-nanotube-resonator encapsulating a finite nanoparticle”. In: *Computational Materials Science* 50.9 (2011), pp. 2741–2744. ISSN: 0927-0256. DOI: https://doi.org/10.1016/j.commatsci.2011.04.033. URL: https://www.sciencedirect.com/science/article/pii/S0927025611002552.

[80] Jeong Won Kang and Oh Kuen Kwon. “A molecular dynamics simulation study on resonance frequencies comparison of tunable carbon-nanotube resonators”. In: *Applied Surface Science* 258.6 (2012). International Vacuum Congress (IVC-18), pp. 2014–2016. ISSN: 0169-4332. DOI: https://doi.org/10.1016/j.apsusc.2011.05.026. URL: https://www.sciencedirect.com/science/article/pii/S0169433211007161.

[81] Jun Lee and Kang Jeong Won. “Vibrational Analysis of Cantilevered Carbon-Nanotube Resonator with Different Linear Density of Attached Mass: Molecular Dynamics Simulations”. In: *Journal of Computational and Theoretical Nanoscience* 10 (Aug. 2013), pp. 1863–1867. DOI: 10.1166/jctn.2013.3140.

[82] Zahra Nourmohammadi et al. “Methods for Atomistic Simulations of Linear and Nonlinear Damping in Nanomechanical Resonators”. In: *Journal of Microelectromechanical Systems* 24 (Oct. 2015), pp. 1–1. DOI: 10.1109/JMEMS.2015.2411747.

[83] Sankha Mukherjee, Jun Song, and Srikar Vengallatore. “Atomistic simulations of material damping in amorphous silicon nanoresonators”. In: *Modelling and Simulation in Materials Science and Engineering* 24.5 (June 2016), p. 055015. DOI: 10.1088/0965-0393/24/5/055015. URL: https://dx.doi.org/10.1088/0965-0393/24/5/055015.

[84] A Isacsson, J M Kinaret, and R Kaunisto. “Nonlinear resonance in a three-terminal carbon nanotube resonator”. In: *Nanotechnology* 18.19 (Apr. 2007), p. 195203. DOI: 10.1088/0957-4484/18/19/195203. URL: https://dx.doi.org/10.1088/0957-4484/18/19/195203.

[85] Hassen M. Ouakad and Mohammad Ibrahim Younis. “Nonlinear Dynamics of Electrically Actuated Carbon Nanotube Resonators”. In: *Journal of Computational and Nonlinear Dynamics* 5 (2010), p. 011009. URL: https://api.semanticscholar.org/CorpusID:119393229.

[86] Ajay M. Patel and Anand Y. Joshi. “Investigating the influence of surface deviations in double walled carbon nanotube based nanomechanical sensors”. In: *Computational Materials Science* 89 (2014), pp. 157–164. ISSN: 0927-0256. DOI: https://doi.org/10.1016/j.commatsci.2014.03.034. URL: https://www.sciencedirect.com/science/article/pii/S0927025614001852.

[87] Hassen M. Ouakad and Mohammad I. Younis. “Nonlinear Dynamics of Electrically Actuated Carbon Nanotube Resonators”. In: *Journal of Computational and Nonlinear Dynamics* 5.1 (Dec. 2009), p. 011009. ISSN: 1555-1415. DOI: 10.1115/1.4000319. eprint: https://asmedigitalcollection.asme.org/computationalnonlinear/article-pdf/5/1/011009/6912125/011009_1.pdf. URL: https://doi.org/10.1115/1.4000319.

[88] M Rasekh, S E Khadem, and M Tatari. "Nonlinear behaviour of electrostatically actuated carbon nanotube-based devices". In: *Journal of Physics D: Applied Physics* 43.31 (July 2010), p. 315301. DOI: 10.1088/0022-3727/43/31/315301. URL: https://dx.doi.org/10.1088/0022-3727/43/31/315301.

[89] Chunyu Li and Tsu-Wei Chou. "Mass detection using carbon nanotube-based nanomechanical resonators". In: *Applied Physics Letters* 84.25 (June 2004), pp. 5246–5248. ISSN: 0003-6951. DOI: 10.1063/1.1764933. eprint: https://pubs.aip.org/aip/apl/article-pdf/84/25/5246/14319825/5246_1_online.pdf. URL: https://doi.org/10.1063/1.1764933.

[90] N. Silvestre et al. "Sanders shell model for buckling of single-walled carbon nanotubes with small aspect ratio". In: *Composite Structures* 93.7 (2011), pp. 1683–1691. ISSN: 0263-8223. DOI: https://doi.org/10.1016/j.compstruct.2011.01.004. URL: https://www.sciencedirect.com/science/article/pii/S0263822311000183.

[91] M. Amabili. *Nonlinear Vibrations and Stability of Shells and Plates*. Cambridge University Press, 2008. ISBN: 9781139469029. URL: https://books.google.co.ug/books?id=0Ymw-pi7-x4C.

[92] Vera Sazonova et al. "A tunable carbon nanotube electromechanical oscillator". In: *Nature* 431 (Oct. 2004), pp. 284–7. DOI: 10.1038/nature02905.

[93] H. B. Peng et al. "Ultrahigh Frequency Nanotube Resonators". In: *Phys. Rev. Lett.* 97 (8 Aug. 2006), p. 087203. DOI: 10.1103/PhysRevLett.97.087203. URL: https://link.aps.org/doi/10.1103/PhysRevLett.97.087203.

[94] D. Garcia-Sanchez et al. "Mechanical Detection of Carbon Nanotube Resonator Vibrations". In: *Phys. Rev. Lett.* 99 (8 Aug. 2007), p. 085501. DOI: 10.1103/PhysRevLett.99.085501. URL: https://link.aps.org/doi/10.1103/PhysRevLett.99.085501.

[95] Hsin-Ying Chiu et al. "Atomic-Scale Mass Sensing Using Carbon Nanotube Resonators". In: *Nano Letters* 8.12 (Dec. 2008), pp. 4342–4346. ISSN: 1530-6984. DOI: 10.1021/nl802181c. URL: https://doi.org/10.1021/nl802181c.

[96] Benjamin Lassagne et al. "Coupling Mechanics to Charge Transport in Carbon Nanotube Mechanical Resonators". In: *Science* 325.5944 (2009), pp. 1107–1110. DOI: 10.1126/science.1174290. eprint: https://www.science.org/doi/pdf/10.1126/science.1174290. URL: https://www.science.org/doi/abs/10.1126/science.1174290.

[97] Hanna Cho et al. "Tunable, Broadband Nonlinear Nanomechanical Resonator". In: *Nano Letters* 10.5 (May 2010), pp. 1793–1798. ISSN: 1530-6984. DOI: 10.1021/nl100480y. URL: https://doi.org/10.1021/nl100480y.

[98] A. Eichler et al. "Nonlinear damping in mechanical resonators made from carbon nanotubes and graphene". In: *Nature Nanotechnology* 6.6 (June 2011), pp. 339–342. ISSN: 1748-3395. DOI: 10.1038/nnano.2011.71. URL: https://doi.org/10.1038/nnano.2011.71.

[99] Andres Castellanos-Gomez et al. "Strong and tunable mode coupling in carbon nanotube resonators". In: *Phys. Rev. B* 86 (4 July 2012), p. 041402. DOI: 10.1103/PhysRevB.86.041402. URL: https://link.aps.org/doi/10.1103/PhysRevB.86.041402.

[100] Z. Y. Ning et al. “Transversally and Axially Tunable Carbon Nanotube Resonators In Situ Fabricated and Studied Inside a Scanning Electron Microscope”. In: *Nano Letters* 14.3 (Mar. 2014), pp. 1221–1227. ISSN: 1530-6984. DOI: 10.1021/nl4040913. URL: https://doi.org/10.1021/nl4040913.

[101] Tomás Rosas Coelho Chuaqui. “Linear and Non-Linear Vibrations of Single-Layer Graphene Sheets”. Master’s degree dissertation. https://hdl.handle.net/10216/89929: Faculdade de Engenharia da Universidade do Porto, Sept. 2016.

[102] Tienchong Chang. “A molecular based anisotropic shell model for single-walled carbon nanotubes”. In: *Journal of the Mechanics and Physics of Solids* 58.9 (2010), pp. 1422–1433. ISSN: 0022-5096. DOI: https://doi.org/10.1016/j.jmps.2010.05.004. URL: https://www.sciencedirect.com/science/article/pii/S0022509610000943.

[103] B. I. Yakobson, C. J. Brabec, and J. Bernholc. “Nanomechanics of Carbon Tubes: Instabilities beyond Linear Response”. In: *Phys. Rev. Lett.* 76 (14 Apr. 1996), pp. 2511–2514. DOI: 10.1103/PhysRevLett.76.2511. URL: https://link.aps.org/doi/10.1103/PhysRevLett.76.2511.

[104] Arthur W. Leissa and Ronald P. Nordgren. “Vibration of shells”. In: United States, Washington, D.C., 1973. URL: https://api.semanticscholar.org/CorpusID:55481138.

[105] Matteo Strozzi et al. “A Comparison of Shell Theories for Vibration Analysis of Single-Walled Carbon Nanotubes Based on an Anisotropic Elastic Shell Model”. In: *Nanomaterials* 13.8 (2023). ISSN: 2079-4991. DOI: 10.3390/nano13081390. URL: https://www.mdpi.com/2079-4991/13/8/1390.

[106] Augustus Edward Hough Love. “XVI. The small free vibrations and deformation of a thin elastic shell”. In: *Philosophical Transactions of the Royal Society of London.(A.)* 179 (1888), pp. 491–546.

[107] Jr. J. Lyell Sanders. “NONLINEAR THEORIES FOR THIN SHELLS”. In: *Quarterly of Applied Mathematics* 21 (1963), pp. 21–36. URL: https://api.semanticscholar.org/CorpusID:122821184.

[108] José Dias Rodrigues. *Apontamentos de Vibrações de Sistemas Mecânicos*. Porto, Portugal: Departamento de Engenharia Mecânica da Faculdade de Engenharia da Univerisdade do Porto, Jan. 2020.

[109] Pedro Ribeiro and Olivier Thomas. “Nonlinear Modes of Vibration and Internal Resonances in Nonlocal Beams”. In: *Journal of Computational and Nonlinear Dynamics* 12.3 (Jan. 2017), p. 031017. ISSN: 1555-1415. DOI: 10.1115/1.4035060. eprint: https://asmedigitalcollection.asme.org/computationalnonlinear/article-pdf/12/3/031017/6109267/cnd_012_03_031017.pdf. URL: https://doi.org/10.1115/1.4035060.

[110] N. S. Bardell. “The application of symbolic computing to the hierarchical finite element method”. In: *International Journal for Numerical Methods in Engineering* 28 (1989), pp. 1181–1204. URL: https://api.semanticscholar.org/CorpusID:121210724.

[111] Wanmin Han, Maurice Petyt, and Kuo-Mo Hsiao. “An investigation into geometrically nonlinear analysis of rectangular laminated plates using the hierarchical finite element method”. In: *Finite Elements in Analysis and Design* 18.1 (1994), pp. 273–288. ISSN: 0168-874X. DOI: https://doi.org/10.1016/0168-874X(94)90107-4. URL: https://www.sciencedirect.com/science/article/pii/0168874X94901074.

[112] P. Ribeiro. “Hierarchical finite element analyses of geometrically non-linear vibration of beams and plane frames”. In: *Journal of Sound and Vibration* 246.2 (2001), pp. 225–244. ISSN: 0022-460X. DOI: https://doi.org/10.1006/jsvi.2001.3634. URL: https://www.sciencedirect.com/science/article/pii/S0022460X0193634X.

[113] L. Meirovitch. *Computational Methods in Structural Dynamics*. Mechanics: Dynamical Systems. Springer Netherlands, 1980. ISBN: 9789028605800. URL: https://link.springer.com/book/9789028605800.

[114] Pedro Ribeiro. “On the influence of membrane inertia and shear deformation on the geometrically non-linear vibrations of open, cylindrical, laminated clamped shells”. In: *Composites Science and Technology* 69.2 (2009), pp. 176–185. ISSN: 0266-3538. DOI: https://doi.org/10.1016/j.compscitech.2008.09.038. URL: https://www.sciencedirect.com/science/article/pii/S0266353808003874.

[115] Kevin Forsberg. “A review of analytical methods used to determine the modal characteristics of cylindrical shells”. In: 1966. URL: https://api.semanticscholar.org/CorpusID:117311299.

[116] Marc Dequesnes, S V Rotkin, and N R Aluru. “Calculation of pull-in voltages for carbon-nanotube-based nanoelectromechanical switches”. In: *Nanotechnology* 13.1 (Jan. 2002), p. 120. DOI: 10.1088/0957-4484/13/1/325. URL: https://dx.doi.org/10.1088/0957-4484/13/1/325.

[117] W.H. Hayt and J.A. Buck. *Engineering Electromagnetics*. Electrical engineering series. McGraw-Hill, 2001, pp. 150–159. ISBN: 9780072304244. URL: https://books.google.pt/books?id=XN3CQgAACAAJ.

[118] M. Poot et al. “Modelling suspended carbon nanotube resonators”. In: *physica status solidi (b)* 244.11 (2007), pp. 4252–4256. DOI: https://doi.org/10.1002/pssb.200776130. eprint: https://onlinelibrary.wiley.com/doi/pdf/10.1002/pssb.200776130. URL: https://onlinelibrary.wiley.com/doi/abs/10.1002/pssb.200776130.

[119] Eduardo Henrique L. M. Gonçalves. “Vibrations of Carbon Nanotubes by a nonlocal shell model”. MA thesis. Porto: Faculdade de Engenharia da Universidade do Porto, June 2020.

[120] S.K. Georgantzinos and N.K. Anifantis. “An Atomistic-based Spring-mass Finite Element Approach for Vibration Analysis of Carbon Nanotube Mass Detectors”. In: Apr. 2011. ISBN: 978-953-307-209-8. DOI: 10.5772/15973.

[121] Hassen M. Ouakad and Mohammad I. Younis. “Natural frequencies and mode shapes of initially curved carbon nanotube resonators under electric excitation”. In: *Journal of Sound and Vibration* 330.13 (2011), pp. 3182–3195. ISSN: 0022-460X. DOI: https://doi.org/10.1016/j.jsv.2010.12.029. URL: https://www.sciencedirect.com/science/article/pii/S0022460X11000423.

[122] John T. Katsikadelis. “Chapter 12 - Multi-degree-of-freedom systems: Free vibrations”. In: *Dynamic Analysis of Structures*. Ed. by John T. Katsikadelis. Academic Press, 2020, pp. 523–600. ISBN: 978-0-12-818643-5. DOI: https://doi.org/10.1016/B978-0-12-818643-5.00012-1. URL: https://www.sciencedirect.com/science/article/pii/B9780128186435000121.

[123] Yin Zhang and Ya-Pu Zhao. “Mass and Force Sensing of an Adsorbate on a Beam Resonator Sensor”. In: *Sensors* 15.7 (2015), pp. 14871–14886. ISSN: 1424-8220. DOI: 10.3390/s150714871. URL: https://www.mdpi.com/1424-8220/15/7/14871.

[124] G. Leizerovich and S. V. Seregin. “Free vibrations of circular cylindrical shells with a small added concentrated mass”. In: *Journal of Applied Mechanics and Technical Physics* 57 (Sept. 2016), pp. 841–846. DOI: 10.1134/S0021894416050102.

Appendix A

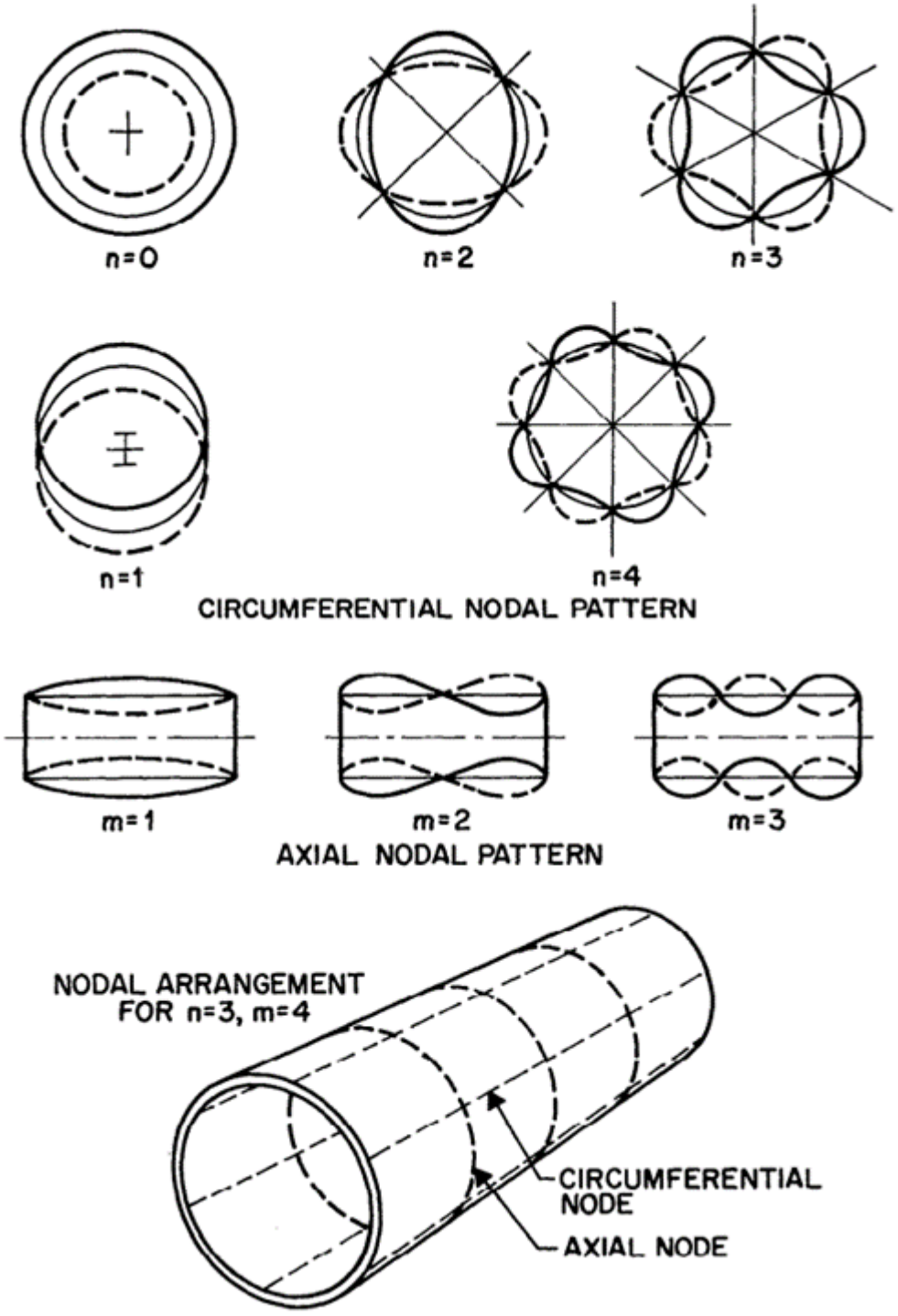

Designation of different modes of vibration based on the circumferential and axial node distribution; reprinted from [115]

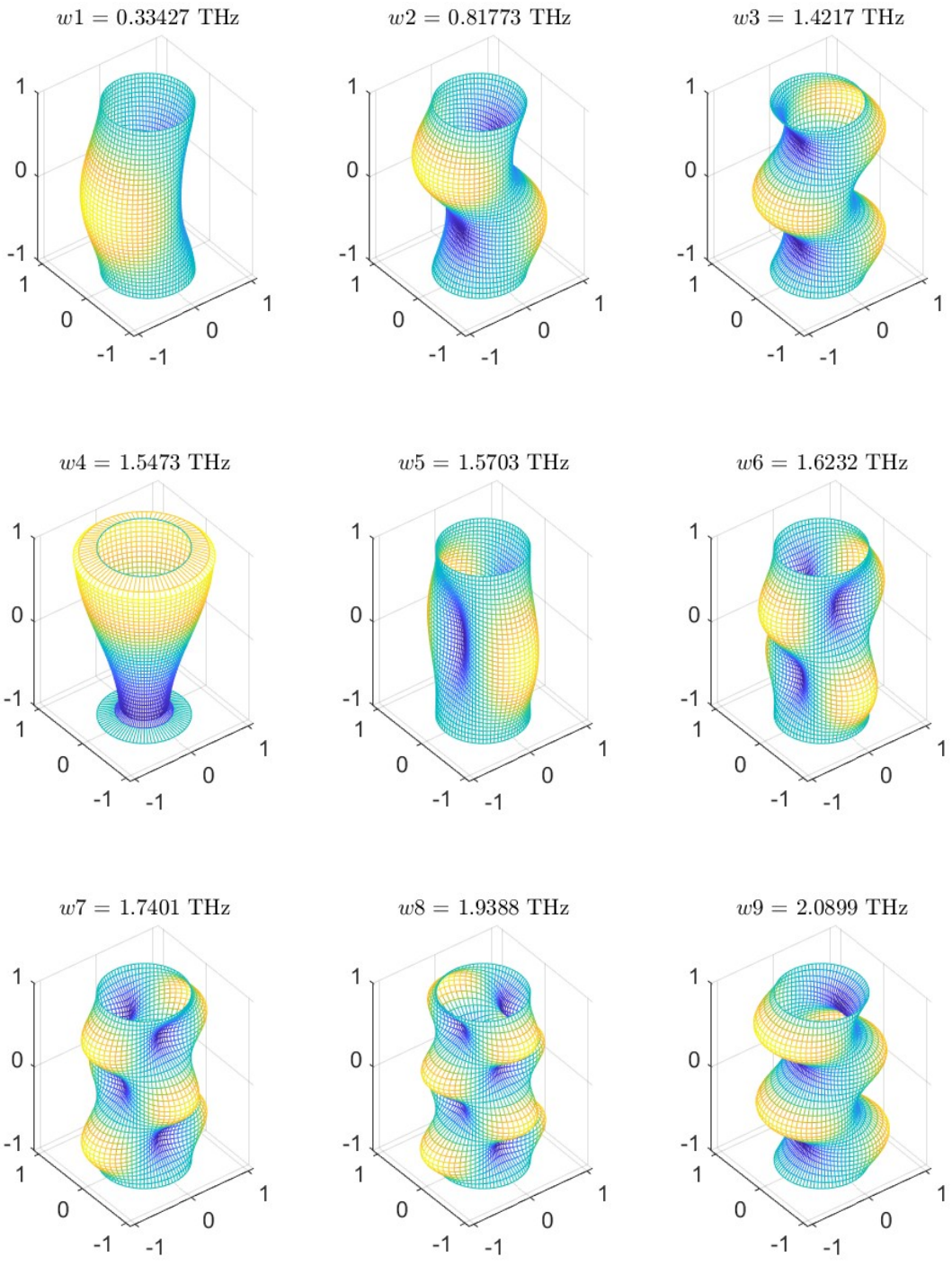
$w1 = 0.33427$ THz
$w2 = 0.81773$ THz
$w3 = 1.4217$ THz
$w4 = 1.5473$ THz
$w5 = 1.5703$ THz
$w6 = 1.6232$ THz
$w7 = 1.7401$ THz
$w8 = 1.9388$ THz
$w9 = 2.0899$ THz

$w10 = 2.2209$ THz

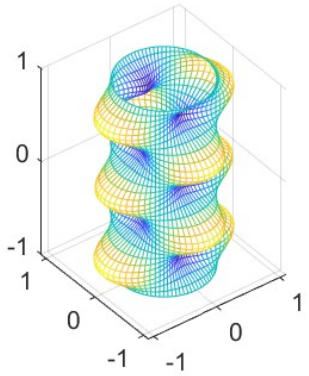

$w11 = 2.5753$ THz

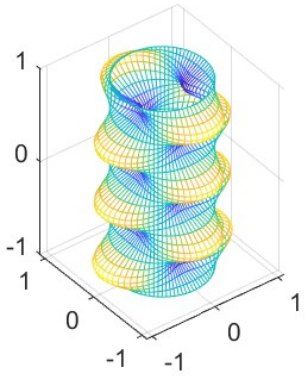

$w12 = 2.7914$ THz

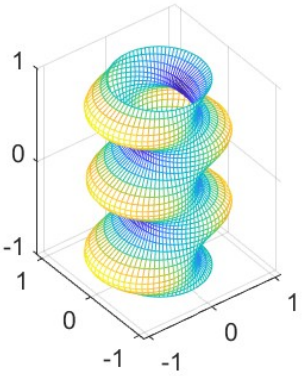

$w13 = 2.9866$ THz

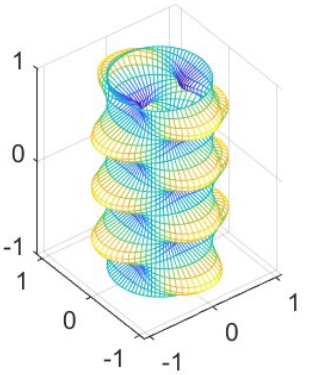

$w14 = 3.0905$ THz

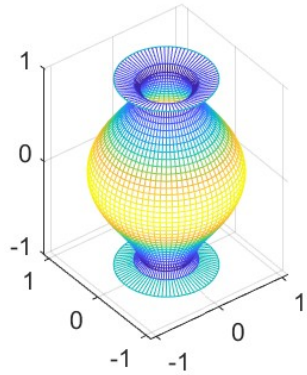

$w15 = 3.4397$ THz

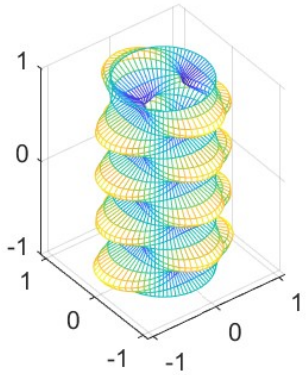

$w16 = 3.5033$ THz

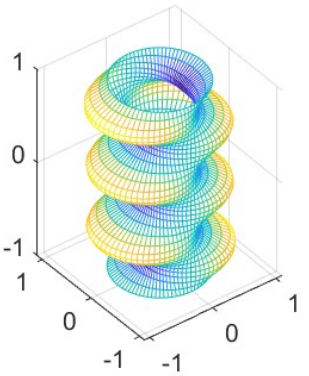

$w17 = 3.9226$ THz

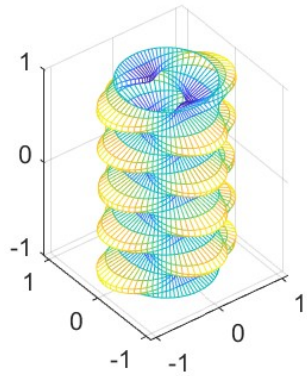

$w18 = 4.2081$ THz

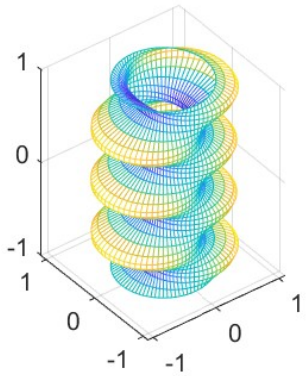

Appendix B

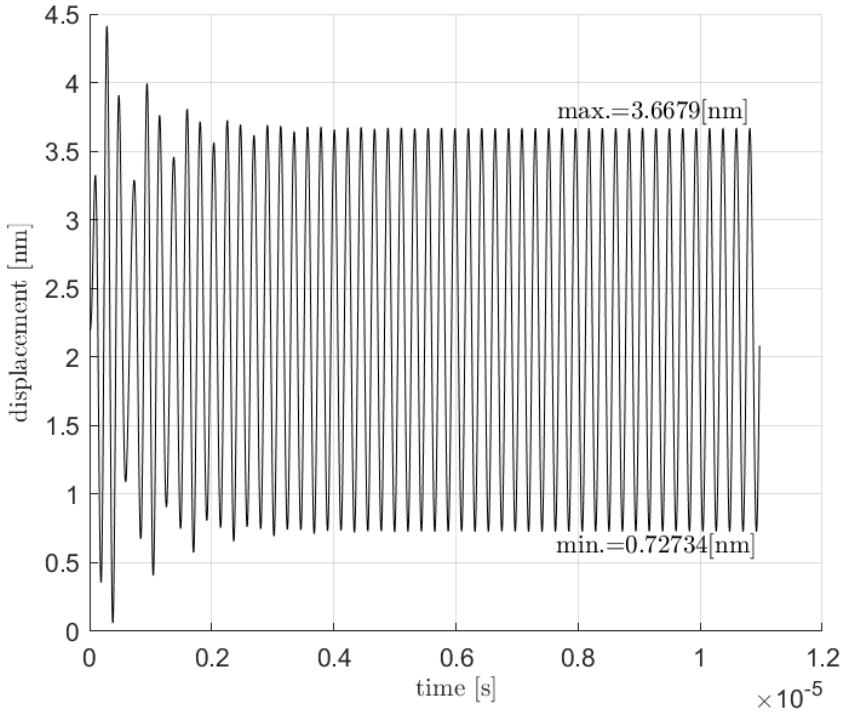

Plot of the displacement in time of the midpoint of the section of the CNT under electrostatic actuation at $\xi = 0$ - Obtained with the full model; $V_{DC} = 0.125$ [V], $V_{AC} = 0.018$ [V] and $\Omega_{AC} = 0.75$

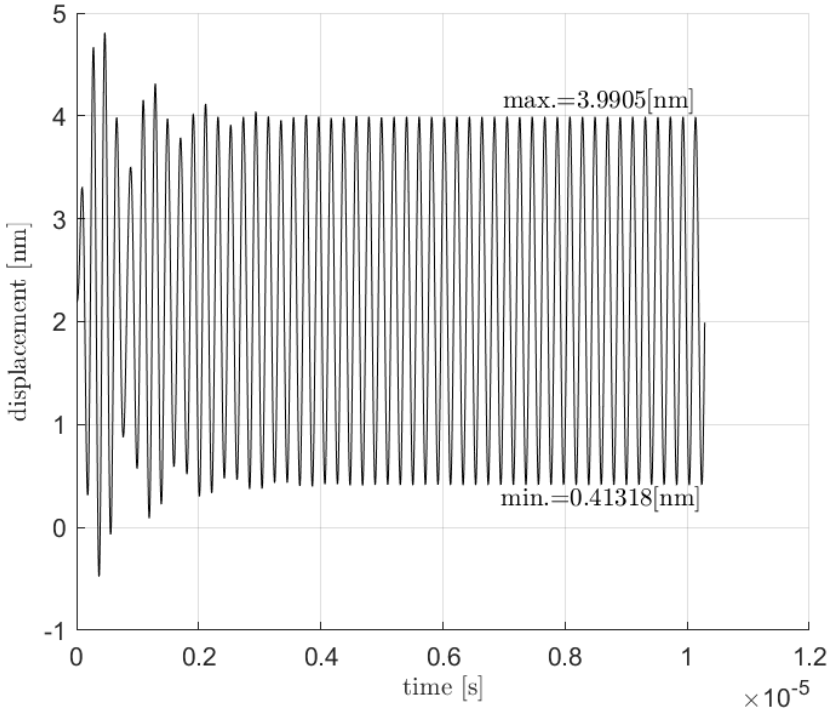

Plot of the displacement in time of the midpoint of the section of the CNT under electrostatic actuation at $\xi = 0$ - Obtained with the full model; $V_{DC} = 0.125$ [V], $V_{AC} = 0.018$ [V] and $\Omega_{AC} = 0.80$

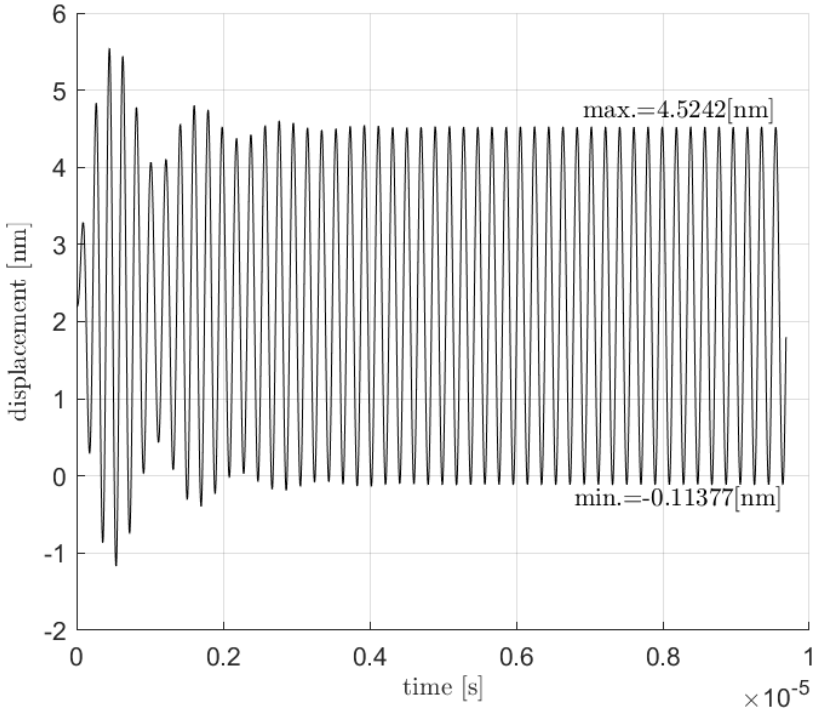

Plot of the displacement in time of the midpoint of the section of the CNT under electrostatic actuation at $\xi = 0$ - Obtained with the full model; $V_{DC} = 0.125$ [V], $V_{AC} = 0.018$ [V] and $\Omega_{AC} = 0.85$

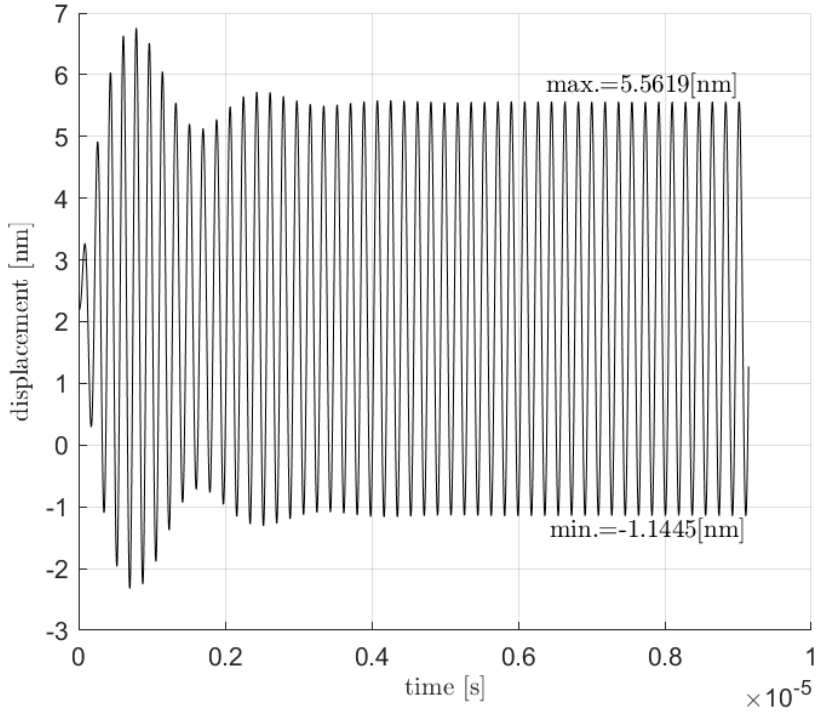

Plot of the displacement in time of the midpoint of the section of the CNT under electrostatic actuation at $\xi = 0$ - Obtained with the full model; $V_{DC} = 0.125$ [V], $V_{AC} = 0.018$ [V] and $\Omega_{AC} = 0.90$

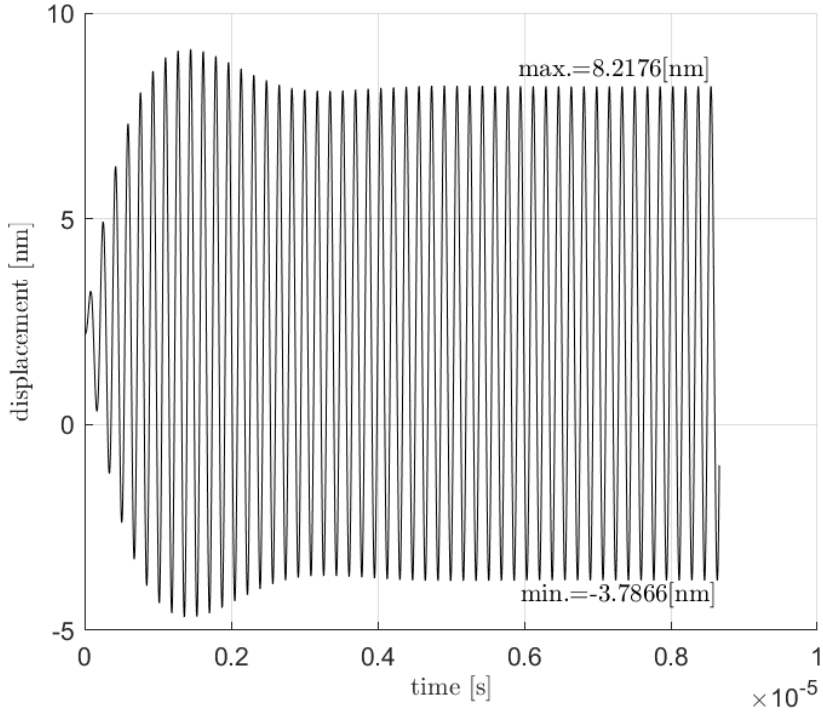

Plot of the displacement in time of the midpoint of the section of the CNT under electrostatic actuation at $\xi = 0$ - Obtained with the full model; $V_{DC} = 0.125$ [V], $V_{AC} = 0.018$ [V] and $\Omega_{AC} = 0.95$

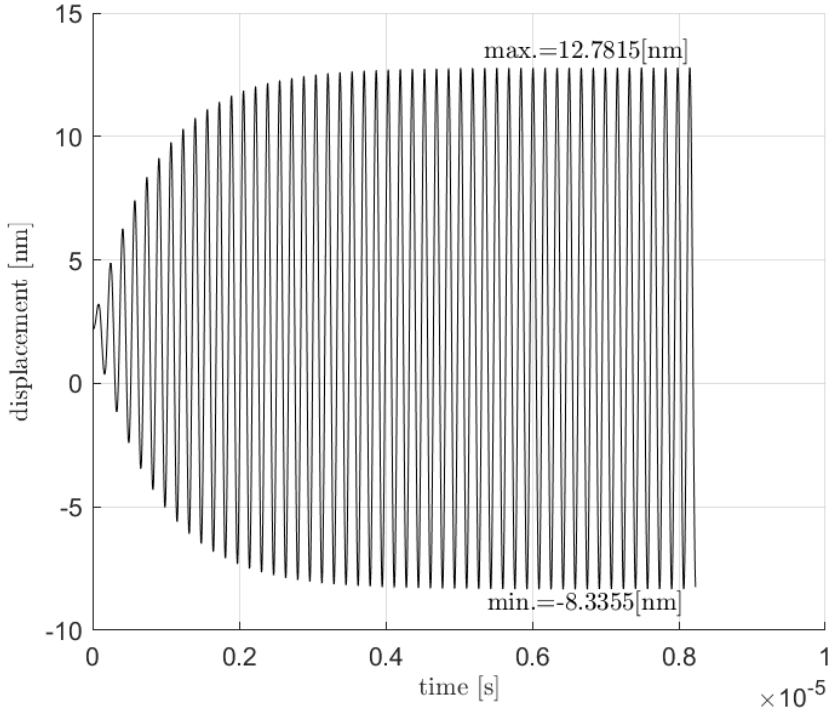

Plot of the displacement in time of the midpoint of the section of the CNT under electrostatic actuation at $\xi = 0$ - Obtained with the full model; $V_{DC} = 0.125$ [V], $V_{AC} = 0.018$ [V] and $\Omega_{AC} = 1.00$

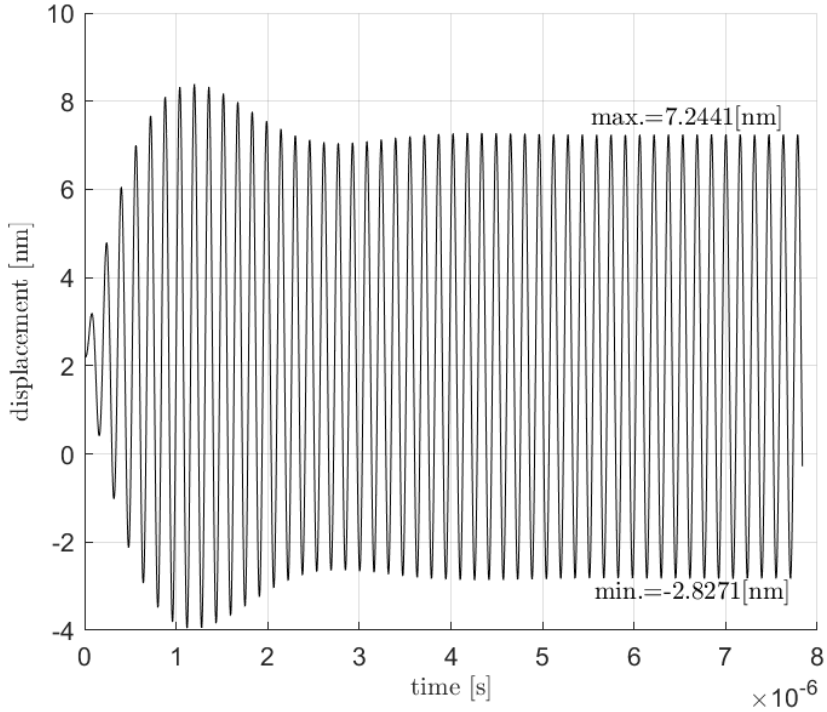

Plot of the displacement in time of the midpoint of the section of the CNT under electrostatic actuation at $\xi = 0$ - Obtained with the full model; $V_{DC} = 0.125$ [V], $V_{AC} = 0.018$ [V] and $\Omega_{AC} = 1.05$

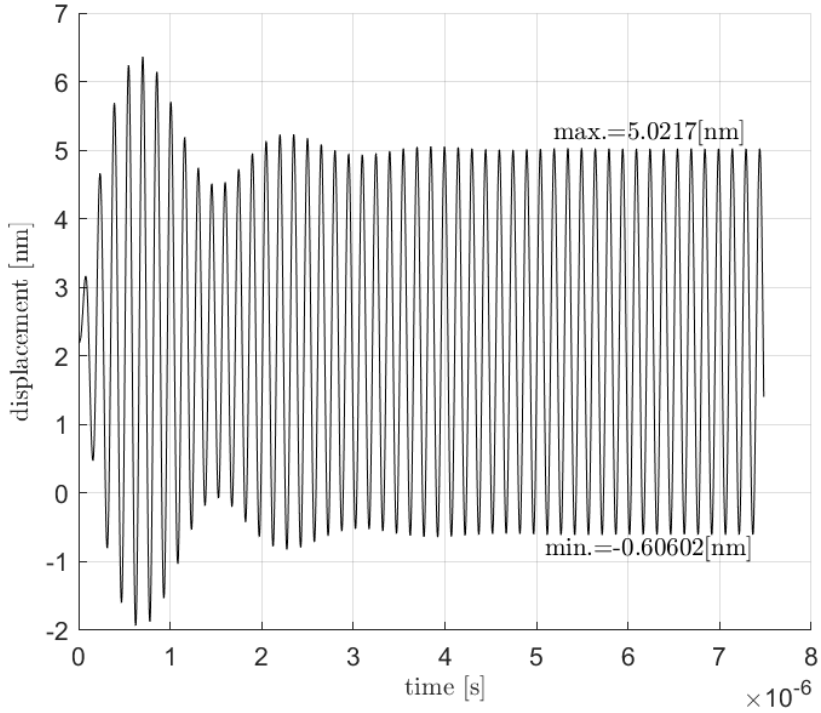

Plot of the displacement in time of the midpoint of the section of the CNT under electrostatic actuation at $\xi = 0$ - Obtained with the full model; $V_{DC} = 0.125$ [V], $V_{AC} = 0.018$ [V] and $\Omega_{AC} = 1.10$

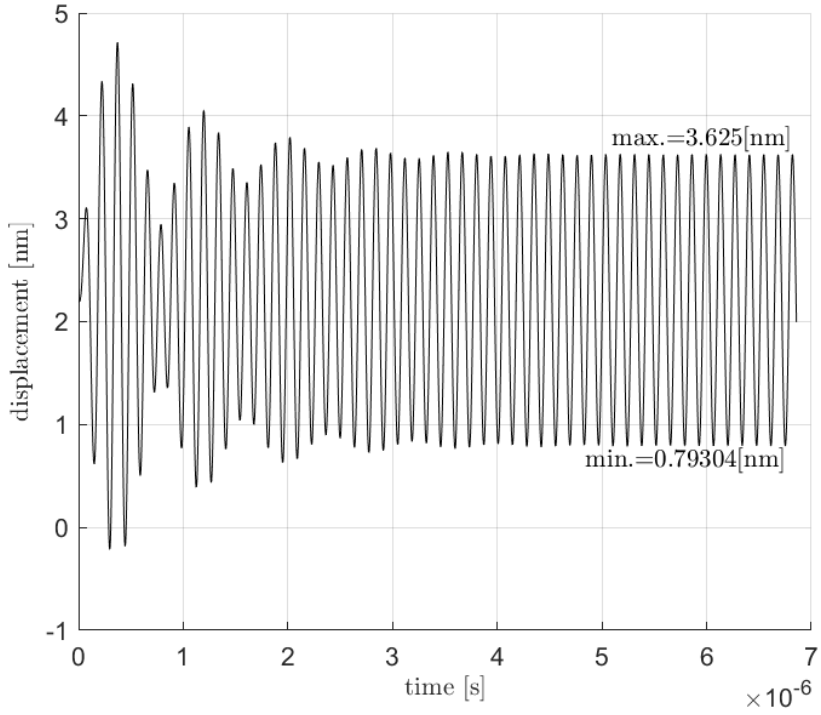

Plot of the displacement in time of the midpoint of the section of the CNT under electrostatic actuation at $\xi = 0$ - Obtained with the full model; $V_{DC} = 0.125$ [V], $V_{AC} = 0.018$ [V] and $\Omega_{AC} = 1.20$

Appendix C

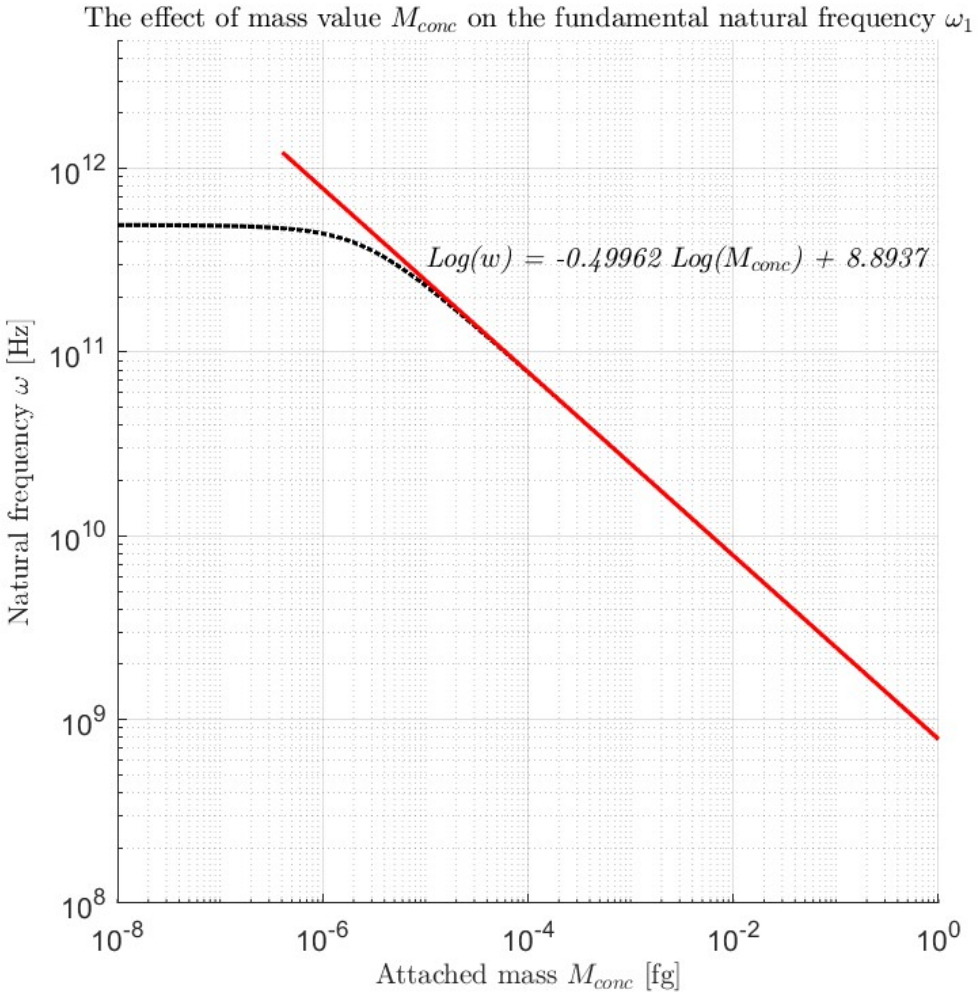

Variation of the fundamental natural frequency with attached mass value and linear approximation - $d = 0.8$ [nm]; $l = 6$ [nm]; with fitted linear regression

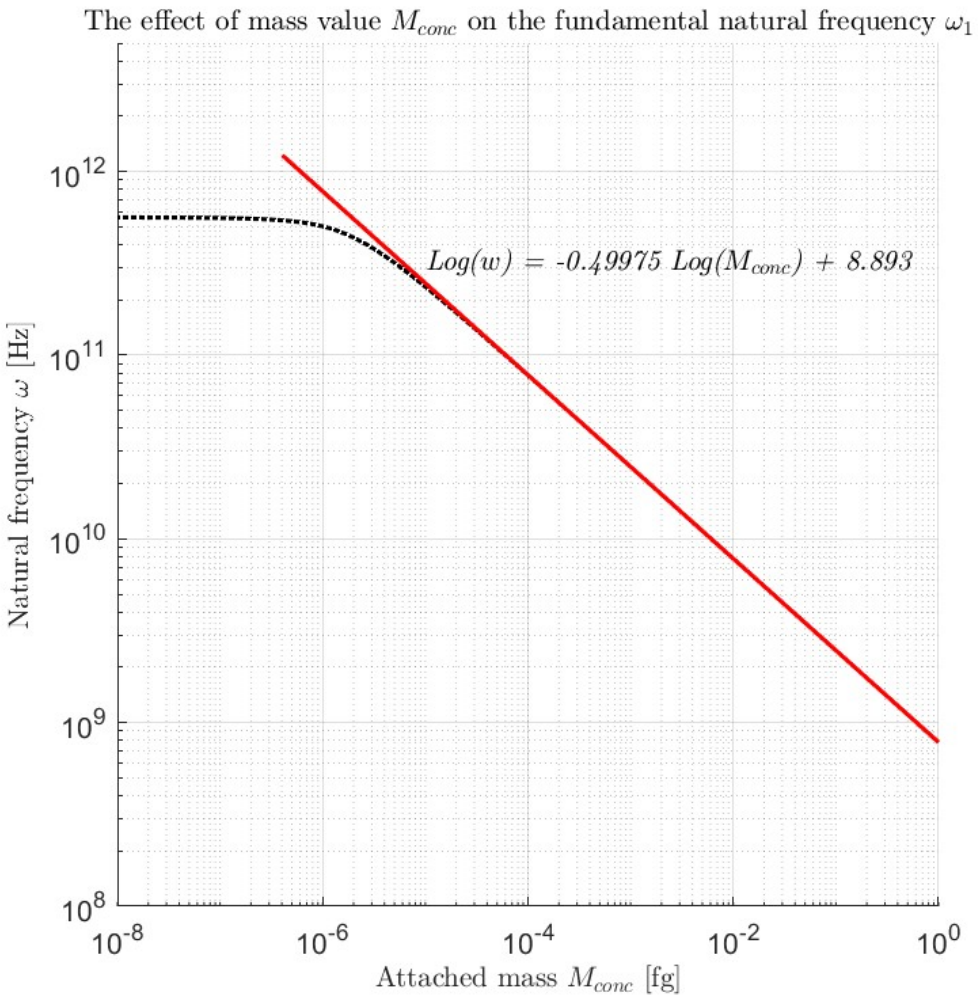

Variation of the fundamental natural frequency with attached mass value and linear approximation - $d = 1.0$ [nm]; $l = 6$ [nm]; with fitted linear regression

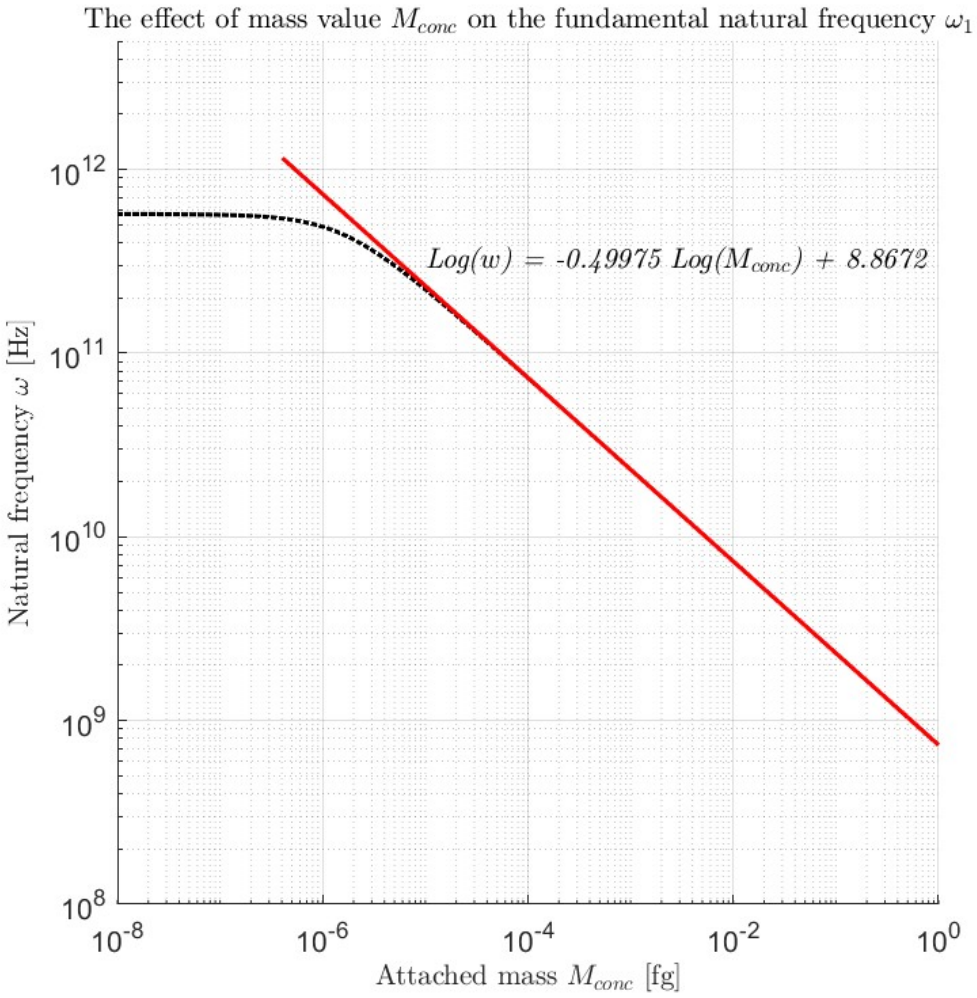

Variation of the fundamental natural frequency with attached mass value and linear approximation - $d = 1.2$ [nm]; $l = 6$ [nm]; with fitted linear regression

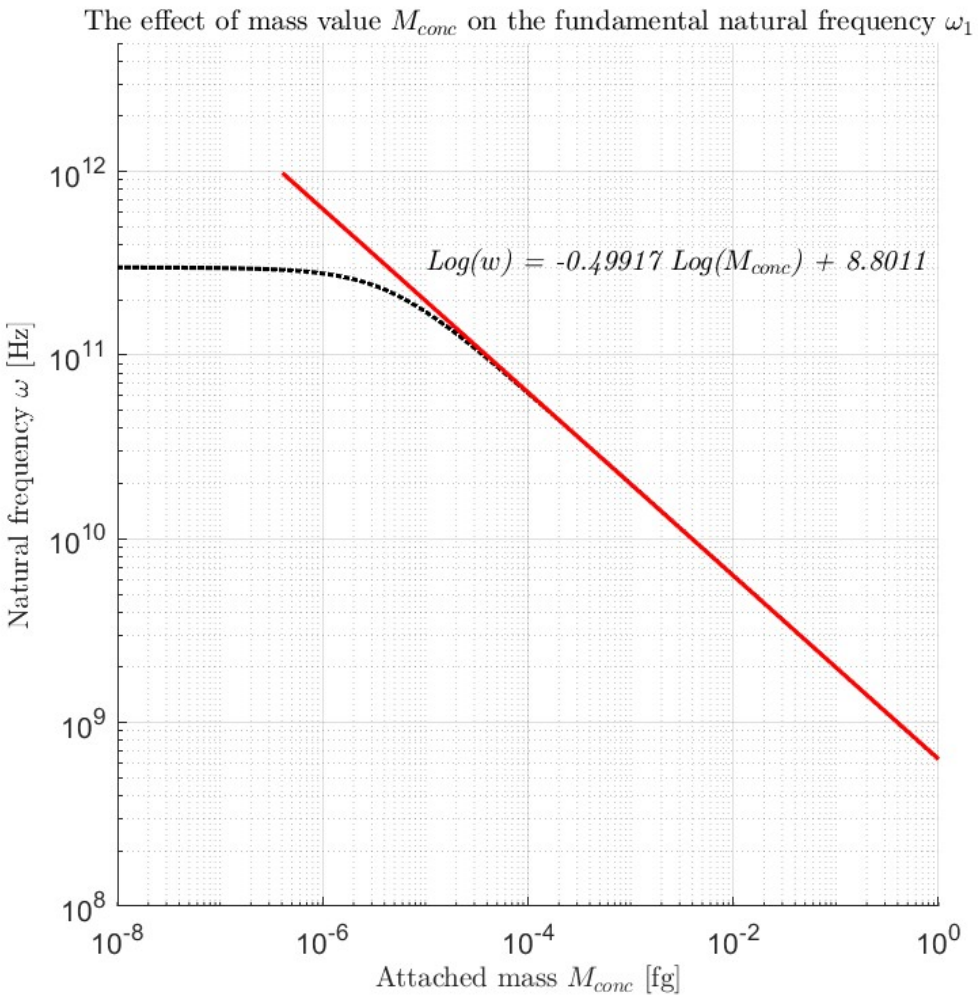

Variation of the fundamental natural frequency with attached mass value and linear approximation - $d = 0.8$ [nm]; $l = 6$ [nm]; with fitted linear regression

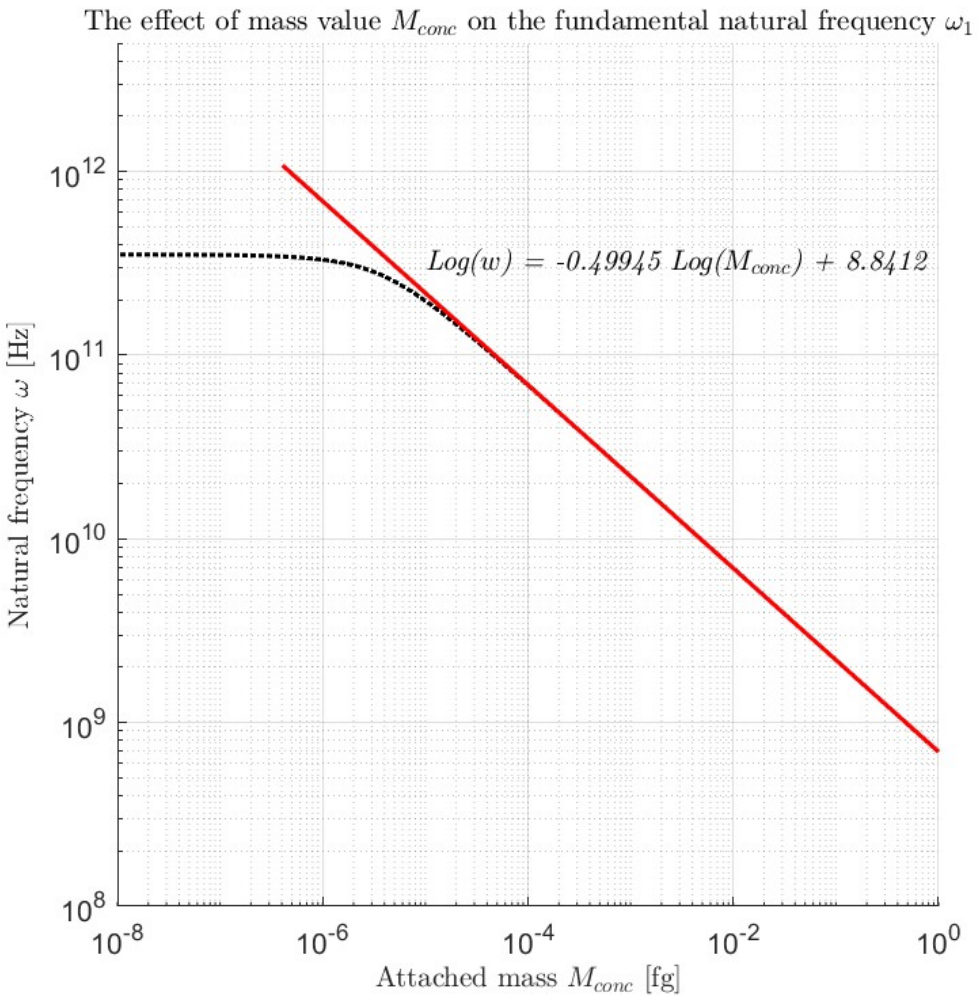

Variation of the fundamental natural frequency with attached mass value and linear approximation - $d = 1.0$ [nm]; $l = 8$ [nm]; with fitted linear regression

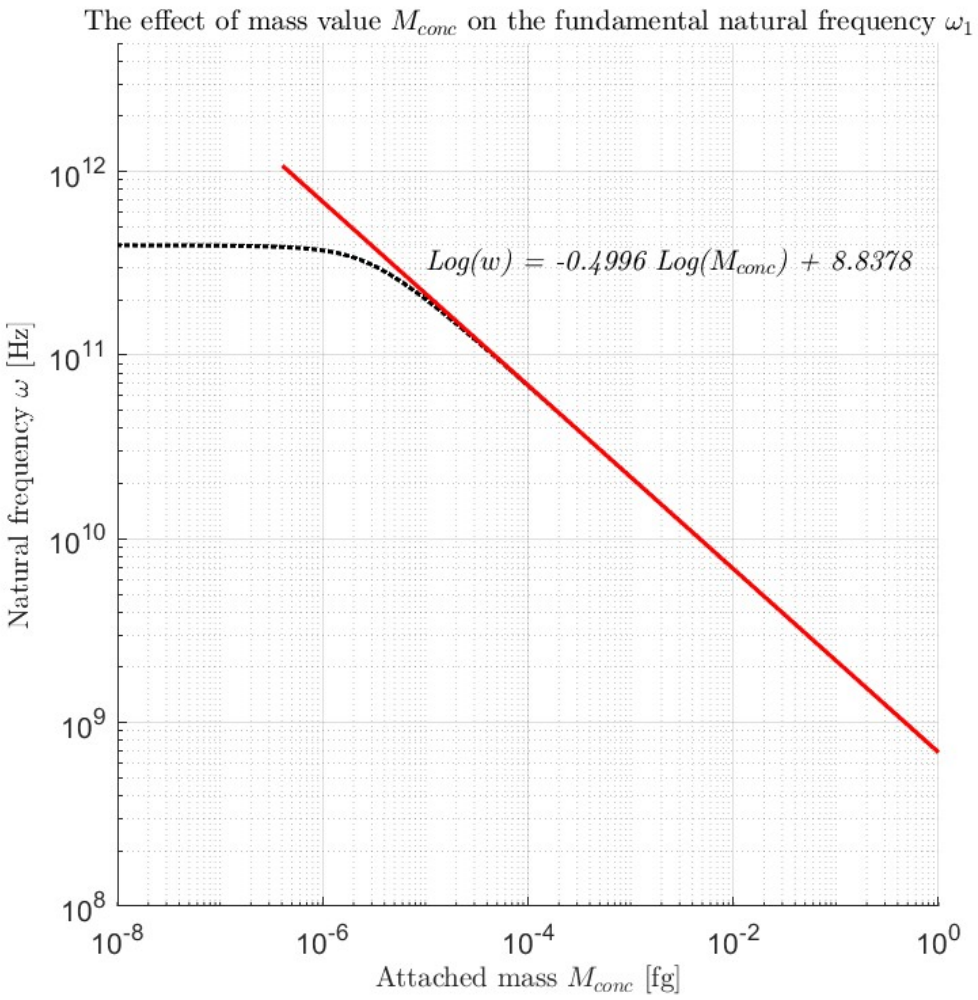

Variation of the fundamental natural frequency with attached mass value and linear approximation - $d = 1.2$ [nm]; $l = 8$ [nm]; with fitted linear regression

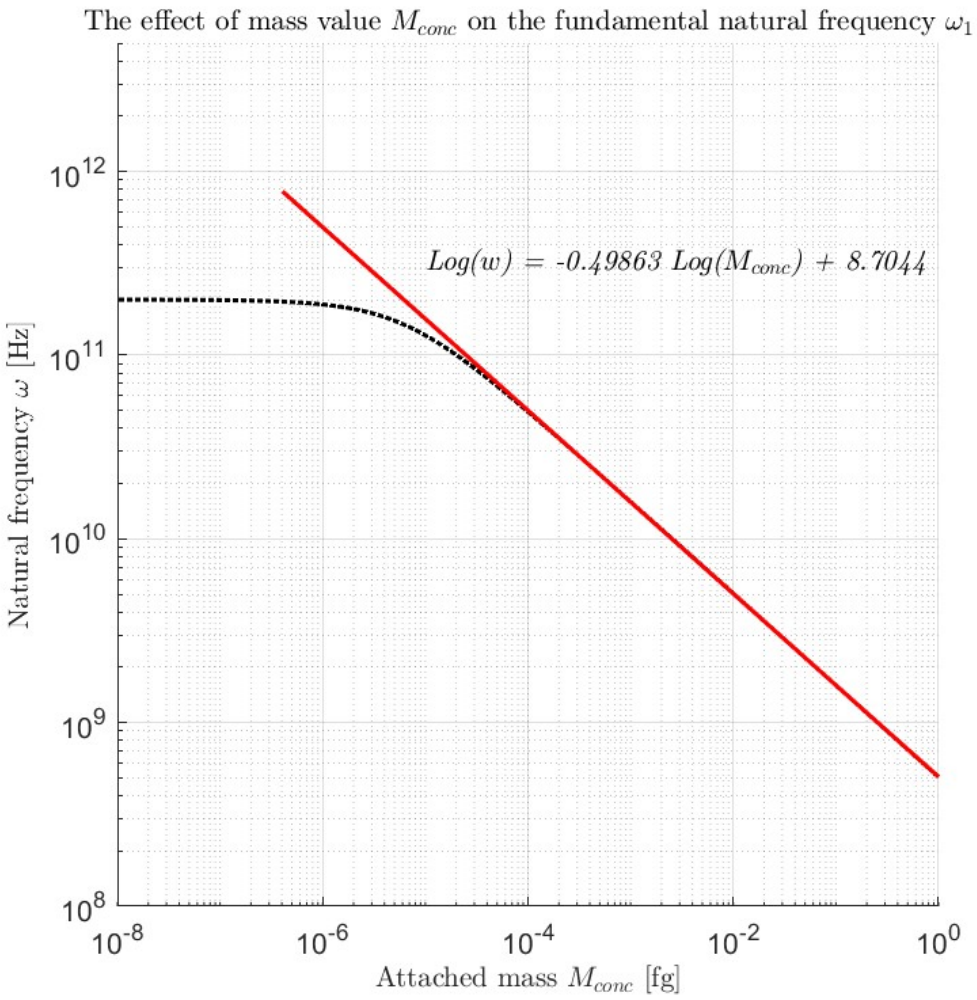

Variation of the fundamental natural frequency with attached mass value and linear approximation - $d = 0.8$ [nm]; $l = 10$ [nm]; with fitted linear regression

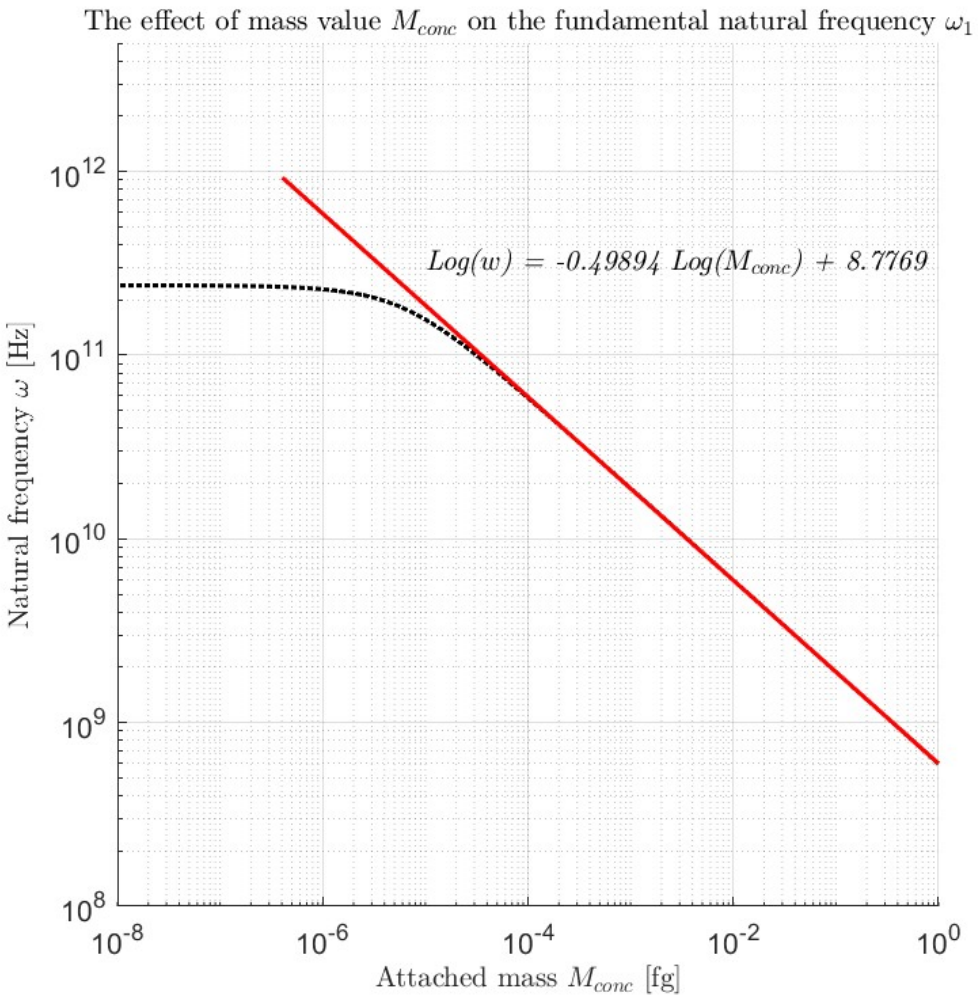

Variation of the fundamental natural frequency with attached mass value and linear approximation - $d = 1.0$ [nm]; $l = 10$ [nm]; with fitted linear regression

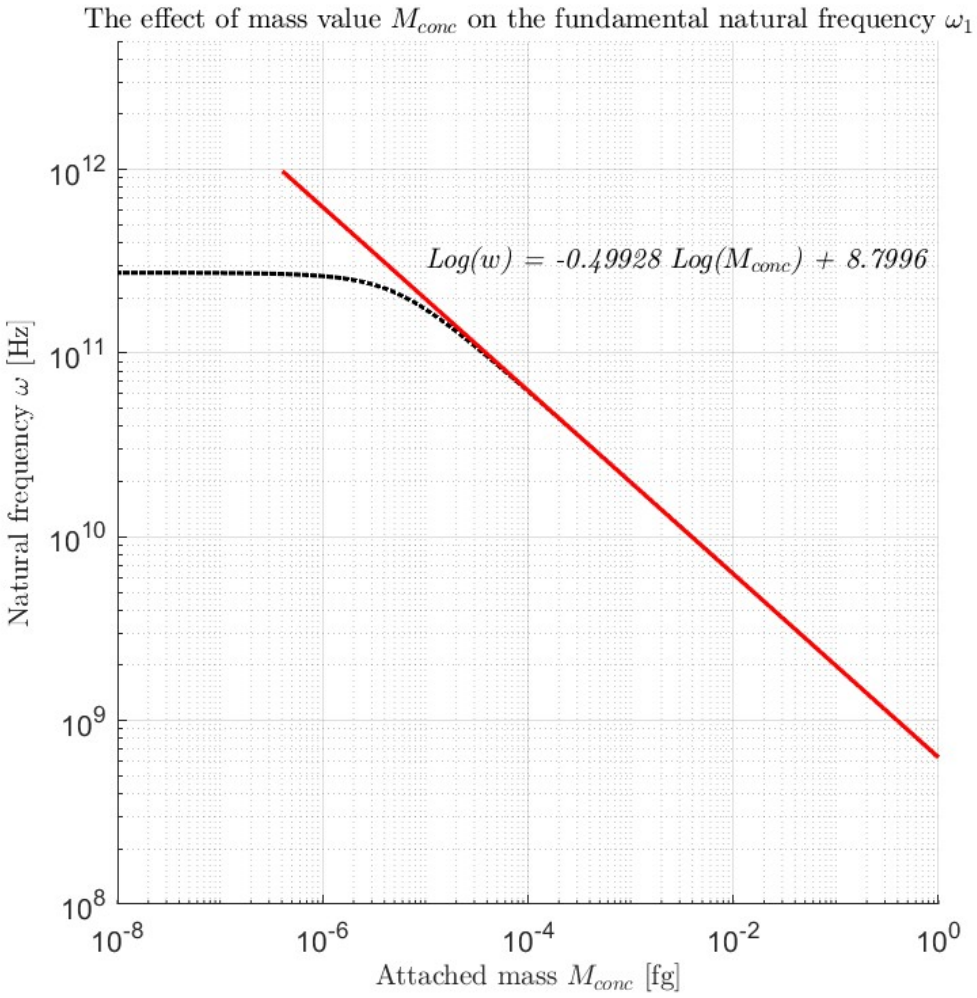

Variation of the fundamental natural frequency with attached mass value and linear approximation - $d = 1.2$ [nm]; $l = 10$ [nm]; with fitted linear regression